The role of two-pore channels 2 (TPC2) in melanoma tumourigenesis and metastasis

Ali Ahmed Hanbashi

Worcester College
University of Oxford

Supervised by

Prof. John Parrington

Department of Pharmacology
University of Oxford

A thesis submitted for the degree of
Doctor of Philosophy
Trinity Term, 2022

Declaration

I declare that this thesis is entirely my own work, and except where otherwise stated, describes my own research.

Ali Hanbashi
Worcester College

Abstract

Melanoma is an exceedingly aggressive and resistant to treatment form of cancer. Therefore, the identification of novel therapeutic approaches continues to be a crucial task. Understanding the pathophysiological role of potential drug targets for this disease enables the discovery of new therapeutic strategies. The two-pore channel 2, TPC2, is located on late endosomes, lysosomes, and melanosomes. Here, we evaluated the effect of TPC2 knockout (KO) on human metastatic melanoma (CHL-1) and murine primary melanoma (B16) cells. TPC2-depleted melanoma cell lines were created using CRISPR-Cas9 gene editing. CHL-1, an amelanotic metastatic melanoma cell line, exhibited *in vitro* induced migratory traits after TPC2 depletion. In contrast, B16 TPC2 KO cells displayed a diminished ability to migrate *in vitro*. TPC2 KO activated genes regulated by YAP/TAZ, which are important regulators of tumorigenesis and metastasis, in CHL-1. TPC2 KO and RNA interference knockdown decreased the expression levels of ORAI1, a component of store-operated Ca^{2+} entry (SOCE), and PKC-II, a component of the HIPPO pathway that adversely affects YAP/TAZ activity. These findings are explained by a cellular mechanism mediated by ORAI1/ Ca^{2+}/PKC-II.

Furthermore, CHL-1 and B16 TPC2 KO proteomic signatures were examined to WT cells. The differential expression of proteins between WT and KO cells enables us to evaluate TPC2's role in various crucial pathways and processes. Accordingly, the bioenergetic phenotype of TPC2-deficient cells was assessed.

TPC2 depletion boosted ATP synthesis in CHL-1 and B16 TPC2 KO cells relative to WT cells, but increased lactate generation in B16 cells. TPC2 deficiency enhanced anaerobic respiration in B16 cells but reduced it in CHL-1 cells. OCR/ECAR analysis confirmed TPC2-KO cells' metabolic shift. CHL-1 TPC2 KO cells are more aerobic due to a reduced OCR/ECAR ratio. OCR/ECAR was elevated in B16 KO cells in complete media. B16 KO cells increased oxygen utilisation and lactate production without glucose. In addition, the cytoskeleton and synthesis and release of melanin were altered in TPC2 KO cells.

In vivo evaluation of B16 TPC2 KO melanoma cell lines following subcutaneous injection revealed a significantly reduced tumour volume compared to WT cells. However, histopathological examination of mice injected with KO cells revealed that the hepatic and splenic structures were drastically changed.

Clinical association is vital to determining correlations between molecular discoveries and cancer patient survival. TPC2 high-expression patients had a shorter overall survival time than low-expression patients. Furthermore, high TPC2 expression is associated with lower survival in BRAF mutant melanoma.

In summary, the work presented in this thesis indicates that TPC2 plays vital functions in melanoma's progression, invasion, and metastasis.

Acknowledgements

I must begin by expressing my gratitude to my advisor, Professor John Parrington, for all of his guidance and support throughout the research and preparation of my thesis. In the few years that have passed, I cannot recall ever seeing him without a smile on his face and without offering someone support. He has an exceptional character. Having him as a mentor throughout my DPhil period was invaluable to my development as a researcher.

I am especially grateful to the former and current members of Parrington's lab, who have been wonderful companions throughout my research.

My profound gratitude also extends to the academic staff of the Department of Pharmacology and the researchers in their labs, particularly Professor Antony Galione and Dr. Vasudevan, who allowed me access to their facilities for research and to those of other departments at Oxford, including pathology and biochemistry. I must also extend my appreciation to Dr. Ali Alhoshani. Without their invaluable support, this research would not be feasible.

The support I received from the sponsor of my DPhil studies at Oxford was also very valuable to me. Without the financial support of the College of Pharmacy, Jazan University, Saudi Arabia, and the Saudi Cultural Bureau, London, United Kingdom, this journey would not have been possible.

Special thanks are extended to Graeme Laidler, Hicham Ouallaf, James Weller, Carolyn Thackrah, Jimmy Martin, and Paula Savin for their continuous support and assistance.

I owe a debt of gratitude to two brilliant scientists: Dr. Alaa Hachem and Dr. Antonella D'Amore. Alaa was and remains the most scientifically curious person I've ever met. Antonella is a bright and superb scientist. Without her, this work and many other things would not have been possible.

I am grateful to my Oxford and beyond friends, notably Emad, Muaad, Abdulla, Mehdi, Faisal, Hatem, Faroq, Mohammdy, Hilal, Hadi, Mohammed, Naif , Adel, Fahad, Awaji, Abdulaziz, and Abdul Majeed, for their company.

The everlasting love and support of my family have been an absolute blessing for me. I am and will always be grateful to you, even though I firmly believe that such love and support can never be paid back.

Publications

- D'Amore, A.; **Hanbashi, A.A.**; Di Agostino, S.; Palombi, F.; Sacconi, A.; Voruganti, A.; Taggi, M.; Canipari, R.; Blandino, G.; Parrington, J.; Filippini, A. Loss of Two-Pore Channel 2 (TPC2) Expression Increases the Metastatic Traits of Melanoma Cells by a Mechanism Involving the Hippo Signalling Pathway and Store-Operated Calcium Entry. *Cancers* **2020**, *12*, 2391.

- Navarro-Serna S, Hachem A, Canha-Gouveia A**, Hanbashi A**, Garrappa G, Lopes JS, París-Oller E, Sarrías-Gil L, Flores-Flores C, Bassett A, Sánchez R, Bermejo-Álvarez P, Matás C, Romar R, Parrington J, Gadea J. Generation of Nonmosaic, Two-Pore Channel 2 Biallelic Knockout Pigs in One Generation by CRISPR-Cas9 Microinjection Before Oocyte Insemination. CRISPR J. 2021 Feb;4(1):132-146. doi: 10.1089/crispr.2020.0078. PMID: 33616447.

- Jin X, Zhang Y, Alharbi A**, Hanbashi A**, Alhoshani A, Parrington J. Targeting Two-Pore Channels: Current Progress and Future Challenges. Trends Pharmacol Sci. 2020 Aug;41(8):582-594. doi: 10.1016/j.tips.2020.06.002. PMID: 32679067; PMCID: PMC7365084.

- **Hanbashi, A.**, D'Amore, A. and Parrington, J. (2020), Two-pore channel 2 (TPC2) Role in Melanoma. The FASEB Journal, 34:1-1.

Glossary of Abbreviations

ATP	Adenosine triphosphate
BCA	Bicinchoninic acid
BRAF	v-Raf murine sarcoma viral oncogene homolog B
cDNA	Complementary DNA
CTLA-4	Cytotoxic T-lymphocyte-associated protein 4
DAPI	4′,6-diamidino-2-phenylindole
DMEM	Dulbecco's modified Eagle's medium
DMSO	Dimethyl sulfoxide
DNA	Deoxyribonucleic acid
DTIC	Dacarbazine
ECAR	Extracellular acidification rate
EDTA	Ethylenediaminetetraacetic acid
gRNA	Guide RNA
KO	Knockout
LFQ	Label free quantitation
mRNA	Messenger RNA
MTIC	5-(3-methyl-1-triazeno) imidazole-4-carboxamide
mTOR	Mechanistic target of rapamycin
NAADP	Nicotinic acid adenine dinucleotide phosphate
NF1	Neurofibrillin 1
NRAS	***Neuroblastoma RAS viral*** oncogene homologue
OCR	Oxygen consumption rate

ORAI-1	Calcium release-activated calcium modulator 1
P/S	Penicillin and streptomycin
PCR	Polymerase chain reaction
PD-1	Programmed cell death protein 1
PI(3,5)P2	Phosphatidylinositol *3*,*5*-bisphosphate
PKC	Protein kinase C
RNA	Ribonucleic acid
RT-PCR	Reverse transcription PCR
RT-qPCR	RT quantitative PCR
SDS	Sodium dodecyl sulphate
SDS-PAGE	Sodium dodecyl sulphate–polyacrylamide gel electrophoresis
siRNA	Small interfering RNA
SNPs	Single nucleotide polymorphisms
STIM	Stromal interaction molecule
TCGA	The cancer genome atlas
TPC	Two-pore channel
UV	Ultraviolet
VEGF	Vascular endothelial growth factor
WT	Wild-type

Table of Contents

List of figures

Chapter 1

General Introduction

Melanoma

Introduction

Melanoma is one of the most aggressive and treatment resistant types of cancer. It is caused by the unregulated multiplication of pigment-producing cells – melanocytes – found in the epidermis's basal layer (1–3). Although the majority of melanomas begin on the skin, they can also form in the eye (uvea) or on mucosal surfaces. Malignant melanoma is the worst type of skin cancer, and its incidence has increased significantly over the last 50 years (4–7) . Despite the fact that it accounts for fewer than 5% of all cutaneous malignancies, melanoma is responsible for the majority of skin cancer-related mortality (6).

When detected early enough, excision of the lesion is frequently curative and linked with a favourable survival rate. However, melanoma is a highly aggressive cancer that frequently metastasizes early(8,9). Whenever the cancer has progressed to an advanced stage, further treatment alternatives are required(8–10). Over the last few years, there has been tremendous progress in developing novel treatments for metastatic melanoma. Combination immunotherapies that have been explored more recently have been shown to be successful and improve survival. Patients with metastatic melanoma who received a combination of nivolumab (anti-PD-1 monoclonal antibody) and

ipilimumab (anti-CTLA-4 monoclonal antibody) had a 3-year overall survival rate of 58%, compared to 52% and 34% for those receiving either monotherapy (11).

Epidemiology

Melanoma skin cancers have been growing in prevalence over the last decades, with 132,000 new cases reported each year globally (12). Melanoma accounts for less than 1% of all skin cancer cases yet is responsible for the majority of deaths (13). In the United Kingdom, around 15,400 new cases of melanoma were detected in 2014, making it the sixth most frequent type of cancer. In the last decade, the incidence of melanoma skin cancer has grown by around a third (32%) (14), with males experiencing a greater increase (38%) than females (27%). Melanoma is a disease that can affect young adults, being the most frequent type of cancer in those aged 25 to 29 years and the second most common type of cancer in those aged 15 to 29 years (15).

Risk Factors

Due to the rising frequency of melanoma, particularly among young individuals, there has been a surge in interest in understanding the disease's risk factors. The major risk factors for skin cancer might be intrinsic (genetic and phenotypic) or extrinsic (environmental or exposure), and include sun exposure, numerous nevi, and family history (16). Although inherent risk factors such as fair skin and family history are unchangeable, patients who have been recognized as having greater intrinsic risk can modify their behaviour and exposure to extrinsic risk factors such as ultraviolet (UV) and chemical exposure to reduce their risk of developing skin cancer [17].

Classification of Melanoma

Melanoma develops when a melanocyte transforms into a malignant cell and progresses to create a primary tumour. The initial tumour thickens and invades the lower layers of the dermis over time, resulting in a vertical growth phase that increases the risk of metastasis (18). Subtypes of malignant skin melanoma that have been described historically in terms of clinical and histological aspects include Superficial Spreading, Nodular, Acral Lentiginous and Desmoplastic [19].

However, in actual practice, the terms utilized in this cellular classification have no independent predictive or therapeutic value (20). Molecular classification of melanomas has undergone a radical shift in recent years due to the discovery

of mutually exclusive oncogenic mutations. According to this molecular categorization, biologically heterogeneous subtypes of cutaneous melanoma share a common oncogenic process, exhibit comparable clinical behaviour, and respond similarly to various therapies (21).

In 2015, The Cancer Genome Atlas (TCGA) network conducted the largest integrated investigation of cutaneous melanoma to date, characterizing 333 tumour samples from 331 individuals and defining four primary genomic subgroups using DNA, ribonucleic acid (RNA), and protein analyses (22). This study identified four significant genetic subtypes:

i. v-Raf viral oncogene homolog B1 (BRAF) mutant in murine sarcoma (52 percent)
ii. Mutant version of the neuroblastoma RAS viral oncogene (NRAS) (28 percent)
iii. NF1 (neurofibrillin 1) mutant (14 percent)
iv. Triple wild-type (BRAF, NRAS, and NF1) (14.5 percent)

Even though therapeutic targets like BRAF have previously been identified, this classification of oncogenic mutations may provide insight into potential future drug targets and clinical trial designs.

Treatment Strategies for Melanoma

Despite the fact that the prevalence of malignant melanoma has increased over the last decade, survival rates have improved dramatically due to a better knowledge of the molecular processes involved in the disease's origin and progression (23). There are two treatment approaches available for melanoma: traditional and new therapies.

The conventional therapy for primary melanomas is surgical excision, which is associated with a 5-year survival rate of 95% in thin melanomas and gradually decreases in bigger melanomas and those that have migrated to lymph nodes (24). However, after metastasis, the survival rate following surgical excision drops considerably to fewer than 25% in the United Kingdom(14). Medically, dacarbazine (DTIC) is the most commonly utilized chemotherapy medication in the treatment of metastatic melanomas. It is an alkylating chemical that may be transformed in the liver to 5-(3-methyl-1-triazeno) imidazole-4-carboxamide (MTIC), which can be used to prevent DNA replication in the body(25). The response rate to dacarbazine is extremely low (15–20%), with similar findings (10–15%) when the oral equivalent temozolomide is used (26). Antimicrotubule drugs taxane and vindesine as well as cisplatin and nitrosoureaeas have failed to improve on the results seen with dacarbazine when employed as a single agent chemotherapeutic treatment (27). Overall survival for individuals with metastatic melanoma has not improved with the use of chemotherapy

combinations such cisplatin, vindesine, and dacarbazine (CVD) or carboplatin and paclitaxel (CPX) (28). Due to advancements in other treatments, chemotherapy is no longer commonly employed.

The emergence of novel targeted and immunological therapy has resulted in considerable improvements in the treatment of metastatic melanoma, particularly BRAF-mutant melanoma, over the last few years. Melanomas have the highest burden of somatic genetic changes of all human tumours, resulting in significant variation in disease development and response to treatment(29). In recent years, novel ways to target cancer cells have evolved that are more precise and effective. These include targeted therapies that are based on the tumour's genetic profile and immunotherapies that make use of the body's immune system(30,31). Targeted or immunotherapy trials in advanced-stage cancer patients have accomplished their primary endpoints every year since 2011. These studies have found that seven out of eight drugs that have recently been approved by the Food and Drug Administration (FDA) have been associated with an improvement in patient overall survival when compared to results from conventional treatment(23). These new drugs include small molecule inhibitors of BRAF or MEK, as well as immunotherapeutic antibodies against cytotoxic T lymphocyte-associated antigen 4 (CTLA4) and programmed cell death protein 1 (PD-1).

Two-pore channel 2 (TPC2)

Two-pore channels (TPCs)

Two-pore channels (TPCs; gene name TPCNs) belong to the voltage-gated cation channel superfamily, which can be found in both endolysosomes and vacuoles (32). In order to generate one functional pore, two repeats of a six-transmembrane domain are dimerised in TPCs (33). TPC1, TPC2, and TPC3 isoforms exist. The first and second isoforms are the only ones found in humans and mice, whereas the third isoform exists in a variety of animals, including chickens and rabbits (34).

TPCs are found in the endolysosomal system, although their relative density is dependent on the acidic organelles' development stage and pH difference. TPC1 is found mostly in recycling endosomes, early and late endosomes, and lysosomes, whereas TPC2 is found primarily in late endosomes and lysosomes (35).

Although NAADP regulates both TPC1 and TPC2 activation, TPC1 appears to be also activated by Ca^{2+}. Additionally, ion conduction and permeability are highly variable. TPCs appear to be permeable to calcium and sodium cations but insensitive to potassium cations.

TPC1 has been demonstrated to be permeable to H^{+}, suggesting that it may play a role in the regulation of lysosomal and cytosolic PH. These differences in

gating and ion conductance suggest that TPC1 and TPC2 may have complementary physiological functions as Ca^{2+} release channels in endo-lysosomal compartments (36).

The activation of TPC2 by NAADP versus PI (3,5) P_2 is still a point of contention (37,38). Wang and Cang revealed that human TPC2 expressed in a variety of mammalian cell types is extremely Na^+ selective and possesses a Na^+ conductance in response to phosphatidylinositol 3,5-bisphosphate [PI (3,5) P_2] but not NAADP.

Numerous studies support the hypothesis that TPCs facilitate the release of Ca^{2+} from acidic storage induced by NAADP (36,39,40). Ruas and coworkers recently demonstrated that NAADP–induced Ca^{2+} release is severely reduced in cells with double knockout of TPC1 and TPC2, confirming the idea that both TPC1 and TPC2 are NAADP targets (41). Additionally, the contradictory observations mentioned may be explained by the fact that NAADP may not directly interact with TPCs but may have an effect on the NAADP-evoked TPC2 Na^+ current via an accessory binding protein or Mg^{2+}; hence, different experimental conditions may influence TPC activation(42–44).

TPC2 and cancer: what it is already known about the role of TPC2 in melanoma and pigmentation

The relationship between TPC2 and cancer has generated considerable interest in recent years, owing to the possibility that TPC2 could be a potential target for this disease. TPC2 has a well-established association with differentiation (45,46), which is a critical step in tumour growth. Two analyses of genetic variables indicated TPC2 overexpression as a possible driver of chromosome 11q13 amplification reported in a variety of cancer types (47,48).

Additionally, a recent study by Nguyen et al. showed that inhibiting TPCs inhibits the adhesion and migration of T24 (bladder cancer), HUH7 (hepatocarcinoma), and 4T1 (breast cancer) cancer cells *in vitro*, as well as inhibiting the generation of lung metastases in a mouse model of breast cancer cells. Inhibition of TPCs results in a build-up of 1-integrin in endocytic vesicles and impairs the production of lamellipodia (49).

Additionally, our lab was involved in the discovery that TPCs are essential for various features of VEGF-induced angiogenesis *in vitro*, including endothelial cell migration and tube formation (50). Angiogenesis is the physiological process by which new blood vessels are formed from pre-existing ones and is a critical mechanism for tumour growth and metastatic dissemination. Furthermore, *in vivo* matrigel experiments demonstrated that Ned-19 and TPC2 prevent VEGF-induced vascularisation, but not in TPC2 knockout mice.

However, TPC2 mutant mice appear to develop normally, implying that compensatory modifications sustain angiogenesis during these animals' development (51). Melanoma is a type of malignancy that arises from pigmented melanocytes. Several studies have identified single nucleotide polymorphisms (SNPs) in the TPCN2 gene as possible risk factors for melanoma development (52). Indeed, variations in the TPCN2 gene have been linked to human skin and hair colour (53). A TPC2 variant with a single amino acid change was related with a decreased risk of malignant melanoma, whereas a TPC2 variant with a nucleotide change in an intronic region was associated with an increased risk of malignant melanoma (54).

Pigmentation abnormalities in Xenopus oocytes are induced by overexpression of TPC2, but not TPC1, and this effect is mediated via interactions between distinct members of the Rab family of trafficking proteins. A recent study also found a link between two separate TPC2 pigmentation variations and a switch from brown to blond hair. These two variations exhibited conformational alterations that altered the channel's sensitivity to PI (3,5) P_2 or ATP, respectively. Indeed, stimulation of PI (3,5) P_2 increases the activity of the variant M484L, whereas the variant G734E is less responsive to ATP and more sensitive to mTOR inhibitors than the WT (55).

TPC2 is localized on melanosomes, where it mediates a Na^+-selective current that regulates the membrane potential, pH, and pigmentation of melanosomes. (56). TPC2 activity in melanosomes is regulated by PI (3,5) P_2, a pigment-regulating protein that may act on melanosome formation (57). TPC2-deficient melanosomes demonstrated increased alkalization of the lumen pH, resulting in an increase in tyrosinase activity, the enzyme responsible for melanin formation. The size of melanosomes was also enlarged in TPC2 KO MNT1 cells when compared to WT controls. The mechanism by which TPC2 modulates melanosome pH is unknown; indeed, Bellono and Ambrosio propose two distinct pathways mediated by Na^+/PI (3,5) P_2 and Ca^{2+}/NAADP (58,59).

Thesis Aims

Melanoma is a cancer that is extremely aggressive and resistant to treatment. Consequently, the development of novel therapeutic approaches remains an essential objective. Strategies can be discovered by understanding the role of targets in the model. Therefore, this thesis is developed to achieve the following objectives:

Aim 1: The role of TPC2 in tumourigenesis and metastasis *in vitro*.

Aim 2: TPC2 related biological mechanisms in melanoma cell lines.

Aim 3: The role of TPC2 *in vivo* and determination of clinical associations.

Chapter 2

Materials and Methods

Cell lines and cell culture

B16-F0 (ATCC CRL-6322) murine melanoma cells and CHL-1 (ATCC) human melanoma cells were cultured in Dulbecco's modified Eagle's medium (Sigma) supplemented with antibiotics (P/S, Sigma), 10% fetal bovine serum (Gibco), and 2 mmol/L glutamine (Sigma).

Cell-based assays

Real time monitoring of cell proliferation by xCELLigence system

This assay used an xCELLigence RTCA DP instrument (ACEA Biosciences, San Diego, CA, USA) that was set to 37°C and 5% CO_2. The experiments were conducted using modified microelectrodes attached to the bottom of 16-well plates to determine the attachment direction, cell distribution, and proliferation based on impedance. To begin, 50 µL of cell-free growth medium (10% FBS) was added to each well. For approximately 30 minutes, the plates were left at room temperature. Then, for 30 minutes, the background impedance of each well was measured. At that point, cells were harvested directly from exponential phase cultures using a standardized detachment procedure utilizing 0.05 percent Trypsin-EDTA. The cells were counted using the LUNA (Logos Biosystem, Seoul, South Korea) device. The cells were then seeded directly into the wells

using a 50 μL volume of the cell suspension (with about 10,000 cells per well). The plates were left at room temperature for approximately thirty minutes to allow for cell attachment, and then placed under lock in the RTCA DP device, which was positioned in the incubator, while the xCELLigence system automatically monitored the impedance value of each well. These values were expressed as confidence intervals (CI) (Cell Index). The xCELLigence system was used to monitor the Cell Index of each well automatically every fifteen minutes. For five days, cells were monitored in real time.

Invasion assay

After 24 hours of incubation, 1 x 10^5 cells were seeded on the transwell coated with reduced growth factor Matrigel (BD). The cells were fixed and stained with DAPI. For each transwell, five fields were counted to determine the number of cells.

ATP level assay

Intracellular ATP levels were determined according to the manufacturer's recommendations using a commercially available kit (ab83355, Abcam, Cambridge, MA, USA). Cells were seeded at 1×10^6 cells per well. Cells were harvested, resuspended, deproteinized, and combined with the reaction reagent. The samples collected were weighed at 535/587 on a SpectraMax i3x (Molecular Devices, San Jose, CA, USA).

Lactate level assay

L-lactate levels were determined using the L-lactate Assay kit in accordance with the manufacturer's recommendations (ab65331, Abcam, Cambridge, MA, USA). Cells were seeded at a density of 1×10^6 per well. Harvested cells were resuspended, deproteinized, and added to the reaction reagent. The collected samples were measured at 535/587 on a SpectraMax i3x (Molecular Devices, San Jose, CA, USA).

Mitochondrial membrane potential

Changes in the mitochondrial membrane potential (ΔΨm) were determined using the fluorescent reagent tetraethylbenzimidazolylcarbocyanine iodide (JC-1) and the JC-1-Mitochondrial Membrane Potential Assay kit (Abcam, Cat. No. ab113850) in accordance with the manufacturer's instructions. In a 96-well plate, cells were plated at a density of 50,000 cells per well and allowed to adhere overnight. Stressed cells were cultured in 0.5% FBS. The cells were then washed once with 1 x dilution buffer before being treated with 20 M JC-1 dye in 1 x dilution buffer for 20 minutes at 37°C in the dark. After removing the JC-1 dye and washing the cells with 1 dilution buffer, 100 μL of fresh 1 dilution buffer was added to each well. Using a Spark multimode microplate reader, the red fluorescence excitation (535 nm)/emission (590 nm) and green fluorescence excitation/emission (475 nm/530 nm) were detected (Tecan Group Ltd.). After subtracting the background fluorescence from the fluorescence of treated cells, the ratio of red (polarised) fluorescence to green (depolarized) fluorescence was obtained.

Protein analysis

Western blotting

Cells were collected at 70-80% confluence and harvested for this assay. The cells were rinsed twice with ice-cold PBS before being scraped into 1 mL of PBS and centrifuged at 1200 rpm for 5 minutes at 4 °C. After discarding the supernatant, 100 µL of a radioimmunoprecipitation assay buffer containing protease and phosphatase inhibitors (Thermo Scientific, #78444) was added. After 30 minutes of incubation on ice, the cell lysate was centrifuged for 15 minutes at 14,000 rpm and 4 °C to remove cell debris. Protein concentration was determined using the Pierce Bicinchoninic Acid (BCA) protein assay (Thermo Fisher Scientific, UK). At 95°C for 5 minutes, equal amounts of protein were denatured in 3 x Laemmli Buffer (70 mM Tris pH 6.8, 5% (v/v) -mercaptoethanol, 40% (v/v) glycerol, 3% (w/v) SDS, 0.05 (w/v) Bromophenol Blue). On 4 - 20 % SDS polyacrylamide gels, proteins were separated according to their molecular weight. Proteins were transferred to PVDF (polyvinylidene difluoride) membranes (Millipore) in transfer buffer (48 mM Tris, 39 mM glycine, 20 percent methanol, 1.3 mM SDS, final pH 9.2) at a constant current of 120V for 1.5 hours. With Intercept (PBS) blocking buffer (Licor), membranes were blocked for an hour at room temperature to reduce nonspecific protein binding. Membranes were incubated overnight at 4°C in a shaking incubator with diluted primary antibodies. After four 5-minute washes with

TBS-T, membranes were incubated for one hour at room temperature with IRDyeanti-rabbit or anti-mouse IRDye® 800CW and IRDye® 680RD secondary antibodies (Abcam). The membranes were then rinsed three times more before the membrane was scanned on an Odyssey® Imaging System (Licor).

Immunofluorescence

Cells were grown on coverslips for at least 18 hours before being washed, fixed, permeabilised, blocked, and incubated overnight with primary antibodies. Subsequently, the coverslips were washed with PBS, incubated for 1 hour at room temperature with Alexa-fluor 488 conjugated secondary antibodies (Life Technologies), washed again with PBS, and embedded in Prolong DAPI-containing antifade mountant (Invitrogen). The fluorescence was detected using a 40x objective and an Olympus spinning disk confocal microscope. The images were acquired as groups of colour images and analyzed using Image J software.

Proteomic analysis

Liquid chromatography-tandem mass spectrometry analysis.

The proteomic dataset was generated using LC–MS/MS on CHL-1 and B16 (WT and KO) samples. The samples were reduced (30 minutes at room temperature) with 5 mL of 200 mM dithiothreitol and alkylated (30 minutes at room temperature) with 20 mL of 200 mM iodoacetamide, followed by methanol-chloroform precipitation. The pellets were reconstituted in 6 M urea in 400 mM TrisHCl, pH 7.8. The urea was diluted to 1 M in 400 mM Tris-HCl, pH 7.8, and proteins were digested at a ratio of 1:50 with trypsin overnight at 37°C. Following acidification to a final concentration of 1% formic acid, the samples were desalted using Sola HRP SPE cartridges (ThermoFisher Scientific) and dried in a SpeedVac (3-6 hours).

Additionally, samples were desalted online (PepMAP C18, 300 mm 3 5 mm, 5 mm particle, ThermoFisher Scientific) for 1 minute at a flow rate of 20 mL/min and separated over 60 minutes on an EASY-Spray column (PepMAP C18, 75 mm 3 500mm, 2 mm particle, ES803, ThermoFisher Scientific) using a gradient of 2–35 percent acetate. Separation and analysis were carried out using standard parameters (Universal Method (60)) a Dionex Ultimate 3000 RSLC system coupled to an Orbitrap Fusion Lumos platform (both ThermoFisher Scientific). MS scans between 400 and 1,500 m/z were acquired at a resolution of 120,000 with an AGC target of 4.0E5. MS/MS spectra were acquired in the linear ion

trap (rapid scan mode) following collision-induced dissociation (CID) fragmentation at a collision energy of 35% and an AGC target of 4.0E3 for up to 250 ms, with a maximum duty cycle of 3 seconds, prioritizing the most intense ions and injecting ions for the entire parallelizable time available. For 30 seconds, selected precursor masses were omitted (60)

Quantitative analysis of the mass spectrometry data was performed using the MaxQuant software platform (Cox and Mann, 2008) (version 1.6.2.3), with database searches against either the reviewed Uniprot Homo sapiens database or Mus musculus database. A reverse decoy database was created, and results for peptide spectrum matches and protein identifications were displayed with a 1% FDR. Trypsin, two missed cleavages, a fixed modification of cysteine carbamidomethylation, and variable modifications of methionine oxidation and protein N-terminal acetylation were used as search parameters. The MaxLFQ algorithm was used to perform label-free quantification with an LFQ minimum ratio count of 2. The 'Match between runs' function was used with 0.7- and 20-minute match and alignment time limits, respectively.

Quantitative analysis of mass spectrometry data

The quantitative analysis of significant differences in protein abundance between WT and KO samples, as well as data visualization, were carried out using the Perseus software platform (61)(version 1.5.2.4) and biological replicate LFQ values. The quantitative analysis was omitted for peptides for which more than two values were missing from three biological replicates. The remaining data were uploaded to Perseus as a data matrix with the respective LFQ intensities as main columns. Filtering on categorical columns reduced the data matrix by removing protein groups identified solely by site, reverse decoy hits, and potential contaminants. Logarithmic transformations (log2(x)) and median subtraction were used to normalize the data.

Missing data points were imputed using the normal distribution and visualized as LFQ intensity histograms with imputed values (per biological replicate). On validated values, principal component analysis (PCA) was performed. A volcano plot was created using the LFQ intensities and a two-way Student's t-test was used to determine whether there was a significant difference in protein abundance between the WT and KO samples. With 250 randomizations and S0 = 0.1, a permutation-based false-discovery rate (FDR) was determined (default).

Functional and pathway analysis.

The WEB-based Gene SeT AnaLysis Toolkit (http://www.webgestalt.org/; revision 2017) is a widely used software tool for functional enrichment analysis in seven biological contexts. As a result, this software was used to conduct GO enrichment analysis in the current study. The false discovery rate (FDR) for the GO and pathway analysis of the DEGs was set to 0.05(62).

Generating TPC2 knockout cell lines using CRISPR-Cas9

Guide RNA design using Synthego Design Tool

To minimize potential off-target effects, guide RNAs were designed using the Synthego Design Tool. Gene name and species were entered, and the top three gRNAs were selected to knock out TPC2. The following primer sequences were used for genotyping:

Table 1. Primer's sequence of CRISPR-Cas9 genotyping.

Gene	Primer sequence
TPCN2 Mouse	F: GGTATTACTCGAACGTCTGCCAACGGT
	R: TTCAAAGCCAAAGCTCACTAGCAA
TPCN2 Human	F: GATAGGGCGGTTACCATCATC
	R: CTCACCGGGTCAAAGTACAA

Lipofectamine 2000 transfection

For CRISPR-Cas9, B16 and CHL-1 cells were seeded overnight to achieve a confluence of approximately 50%-60% the following day. 3 μM Cas9 nuclease, 3 μM single guide RNA (sgRNA), and 1 μL Lipofectamine CRISPRMAX Cas9 Plus reagent were added to 30 μL OPTIMEM, reduced serum free medium. RNPs were incubated at room temperature for ten minutes. Transfection solution was prepared in a separate tube using 1.5 μL Lipofectamine

CRISPRMAX Transfection Reagent in a final volume of 25 µL and incubated for 5 minutes at room temperature. The tube contents were incubated for 10 minutes. Each sgRNA was transfected into 5 x 10^4 suspended cells. The single clone assay was performed three days later. B16 cells were seeded on coverslips and used at a confluence of 70% in a 24-well plate for TPC2 overexpression and silencing. In a 12-well plate, 100,000 CHL-1 cells were seeded. TPC2 siRNA (Qiagen) was used at a concentration of 10 nM. Lipofectamine 2000 (Life Technologies) was used to transfect the cells according to the manufacturer's protocol.

Single clone assay

2,000 cells were seeded in 200 µL of 20% FBS DMEM in each well of a 96-well plate. On the first row, a first dilution series was performed; 100ul were transferred to the following wells. The second dilution series was performed by adding 100 µL to the first row and 100 µL to each subsequent row until the plate reached the end, resulting in a final volume of 200 µL per well.

RNA analysis

RNA extraction

RNA was isolated using the RNeasy kit (QIAGEN, #75144) according to the manufacturer's instructions from cell lysates collected from cultivated cells or homogenised tumour tissue. In 700 µL of RTL buffer containing 0.1 M -mercaptoethanol, cells were lysed. Cell lysate was transferred to an extraction column for the RNA to bind to the membrane. The membrane was then treated with DNase I (QIAGEN, 15200-50) diluted in RDD buffer to digest the genomic DNA. The column was incubated for 15 minutes at room temperature and then washed with 350 µL of RW1 buffer. The RNA was eluted in 30 µL of DEPC-treated RNase-free Water and then quantified using a NanoDrop 2000c Spectrophotometer.

Reverse transcription (RT)

RNA samples were reverse-transcribed into complementary DNA (cDNA) using the SuperScript® III First-Strand Synthesis SuperMix (Invitrogen, #11752-050) according to the manufacturer's instructions. 2 µL of the enzyme mixture comprising reverse transcriptase, 1 µg of total RNA, and 10 µL of the 2 x RT reaction buffer (containing random primers and dNTPs) were added to a PCR tube, followed by the addition of RNase-free water to form the final volume of

20 μL. The contents were mixed gently and placed in a Thermo Cycler for 10 minutes at 25°C, 30 minutes at 50°C, and 5 minutes at 85°C, respectively. The cDNA samples were utilised immediately or frozen at -20°C.

Quantitative real-time PCR (qRT-PCR)

QRT-PCR reactions were performed using SYBR Select master mix (PowerUP, Thermo) according to the manufacturer's instructions. 20 ng of cDNA and 10 pmol of forward and reverse primers were added to 10 μL of 2 x SYBR Select Master Mix with SYBR GreenER Dye for each reaction. 20 μL of RNase-free water was added to make up the total volume. The reaction mixture was then loaded to the Applied Biosystems QuantStudio 5 Real-Time PCR System in order to measure the expression relative to a housekeeping gene. The real-time PCR was performed with primers specific for ANKDR1, CTGF, CYR61, YAP, TAZ, TPC2, ORAI1, STIM1, PKC-II, INF2 (Invitrogen). As an internal control, GAPDH and actin were used. The Ct method was used to determine the relative level of mRNA expression.

Table 1. Primer sequences for qPCR

Gene	Forward	Reverse
CTGF	AGGAGTGGGTGTGTGACGA	CCAGGCAGTTGGCTCTAATC
CYR61	CCTTGTGGACAGCCAGTGTA	ACTTGGGCCGGTATTTCTTC
ANKRD1	AGTAGAGGAACTGGTCACTGG	TGGGCTAGAAGTGTCTTCAGAT
YAP	GCACCTCTGTGTTTTAAGGGTCT	CAACTTTTGCCCTCCTCCAA
TAZ(WWTR1)	GGCTGGGAGATGACCTTCAC	CTGAGTGGGGTGGTTCTGCT
GAPDH	GGAGCGAGATCCCTCCAAAAT	GGCTGTTGTCATACTTCTCATGG
STIM	ATCTCACAGCTCATGGTATGCTCC	GGAAGGTGCCAAAGAGTGTGTTTC
ORAI	TACTTGAGCCGCGCCAAGCTTAAA	ACCGAGTTGAGATTGTGCACGTTG
PKCβII	GACCAAACACCCAGGCAAAC	GATGGCGGGTGAAAAATCGG
INF2	CACATCCAACGTGATGGTGAAG	GGAGAGCTCGTTCATGACAATG

Measurements of metabolic fluxes

In a Seahorse XF96 Cell Culture Microplate (Seahorse Bioscience, Billerica, MA, USA), adherent cells were seeded at a density of 2 x 10^4 cells per well in normal growth media (cell line specific). Plates were rocked at 25°C for 20–40 minutes to ensure an even distribution of cells within wells. After that, the plate was incubated overnight at 37°C to allow the cells to adhere. The next day, growth media were replaced with Seahorse Phenol Red-free DMEM with or without glucose. Using an XF96 Extracellular Flux Analyzer, cellular respiration (oxygen consumption rate (OCR) and extracellular acidification rate (ECAR) were determined. Each group had a mean value calculated.

In vivo tumour growth assay

Animals were obtained from Jackson Laboratories as 7–8-week-old female C57BL/6J mice that are free of specific pathogens (SPFs) (Bar Harbor, ME). The animals were housed in a controlled environment. TPC2 B16 wild-type and B16 TPC2 knockout cells was subcutaneously injected into the right flank of experimental mice (1 x 10^7 cells in 0.2 mL). Over the course of the study, tumour volumes and body weights were measured and recorded twice weekly. The study lasted 28 days. The Institutional Animal Care and Use Committee at King Saud University (KSU) approved the protocol for the animal experiments described in this proposal.

Histopathology

Mice livers and spleens were removed at the conclusion of the experiment, cut into small pieces, and fixed in 10% neutral buffered formalin. Dehydrated samples were embedded in wax and then sectioned at a thickness of 5 µm. HER stain was used to stain the sections, which were then examined and photographed microscopically (Motic-2000). Sections of spleen were subjected to area measurements of lymph nodes using microscope programs at a magnification of 100x for ten fields in each group, and then volume was calculated using the formula: A sphere's volume is equal to 4/3r3. The data were analyzed statistically using the ANOVA test, with a P value of 0.05 considered significant. The data were expressed as Standard Error of the Mean (SEM).

Kaplan Meier analysis

GEPIA (63) was used for our Kaplan maier analysis, this being a webserver that extracts data from the Cancer Genome Atlas (TCGA) data portal and the GTEx normal tissue database (http://gepia. Cancer-pku.cn).

On the basis of TPCN2 gene expression, overall survival (OS) and disease-free survival (DFS) were also analyzed. The GEPIA considers the Log-rank test when it comes to hypothesis testing. A hazard ratio (HR) was chosen based on the Cox PH model and this also included appropriate information to depict the dotted line as the 95 percent confidence interval (CI). The median value of 50% (TPCN2 expression) was used to divide the TPCN2 high- and low-expression cohorts. As a result, samples with TPCN2 expression levels greater than or equal to 50% were used as the high-expression cohort (cutoff-high) and samples with TPCN2 expression levels of less than 50% as the low-expression cohort (cutoff-low), respectively.

Statistical analyses

As indicated in the Methods section, each experiment was conducted in biological triplicates or more. The parametric, unpaired, two-tailed Student's t-test was applied to determine the statistical significance of two-group experimental results.. Multiple-group data sets were compared using one-way analysis of variance (ANOVA) and Bonferroni post hoc tests. The data are expressed as means ±SEM. $P < 0.05$ was deemed to indicate statistical significance. Excel and GraphPad Prism software version 6.0 were utilised for the purpose of conducting the analysis on the experimental parameters.

Chapter 3

The effect of TPC2 knockout on tumourigenesis and metastasis in vitro in melanoma cell lines

Part of the material presented in this chapter was published in D'Amore, A.; Hanbashi, A.A.; Di Agostino, S.; Palombi, F.; Sacconi, A.; Voruganti, A.; Taggi, M.; Canipari, R.; Blandino, G.; Parrington, J.; Filippini, A. Loss of Two-Pore Channel 2 (TPC2) Expression Increases the Metastatic Traits of Melanoma Cells by a Mechanism Involving the Hippo Signalling Pathway and Store-Operated Calcium Entry. *Cancers* 2020, *12*, 2391. I have generated all the data presented in this chapter except for figures 7 and 8, which were generated in collaboration with Dr. D'Amore.

Introduction

Melanoma is a malignant tumour originating from transformed melanocytes – cells that normally produce melanin (64). The B16 mouse melanoma cell line was isolated in 1930 and has been widely utilized in over 17,000 publications to date (65). Through *in vivo* and *in vitro* variant selection, the B16 line was developed in Fidler's laboratory. This cell is highly pigmented and has been extensively utilized to evaluate melanoma cell biology, tumour formation, and anti-tumour immune responses (66) Amelanotic melanoma is a rare form of human melanoma cancer and generally difficult to diagnose in the first stage due to its lack of pigmentation. Therefore, finding new markers to recognize this form of melanoma at an early stage of tumourigenesis is an important goal that could have major therapeutic benefits. CHL-1 cells are a model of a human amelanotic melanoma and are derived from a metastatic site. Exploring the role of TPC2 in the CHL-1 and B16 cell lines was the primary objective of this section.

Generation of TPC2 knockout cells in the CHL-1 and B16 cell lines using CRISPR-Cas9

To create a stable TPC2 knockout CHL-1 cell line, we used CRISPR-based genome engineering technology. The workflow for generating a CRISPR knockout comprises three steps. First, guide RNAs (gRNAs) are designed using Synthego's CRISPR Design Tool to maximize the on-target score while minimizing off-target effects. Second, CRISPR components are introduced into cells, resulting in high editing and knockout (KO) efficiencies. Third, edited regions are sequenced and analyzed using Synthego's ICE tool, generating NGS-quality results in seconds. After testing three gRNAs, the gRNA with the highest KO score was selected to create a frameshift. The gRNA (CGUGCUGGUGAGUGAGGAUG) targeted the CCTCCACAAAAGCCAAGATC sequence in the TPCN2 exon 4 in the *Homo sapiens* genome as illustrated in Figure 1A. Synthego's ICE tool was used to assess the efficiency of the gene editing in different clones and the clone with the highest KO score was selected to be further analyzed (Figure 1B). The selected clone showed 95% editing efficiency and Model Fit (R^2) equal to 0.955 (Figure 1C). The ICE also showed the Sanger sequence view of wild-type (control) sequences in the region around the guide sequence and edited sample which showed mixed sequencing bases after the cut site as a result of cutting and error-prone repair (Figure 1D).

A

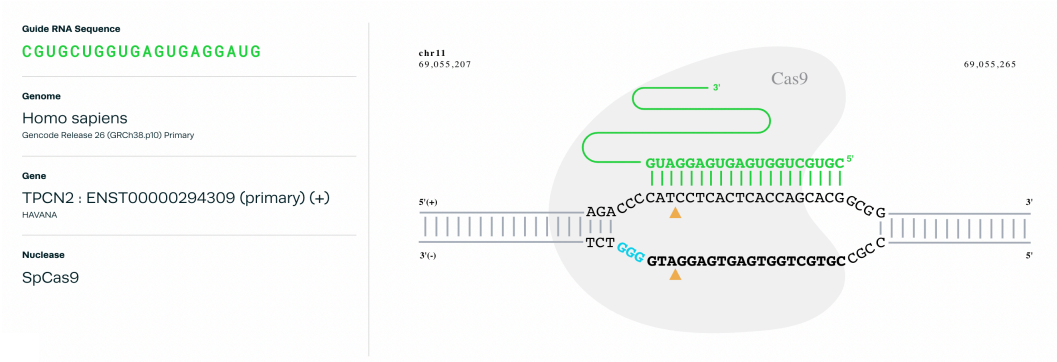
Guide RNA Sequence
CGUGCUGGUGAGUGAGGAUG
Genome
Homo sapiens
Gencode Release 26 (GRCh38.p10) Primary
Gene
TPCN2 : ENST00000294309 (primary) (+)
HAVANA
Nuclease
SpCas9
chr11
69,055,207
69,055,265
Cas9
GUAGGAGUGAGUGGUCGUGC
AGACCCCATCCTCACTCACCAGCACGGCGG
TCTGGGGTAGGAGTGAGTGGTCGTGCCGCC

B

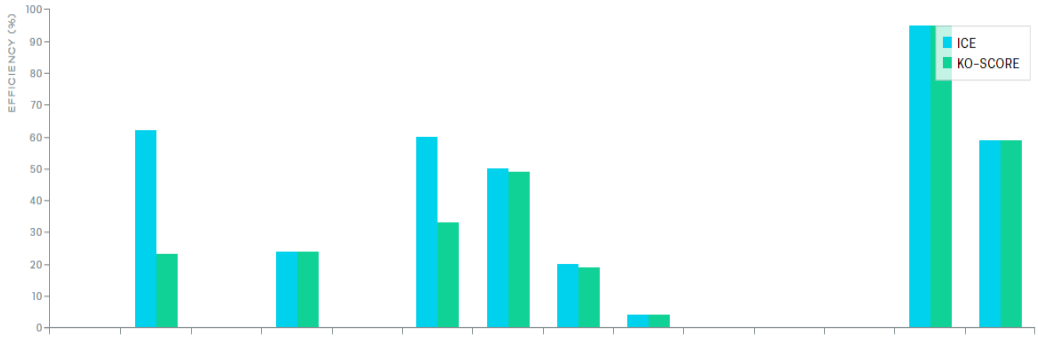
EFFICIENCY (%)
ICE
KO-SCORE

C

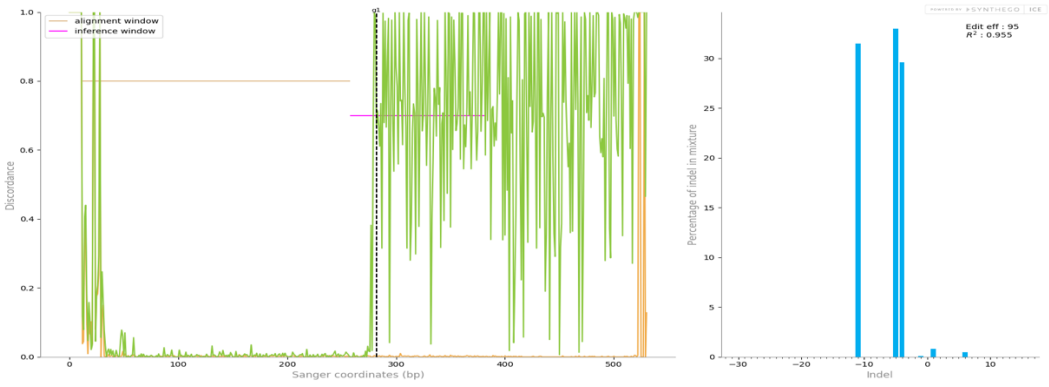
alignment window
inference window
Discordance
Sanger coordinates (bp)
Edit eff : 95
R² : 0.955
Percentage of indel in mixture
Indel

D

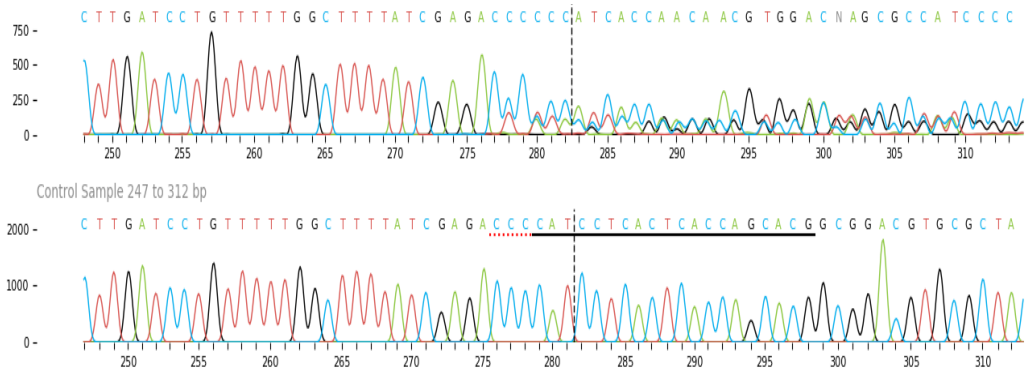
Control Sample 247 to 312 bp

Figure 1. Generation of CHL-1 cell line TPC2 Knockout using CRISPR-Cas9.
A) Schematic of CRISPR-Cas9 strategy used for CHL-1 human melanoma cell line. B) ICE analysis of possible KO clones, CHL-1 clone G10 was selected. KO-Score indicates the percentage sequences that are putative knockout. C) The discordance and the indel plots which show the level of alignment per base between the wild type (control) and the edited sample in the inference window (the region around the cut site) and the indel plot displays the inferred distribution of indels in the entire edited population of genomes. D) Sanger sequence view of edited and wild-type (control) sequences in the region around the guide sequence. The horizontal black underlined region represents the guide sequence. The horizontal red underlined region is the PAM site. The vertical black dotted line represents the actual cut site.

DNA and amino acid sequences of wild type and edited CHL-1 cells were analyzed to further confirm the knocking out of TPC2. In Figure 2A, the Sanger sequences of the targeted site of wild type and edited cells were aligned, and a 5 base pair deletion was detected at the cut site of modified cells. This is a frameshift mutation that led to a premature stop codon. The DNA sequences were translated to amino acids by CLC sequence viewer 8. The alignment of amino acids showed the effect of the frameshift. To provide additional validation, the levels of TPC2 RNA expression were assessed in both cell lines. When CHL-1 altered, cells were compared to wild type cells, TPC2 expression was significantly reduced (Figure 2C). CRISPR-Cas9 technology thus allowed the generation of stable TPC2-deficient CHL-1 cells.

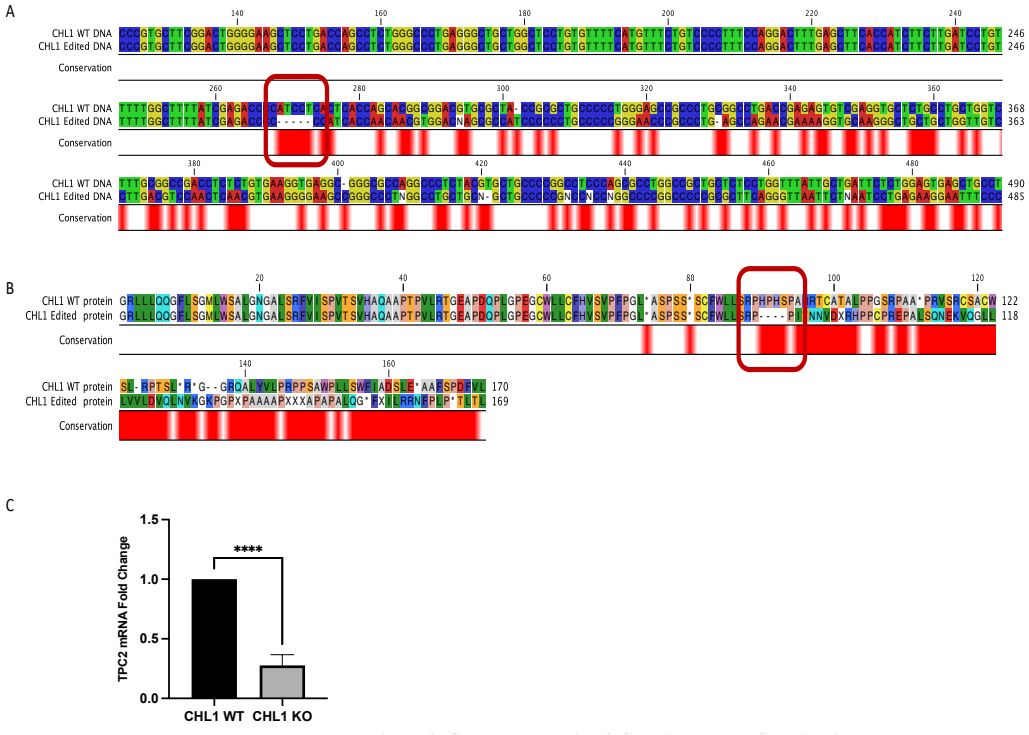

Figure 2. Sequence analysis of CHL-1 WT and CHL-1 edited cells generated by CRISPR-Cas9 targeting.

A) DNA sequence alignment of wild type and edited cells. The alignment shows a 5 base pair deletion (red box) in the CHL-1 edited cells. B) Amino acid sequences generated from the upper DNA sequences were aligned and a confirmation of change was observed after the cut site (red box). C) qPCR analysis for TPC2 transcript levels in CHL-1 (WT and KO) cells.

Similarly, CRISPR-based genome engineering technology was used to establish a stable TPC2 depleted B16 cell line. As shown in Figure 3A, the gRNA (CCUCCACAAAAGCCAAGAUC) targeted the CCTCCACAAAAGCCAAGATC region in the TPC2 axon 4 of the *Mus musculus* genome. The ICE tool from Synthego was used to assess the efficacy of gene editing in several clones, and the clone with the highest KO score was chosen to be further investigated (Figure 3B). The chosen clone has a Model Fit (R2) of 0.96 and a 96 percent editing efficiency (Figure 3C). The ICE also displayed a Sanger sequence view of wild-type (control) sequences in the region surrounding the guide sequence, as well as an edited sample with mixed sequencing bases after the cut site due to cutting and error-prone repair (Figure 3D).

A

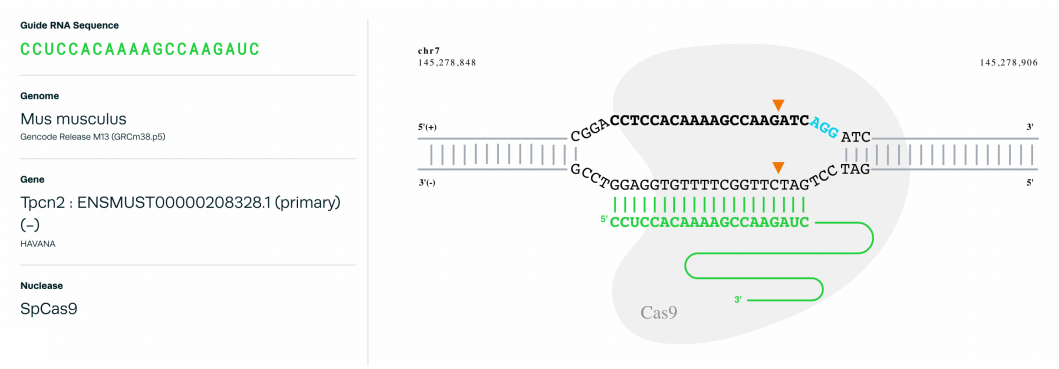
Guide RNA Sequence
CCUCCACAAAAGCCAAGAUC
Genome
Mus musculus
Gencode Release M13 (GRCm38.p5)
Gene
Tpcn2 : ENSMUST00000208328.1 (primary) (–)
HAVANA
Nuclease
SpCas9
chr7
145,278,848
145,278,906
5'(+)
3'
3'(-)
5'
CGGACCTCCACAAAAGCCAAGATCAGG ATC
GCCTGGAGGTGTTTTCGGTTCTAGTCC TAG
5' CCUCCACAAAAGCCAAGAUC
3'
Cas9

B

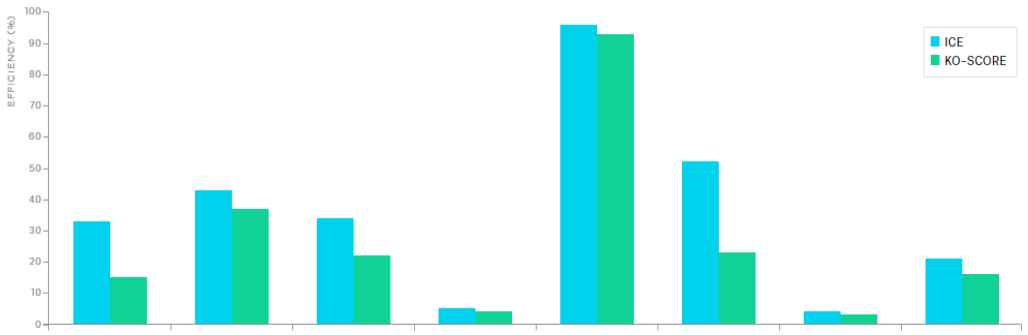
EFFICIENCY (%)
ICE
KO-SCORE

C

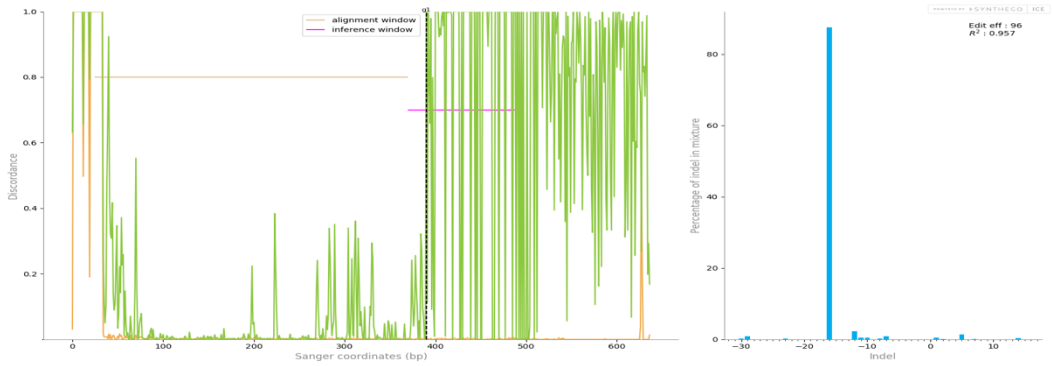
alignment window
inference window
Discordance
Sanger coordinates (bp)
Edit eff : 96
R² : 0.957
Percentage of indel in mixture
indel

D

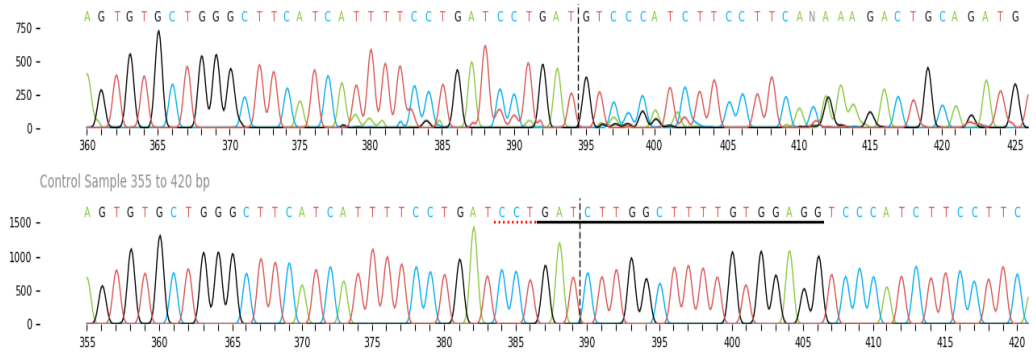
A G T G T G C T G G G C T T C A T C A T T T T C C T G A T C C T G A T G T C C C A T C T T C C T T C A N A A A G A C T G C A G A T G
Control Sample 355 to 420 bp
A G T G T G C T G G G C T T C A T C A T T T T C C T G A T C C T G A T C T T G G C T T T T G T G G A G G T C C C A T C T T C C T T C

Figure 3. Generation of B16 cell line TPC2 knockout using CRISPR-Cas9.
A) Schematic of CRISPR-Cas9 used for B16 murine melanoma cell line B) ICE analysis of possible KO clones, from which B16 clone H4 was selected. KO-Score indicates the percentage sequences that are putative knockouts. C) The discordance and the indel plots which show the level of alignment per base between the wild type (control) and the edited sample in the inference window (the region around the cute site) and the indel plot displays the inferred distribution of indels in the entire edited population of genomes. D) Sanger sequence view of edited and wild-type (control) sequences in the region around the guide sequence. The horizontal black underlined region represents the guide sequence. The horizontal red underline is the PAM site. The vertical black dotted line represents the actual cut site.

To confirm the knocking out of TPC2, DNA and amino acid sequences of wild type and altered B16 cells were analyzed. The Sanger sequences of the targeted location of wild type and edited cells were aligned in Figure 4A, and a 4 base pair deletion was found at the modified cells' cut site. A premature stop codon resulted from a frameshift mutation. CLC sequence viewer 8 was used to convert the DNA sequences to amino acids (Figure 4B). The frameshift was visible in the alignment of amino acids. TPC2 RNA expression levels were measured in both cell lines to provide additional validation. TPC2 expression was significantly reduced when B16 modified cells were compared to wild type cells (Figure 4C).

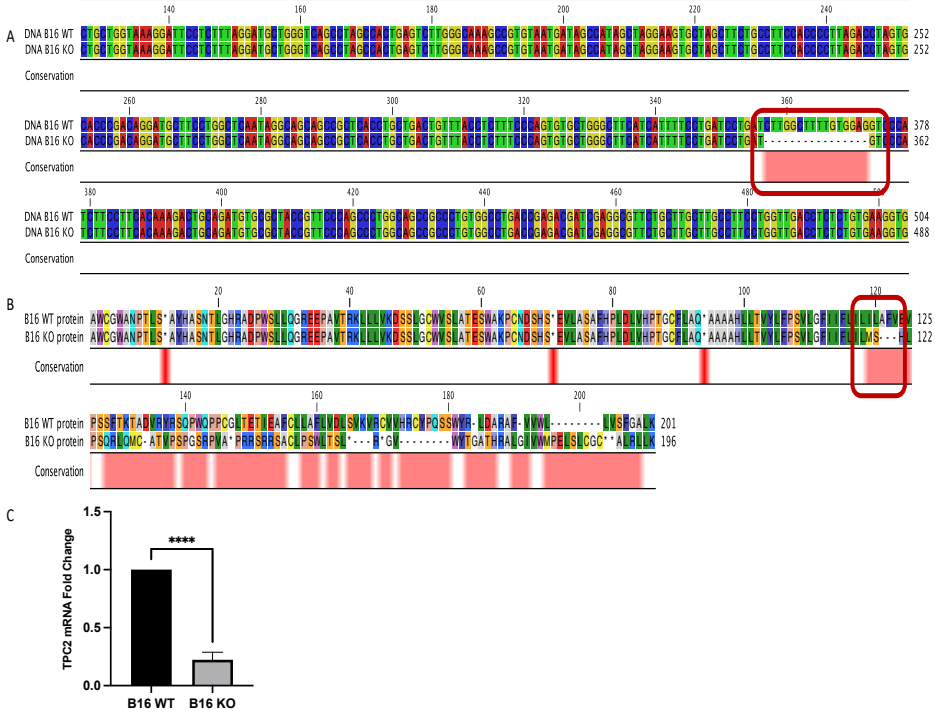

Figure 4. Sequence analysis of B16 WT and B16 edited cells generated by CRISPR-Cas9 targeting.

A) DNA sequence alignment of wild type and edited cells. The alignment shows a 5 base pair deletion (red box) in the B16 edited cells. B) Amino acid sequences generated from the upper DNA sequences were aligned and a confirmation of changes was observed after the cut site (red box). C) qPCR analysis for TPC2 transcript levels in B16 (WT and KO) cells.

Migration and proliferation

Invasion of cancer cells, also known as metastasis, is a significant hallmark of cancer. The metastatic cascade is a complex process that is related to invasion. It involves the invasion of surrounding tissues, intravasation, transit through the circulatory system, arrest at a secondary site, and extravasation and growth in a secondary organ. A transwell assay was used to evaluate the invasive ability of cells *in vitro*. Cell invasion is quantified by counting the number of individual cells that invade a transwell porous membrane coated with extracellular matrix. When compared to CHL-1 WT cells, CHL-1 KO cells showed a statistically significant increase in their ability to invade membranes as shown in Figure 5A.

Cell proliferation refers to the rate at which a cancer cell copies its DNA and divides into two cells. An increase in the rate at which cancer cells divide indicates that the cancer is developing more quickly or that it is becoming more aggressive in its progression. Therefore, it is crucial to understand how TPC2 KO cells proliferate. The xCELLigence real-time cell analysis (RTCA) system was used to study this phenotype. The RTCA system is a cutting-edge device that enables real-time monitoring of cell growth via a label-free cell-based assay that monitors impedance fluctuations in the culture media. Normalized cell index curves (Figures 5B, C) were generated for all impedance profiles during a 120-hour period. They were calculated using the CI, which is a dimensionless relative

value that represents the impedance change divided by the background value and so indicates the total number of cells and the quality of their attachment. The CI fluctuated with time, producing time-dependent impedance profiles during an experiment. The normalized CI values for CHL-1 WT cells were 0.43, 0.47, 0.63, 0.99, and 1.32 for every 24 hours in the experiments, while the normalized confidence intervals for CHL-1 KO cells were 0.56,0.79, 0.97,1.02, and 0.6 (Figure 5B, C). These results indicated that TPC2 KO has an initial positive effect on the initial stages of CHL-1 growth and then further accelerates it. However, after 100 hours, CHL-1 KO cells displayed a drastic reduction in growth rate, but WT cells continued to proliferate.

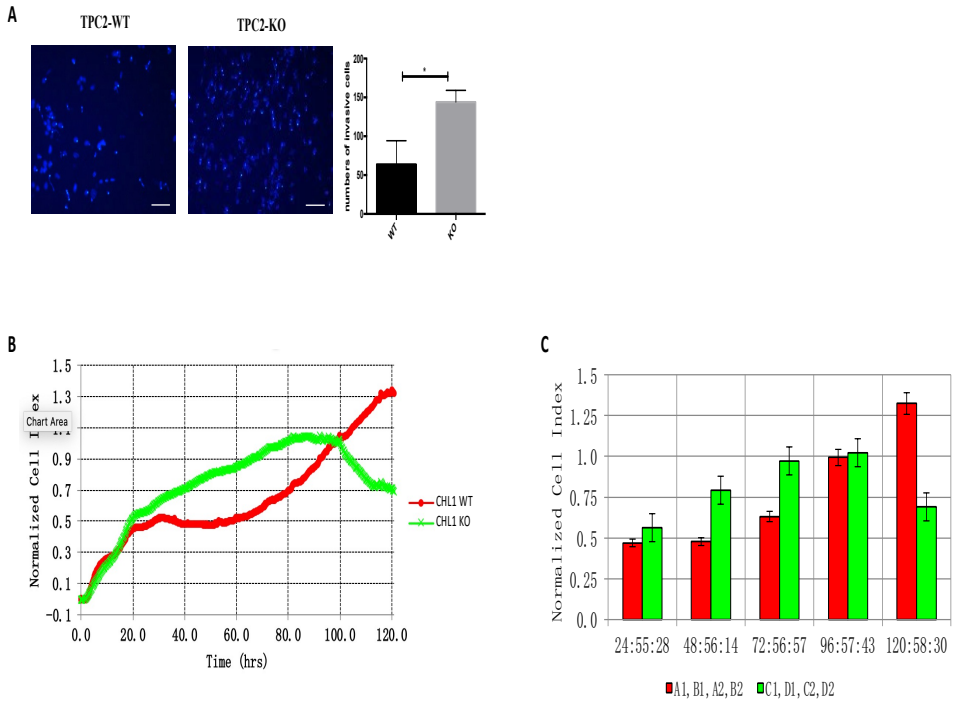

Figure 5. Invasion and proliferation phenotype of CHL-1 WT vs KO cells.

A) Transwell assay after 24 hours incubation on Matrigel matrix. The scale bar represents 20 µm. B, C) The RTCA proliferation curves and values. The proliferation rate was monitored for 120 hours by measuring CI values. A show the change in CI for the whole experiment's duration while D shows CI measures at specific time points.

The next trait to be assessed was a cell's invasion capacity. Comparing B16 WT cells to TPC2 KO cells, it was found that the ability of the KO cells to invade the transwell membrane was significantly reduced (Figure 6A). Tumour vasculogenic mimicry is a unique cancer signature that has emerged in recent years (VM). VM is a term used to describe the formation of patterned three-dimensional (3D) channel networks by malignant melanoma cells(67). Interestingly, we discovered that TPC2 KO cells are incapable of forming vessel-like structures in comparison to WT cells (Figure 6B).

Furthermore, real-time monitoring of cellular proliferation was performed for 120 hours utilising RTCA. The normalized CI values for B16 WT cells were 3.2, 4.4, 5.7, and 8.4 for each of the 24-hour periods, while the normalized confidence intervals for B16 TPC2 KO were 9.3, 9.6, 15.3, and 4.4 (Figure 6C, D). According to these findings, TPC2 KO initially enhanced growth for three days after application. As was the case with CHL-1 TPC2 KO cells, the rate of B16 KO cell growth was reduced on the fourth day, although the rate of B16 WT cell growth remained constant.

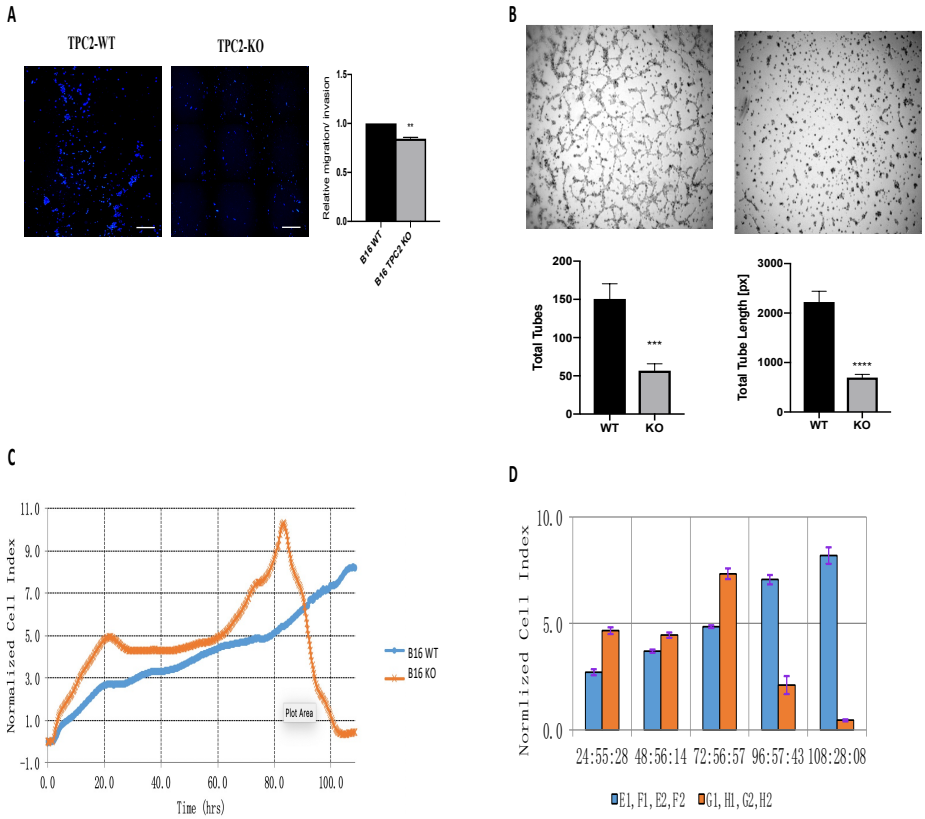

Figure 6. Invasion and proliferation phenotype of B16 WT vs TPC2 KO cells.

A) Transwell assay after 24 hours incubation on Matrigel matrix. The scale bar represents 20 µm. B) Representative images of tube formation assays comparing WT and KO (left panel) for 4 hours, and the quantitative data of tube formation assays (right panel). ***, P=0.0001; ****, P<0.0001 C, D) The RTCA proliferation curves and values. The proliferation rate was monitored for 120 hours by measuring CI values. A show the change in CI for the whole experiment's duration while D shows CI measures at specific time points.

Overall, CHL-1 TPC2 KO and B16 TPC2 KO cells showed different invasion capability compared to their WT controls. CHL-1 KO cells showed an increase in their ability to invade the transwell membrane whereas B16 KO cells were less invasive. In real-time monitoring of cellular proliferation, both CHL-1 and B16 KO cells showed a similar trend whereby KO cells showed a higher proliferation rate for three days then the rate dropped while WT cells showed a more gradual increase in the growth rate, but this was maintained after three days.

TPC2 and the Hippo pathway

The potential links with an important developmental pathway associated with tumour initiation and progression were studied to obtain insights into the molecular mechanisms driving the apparent increased aggressiveness of CHL-1 TPC2 KO cells. Recent advances in cancer research have shown the pivotal roles played by YAP/TAZ and the transcriptional effectors of Hippo signalling in tumour initiation and progression. Their activity has been linked to poor prognosis and can influence proliferation, invasion, and metastasis(68). Increased YAP levels have been associated with reduced survival in individuals with melanoma (69), and TAZ activation has been associated with lung cancer brain metastases (70). The expression of ankyrin repeat domain-containing protein 1 (ANKRD1), cysteine-rich 61 (CYR61), and connective tissue growth factor (CTGF), which are regarded to be genuine YAP/TAZ target genes, was examined to determine the activation state of YAP/TAZ (71). This analysis showed all these target genes were significantly upregulated in CHL-1 TPC2 KO cells, showing that the YAP/TAZ transcriptional activation pathway was activated in these cells (Figure 7A). In order to validate the existence of direct crosstalk between TPC2 and YAP/TAZ target genes, we transiently silenced TPC2 in the CHL-1 cell line for 24 hours. We observed an increase in the expression of ANKRD1, CTGF, and CYR61 at 24 hours post transfection (Figure 7B, C). These

findings confirm the link between TPC2 and YAP/TAZ target genes and imply that TPC2 plays a novel role in late-stage cancer.

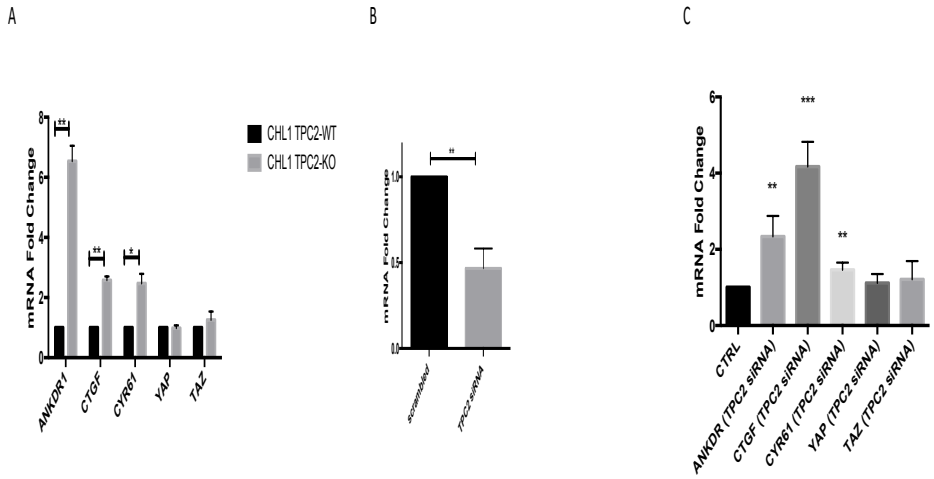

Figure 7. TPC2 KO and silencing induces YAP/TAZ target genes.

A) q-PCR analysis of YAP/TAZ target genes in CHL-1 TPC2-WT and KO cell lines. B) TPC2 transient inhibition after 24h from CHL-1 transfection. C) q-PCR analysis of YAP/TAZ target genes after transient silencing of TPC2.

A critical issue to address is how the absence of an endolysosomal ion channel such as TPC2 affects the activity of YAP/TAZ. We and others have demonstrated that TPC2 is a modulator of Ca^{2+} signalling responses in cells(72,73). As yet, the only known relationship between YAP/TAZ activity and Ca^{2+} signalling is via store operated Ca^{2+} entry (SOCE), a mechanism in which the endoplasmic reticulum (ER) Ca^{2+} store is replenished via an interaction between the ER protein STIM1 and the plasma membrane ion channel ORAI1(74). In glioblastoma cells, induction of SOCE reduced YAP/TAZ activity via activating PKC-II (75). This kinase is involved in the phosphorylation of MST1/2 and LATS 1/2, two signalling components of the Hippo pathway. YAP/TAZ are phosphorylated and sequestered in the cytoplasm upon activation by phosphorylation. Additionally, the glioblastoma study demonstrated that SOCE-induced elevations in Ca^{2+} resulted in actin cytoskeleton remodelling mediated by INF2 (75). The current study examined ORAI1 and PKC-II expression levels. TPC2 KO cells exhibited significant downregulation of ORAI1 and PKC-II expression (Figure 8A-C); however, STIM1 and INF2 expression remained unaltered. Additionally, a decrease in ORAI1 expression was detected following TPC2 temporary silencing (Figure 8B). An in-depth look at protein localization and expression of ORAI1 was conducted. Immunofluorescence and confocal imaging were used to determine ORAI1 localisation in WT and TPC2 KO cells. ORAI1 and β-actin showed protein expression in both cell lines, and an average

of z-stack images was created to assist in the localization of ORAI1. Unlike in WT cells, where ORAI1 was shown to be dispersed throughout the cytoplasm, ORAI1 was highly localised to the cell membrane in KO cells. The ORAI1 level in CHL-1 TPC2 KO cells was also found to be significantly lower when measured by Western blot (Figure 8D, E).

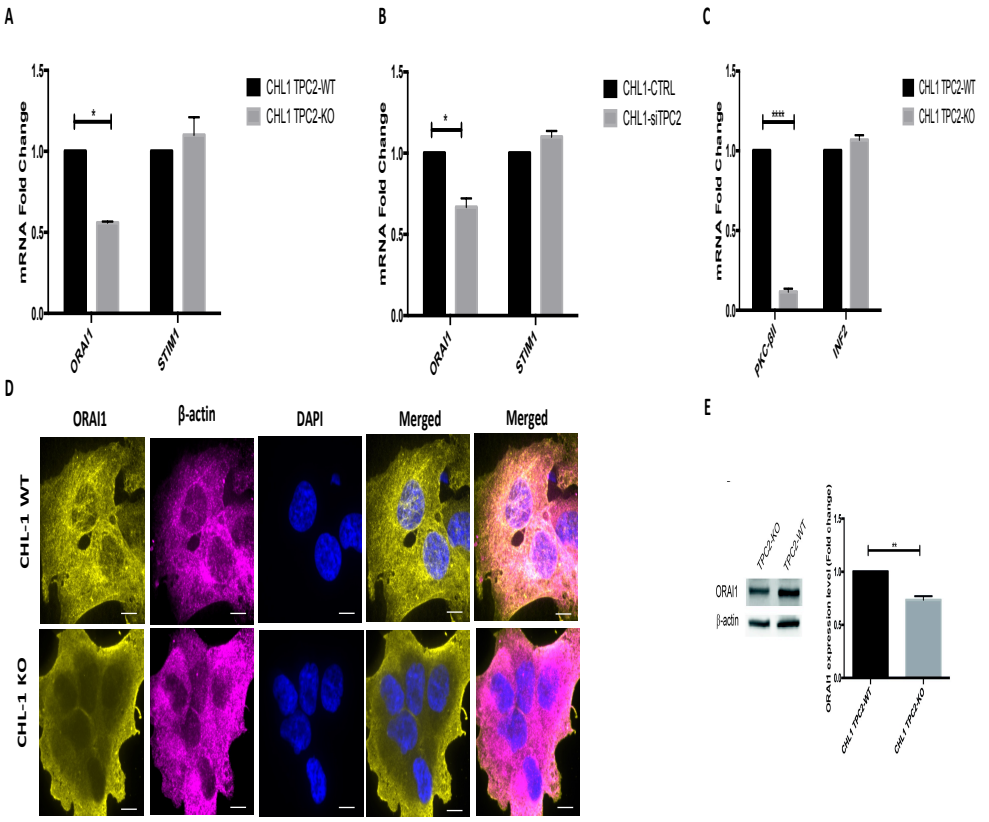

Figure 8. TPC2 KO and silencing reduce SOCE compartments.
A) q-PCR analysis of ORAI1 and STIM1 in CHL-1 WT and TPC2 KO cell lines. B) q-PCR analysis of ORAI1 and STIM1 after transient silencing of TPC2. C) q-PCR analysis of PKC-βII and INF2 in CHL-1 WT and TPC2 KO cell lines. D) Immunofluorescence expression and localization of ORAI1 and β-actin in CHL-1 cells (WT and TPC2 KO). Quantification of ORAI1 fluorescence staining intensity is shown (Mean CTCF values ± SEM). E) ORAI1 expression analyzed by western blot in WT and KO cells. The scale bar represents 10 µm.

Discussion

TPC2 has previously been shown to play a role in the progression of cancer. Nguyen et al. (76) demonstrated that silencing and pharmacological inhibition of this channel impairs the migration of human urinary bladder and hepatic carcinoma cells *in vitro*, as well as murine breast cancer cells *in vitro* and *in vivo*. However, the current study shows for the first time that TPC2 is involved in the aggressiveness of metastatic melanoma cells, and it clearly suggests that this involvement in human metastatic melanoma cells differs from what is already known about the role of TPC2 in other human cancer cell lines generated from original tumours.

To investigate the role of TPC2 in melanoma tumorigenesis and metastasis, TPC2 knockout cells were generated in the CHL-1 and B16 cell lines. CHL-1 cells are derived from a metastatic site and serve as a model of human amelanotic melanoma. CHL-1 cells do not have mutated BRAF, NRAS, or NF1. Therefore, CHL-1 is classified as a triple WT metastatic melanoma cell line based on these premises. B16 cells are a highly pigmented mouse melanoma cell line that have been extensively used to study melanoma cell biology. We employed CRISPR-based genome editing to generate stable TPC2 KO CHL-1 and B16 cell lines. In this study, the investigation of cancer's hallmarks began by an examination of melanoma cells' potential to invade. The metastatic process entails invasion of surrounding tissues, intravasation, circulation, arrest at a secondary site, and extravasation and growth in a secondary organ. The

invasive potential of cells *in vitro* was determined using a transwell test. When CHL-1 KO cells were compared to CHL-1 WT cells, CHL-1 KO cells showed a statistically significant increase in their capacity to infiltrate membranes, whereas B16 KO cells demonstrated decreased invasion ability.

Subsequently, cell proliferation rate was determined. The pace at which a cancer cell replicates its DNA and splits into two cells is referred to as cell proliferation. Increased cell division suggests that the cancer is progressing more rapidly or is becoming more aggressive in its progression. Thus, it is important to study how TPC2 KO cells multiply. This trait was investigated using the xCELLigence real-time cell analysis (RTCA) technology. In real-time monitoring of cellular proliferation, both CHL-1 and B16 KO cells had a similar pattern, with KO cells exhibiting a greater proliferation rate for three days before declining, whereas WT cells continued to proliferate at a higher rate.

To ascertain the molecular basis for this increase in metastatic potential following TPC2 depletion in CHL-1 cells, we examined whether KO had any effect on the Hippo signalling pathway. Recently, it has been demonstrated that this route regulates cell proliferation and differentiation and contributes to the advancement of a variety of illnesses, including cancer (77). MST1/2 and the large tumour suppressor 1/2 (LATS1/2) are Hippo pathway components; thus, MST1/2 phosphorylates and activates LATS1/2, which can then phosphorylate the yes association protein (YAP) and its paralogue, the transcriptional coactivator with PDZ-binding motif (TAZ), inhibiting YAP/TAZ activity. When not inhibited in this manner, translocation of YAP/TAZ to the nucleus

activates target genes involved in cell growth, proliferation, and organ development (77).

Increased YAP levels have been associated with reduced survival in individuals with melanoma (78), and TAZ activation has been associated with lung cancer brain metastases (79). To determine the status of YAP/TAZ activation, the expression of their target genes ankyrin repeat domain-containing protein (ANKRD1), cysteine-rich 61 (CYR61), and connective tissue growth factor (CTGF), was studied. Notably, all of these genes were significantly upregulated in CHL-1 TPC2 KO cells, implying YAP/TAZ activation.

To determine independently whether there is a correlation between decreased TPC2 expression and increased expression of YAP/TAZ target genes, RNA interference (RNAi) was employed to transiently knockdown (KD) TPC2 expression for 24 hours in the metastatic melanoma cell line CHL-1. Notably, elevated expression levels of ANKRD1, CTGF, and CYR61 mRNAs were detected in TPC2 KD cells using this fundamentally different technique [3]. Additionally, an investigation was made of whether the enhanced translocation of YAP/TAZ from the cytoplasm to the nucleus observed in TPC2 KO cells is related with higher activation of YAP/TAZ target genes. Using differential nucleus-cytoplasm protein extraction, an increase in YAP and TAZ in the nucleus was detected following TPC2 KO. Taken together, these data establish a relationship between decreased or absent TPC2 expression and transcriptional activation of YAP/TAZ target genes (80).

In contrast to our findings with CHL-1 cells, we detected no evidence of YAP/TAZ target gene activation following TPC2 KD in B16 cells. This is consistent with our discovery that knocking out TPC2 lowers metastatic characteristics in B16 cells, but not in CHL-1 cells.

A critical topic is how the absence of an endolysosomal ion channel such as TPC2 affects the activity of YAP/TAZ. Our lab and others previously demonstrated that TPC2 acts as a modulator of Ca^{2+} signalling responses (81). Prior to our recent studies, the only known link between YAP/TAZ activity and Ca^{2+} signalling was via store-operated Ca^{2+} entry (SOCE), a process in which the endoplasmic reticulum (ER) Ca^{2+} store is replenished via an interaction between the ER protein STIM1 and the plasma membrane ion channel ORAI1 (82). Thus, stimulation of SOCE reduced YAP/TAZ activity in glioblastoma cells via activation of PKC-II. PKC-II modulates the phosphorylation of MST1/2 and LATS 1/2, two components of the Hippo signalling pathway (77). ORAI1 and PKC-II expression levels were compared in this study. Interestingly, CHL-1 TPC2 KO cells exhibited a significant decrease in ORAI1 and PKC-II expression, but STIM1 and INF2 expression remained unaltered. Additionally, a decrease in ORAI1 expression was detected following TPC2 temporary silencing. This indicates that the absence of TPC2 may result in the activation of YAP/TAZ target genes, resulting in an increase in metastasis. A summary of this chapter's methods and findings is illustrated in Figure 9.

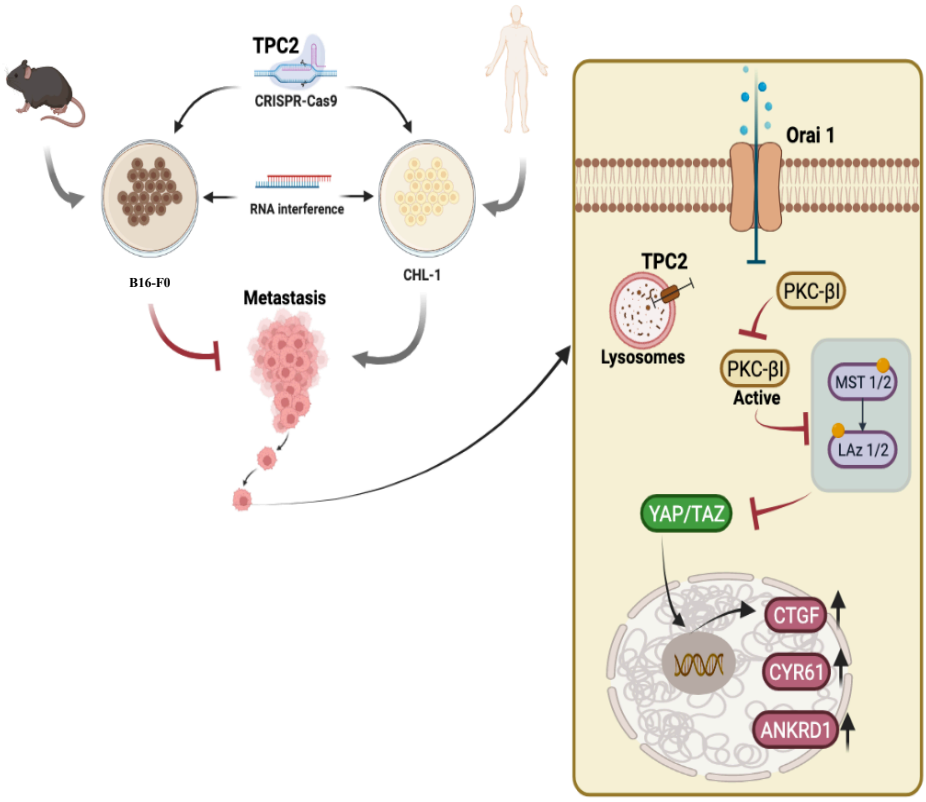

Figure 9. An overview of the chapter's methods and findings.

Chapter 4

TPC2 KO effect on bioenergetic phenotypes, cellular cytoskeleton and melanin synthesis and release.

Introduction

In cancer research, the proteomics approach has gained traction. Proteomics-based technologies have enabled the identification of possible biomarkers and protein expression patterns that can be used to assess tumour prognosis, predict responses to specific therapies, and classify tumours. Additionally, to gain a better understanding of cancer's fundamental biology, proteomics approaches have been used to decipher how signalling pathways in tumour cells are altered, thereby increasing our understanding of how to target various pathways for cancer therapy(83). In this chapter, we examined the proteins that were differentially expressed following TPC2 knockout in B16 and CHL-1 cell lines. After bioinformatics analysis identified the altered cellular process in KO cells, molecular-based analysis was employed to confirm these findings.

Proteomic signature

To further assess the effect of TPC2 KO on the CHL-1 cell line, a proteomic approach was used. Alterations in protein expression between WT and KO CHL-1 cells were analyzed using a label-free proteomics approach. This resulted in the collection of 2772 identified proteins after filtering them using the Perseus software (removing possible contaminants and considering only proteins identified with at least one unique peptide) (Figure 10A).

To ascertain probable expression differences between WT and KO cells, a principal component analysis (PCA) was used to determine the degree of similarity, as illustrated in Figure 10B. The histogram plot of log2-transformed ratio distributions revealed that the protein samples were generally distributed normally with relatively few outliers (Figure 10C). A scatter blot analysis was used to visualize the expression differences between samples (Figure 10D). In WT samples, Pearson correlation values were above 0.9, whereas in KO samples, Pearson correlation values were above 0.92. These findings reflect the group's similarity. To identify proteins that are highly enriched or depleted in KO cells, the fold change and p-value of each protein were plotted. There were 303 proteins that differed significantly (74 upregulated and 87 downregulated). In Figure 10E, F, these proteins are shown in a volcano plot and correlated using hierarchical clustering analysis and a heat map.

A

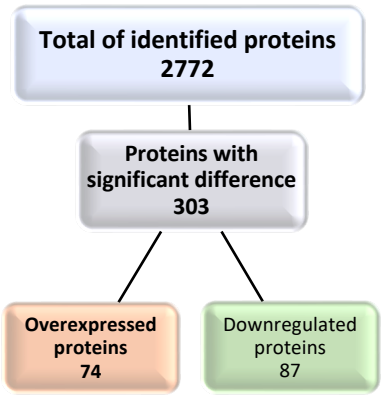
Total of identified proteins
2772
Proteins with significant difference
303
Overexpressed proteins
74
Downregulated proteins
87

B

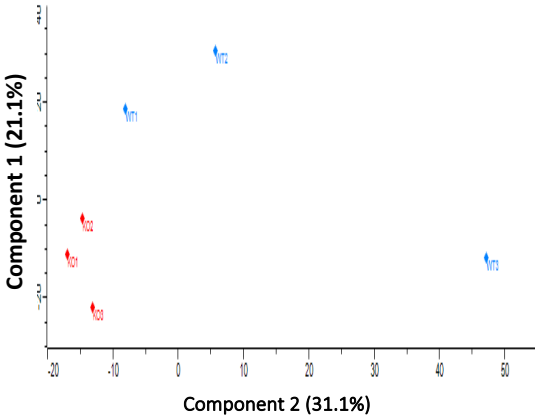
Component 1 (21.1%)
Component 2 (31.1%)

C

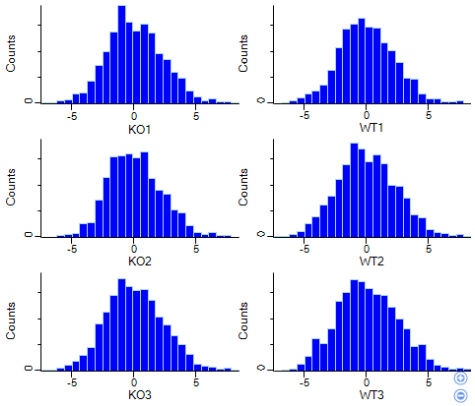
Counts
KO1
WT1
KO2
WT2
KO3
WT3

D

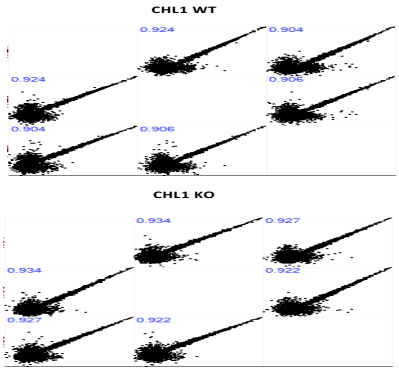
CHL1 WT
CHL1 KO

E

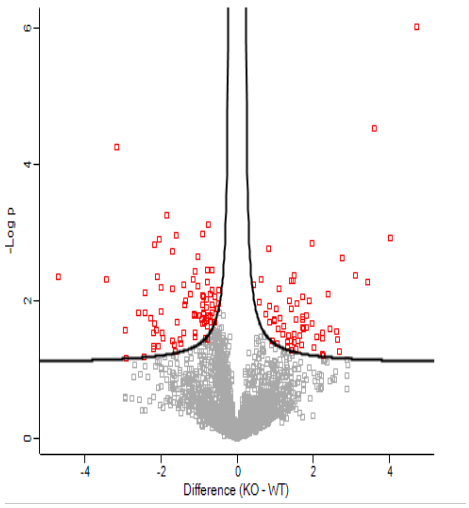
-Log p
Difference (KO - WT)

F

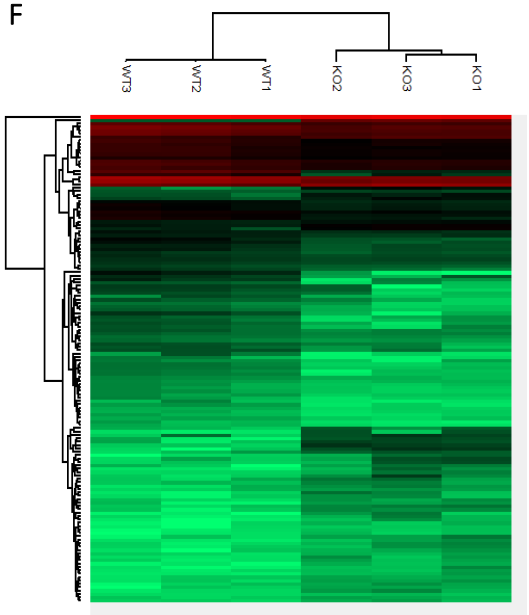
WT3
WT2
WT1
KO2
KO3
KO1

Figure 10. Identification of differentially expressed proteins between WT and TPC2 KO CHL-1 melanoma cells. A) Number of identified proteins during analysis and filtering process. B) Principal component analysis of the measurements; KO cells are shown in red, control cells in blue. C) Histogram plot of the fold-changes for all of the quantified proteins in log2-transformed ratios after normalization. D). Multiscatter analysis. To evaluate the similarity between samples, a multiscatter analysis was performed. A Pearson correlation index close to 1 indicates high similarity. E) Volcano plot analysis of KO vs WT cells. F). Hierarchical clustering analysis with heat map of the 303 proteins (rows) and the samples (columns).

Gene set enrichment analysis (GSEA) was performed using WebGestalt (WEB-based Gene SeT AnaLysis Toolkit) to evaluate the changes in gene ontology and signalling pathways associated with variably expressed proteins in CHL-1 TPC2 KO cells. Among enriched categories in gene ontology, for Cellular Component, there were six positive associated categories and ten negative related categories (Figure 11A). Intercellular junction, actin cytoskeleton, endoplasmic reticulum, extracellular matrix, and mitochondrial inner membrane are all included in these classifications. Under enriched categories, for Biological Process analysis, ten positive associated categories and ten negative linked categories were identified (Figure 11B). Small molecule metabolic process regulation, organelle localization, cytoskeleton organization, intracellular transport regulation, proteasomal protein catabolic process regulation, actin filament-based process regulation, and sensitivity to oxygen levels are among the categories that were altered. When the Molecular Functions of altered proteins were analyzed, two positive associated categories and four negative related categories were identified as enriched categories (Figure 11C). Binding

of cell adhesion molecules, actin binding, and catalytic activity on RNA are all enhanced in TPC2 KO samples.

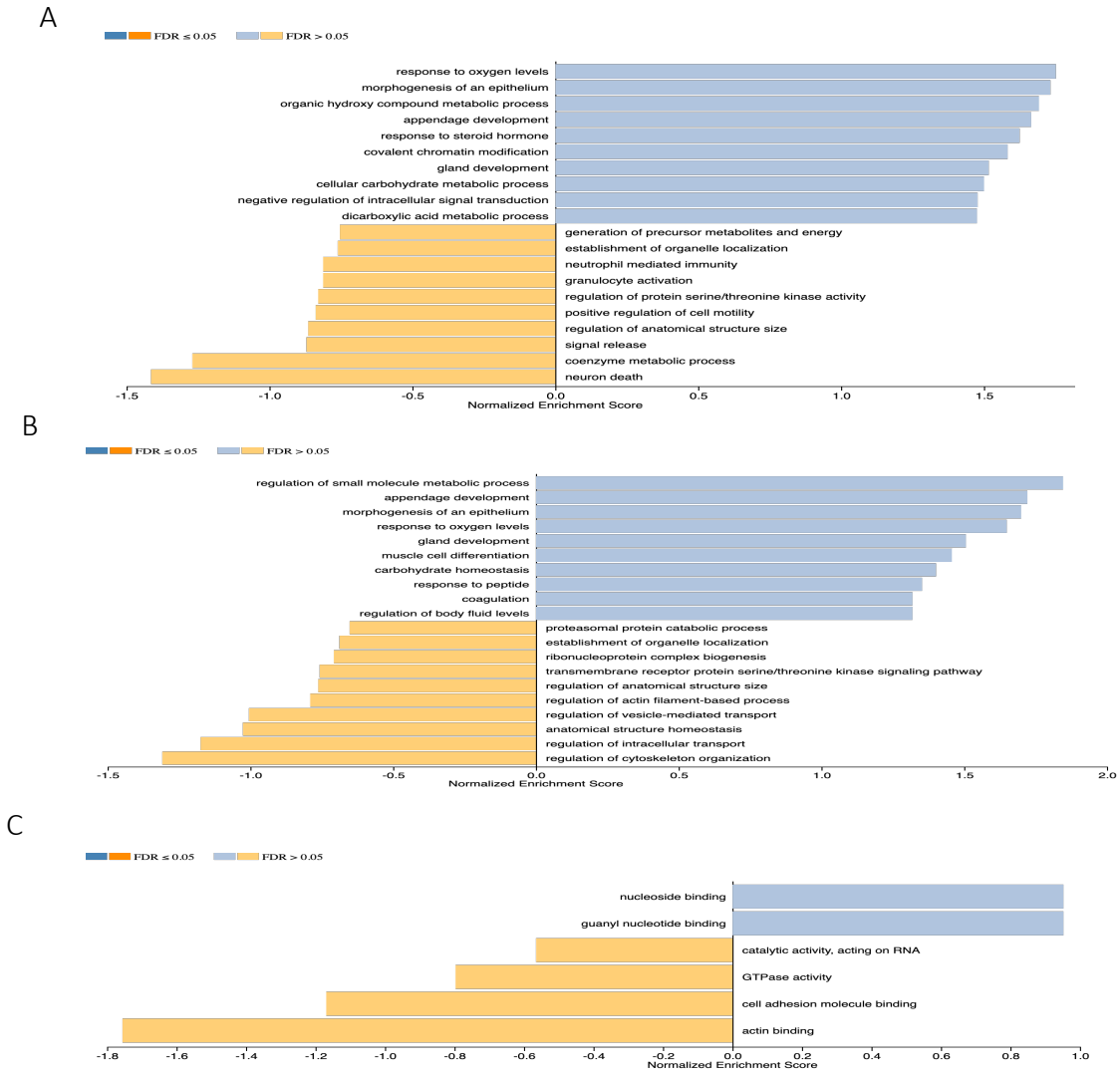

Figure 11. Gene set enrichment analysis (GSEA) using WebGestalt (WEB-based Gene SeT AnaLysis Toolkit) between differently expressed proteins in WT and TPC2 KO CHL-1 melanoma cells. A) Cellular Component. B) Biological Process. C) Molecular Function of the differentially expressed proteins in CHL-1 TPC2 KO cells. Among the 103 unique entrezgene IDs, 72 IDs are annotated in Cellular Component. In Biological Process (BP), 97 IDs are annotated to BP and 84 IDs are annotated to Molecular Function, which are used for the enrichment analysis. 10 positive related categories and 10 negative related categories are identified as enriched categories.

Furthermore, proteins were assigned to Reactome pathways to gain insight about enriched pathways in TPC2 KO samples (Figure 12A). Ten categories with a positive correlation and another ten with a negative correlation are recognized as enriched categories. Signalling by TGF-beta receptor complex, Signalling by WNT, Transport of small molecules, Signalling by Rho GTPases, Cell-cell communication, and Extracellular matrix organization are significantly enhanced. The KEGG (Kyoto Encyclopedia of Genes and Genomes) pathway showed enrichment in Regulation of actin cytoskeleton, Pathways in cancer, Focal adhesion, and Viral carcinogenesis (Figure 12B). Evaluating cancer Wikipathway analysis of changed proteins revealed three categories of positively associated proteins and three categories of negatively related proteins. The TGF-beta Signalling, Cell Cycle, Focal Adhesion-PI3K-Akt-mTOR-signalling, and DNA Damage Response (only ATM dependent) pathways have been enriched based on cancer Wikipathways (Figure 12C).

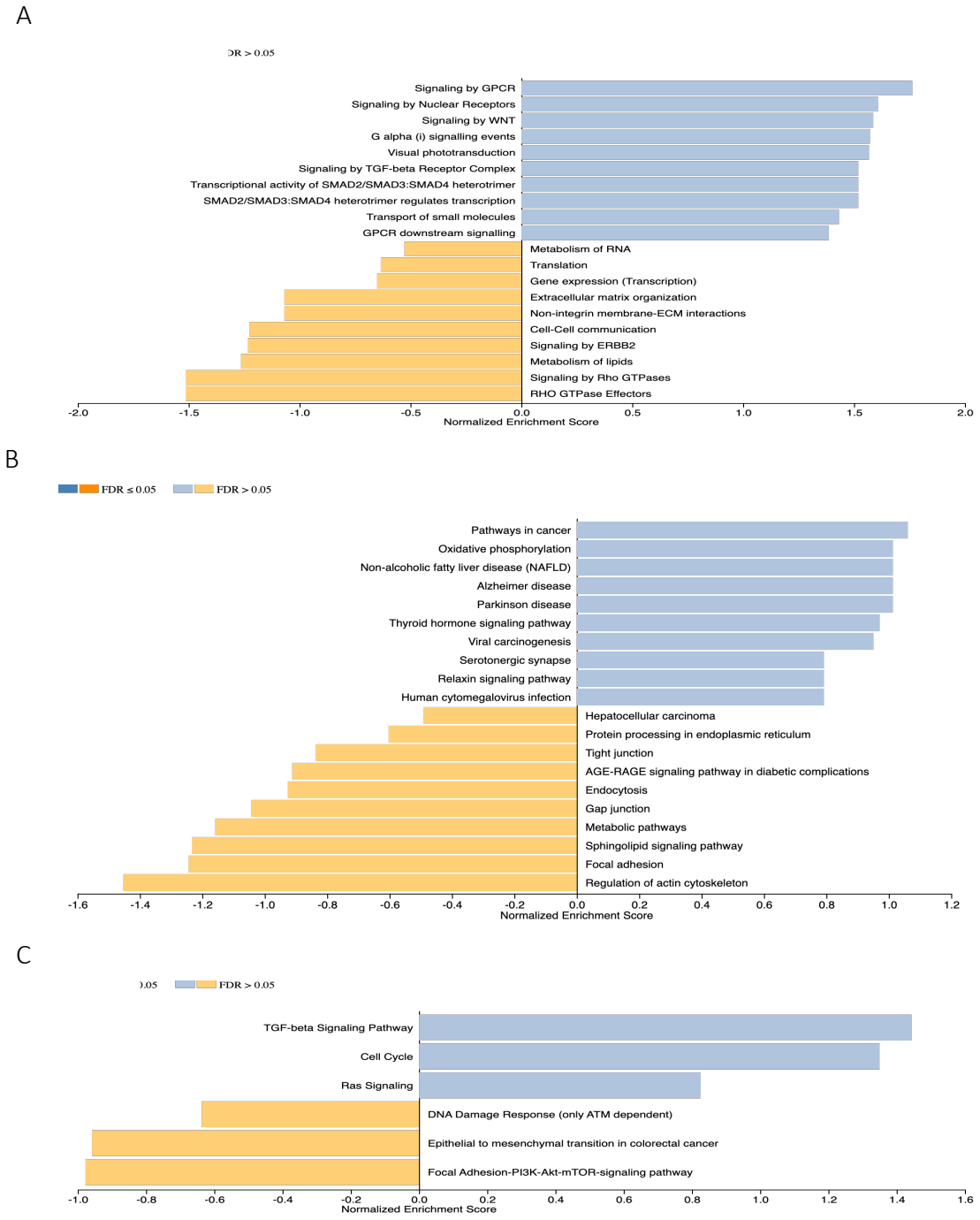

Figure 12. Gene set enrichment analysis (GSEA) using WebGestalt (WEB-based Gene SeT AnaLysis Toolkit) between differently expressed proteins in WT and TPC2 KO in CHL-1 melanoma cells. A) Pathway analysis by REACTOME. B) Pathway analysis by KEGG (Kyoto Encyclopedia of Genes and Genomes) C) Pathway enrichment by Wikipathway cancer of the differentially expressed proteins in CHL-1 TPC2 KO cells. 10 positive related categories and 10 negative related categories are identified as enriched categories.

The protein concentrations of some targets that were altered after TPC2 KO were compared to those from MS quantification data as a first step in confirming the findings. Proteomic study revealed a one-fold reduction in lamin-B1 in KO cells. Nuclear lamin-B1 (LB1) is a structural component of the nucleus that appears to regulate a variety of nuclear processes. The results of the Western blot mirrored the MS quantification data (Figure 13A). Evidence for downregulated proteins in the Focal Adhesion-PI3K-Akt-mTOR signalling pathway was the next finding to be validated. CHL-1 KO cells showed a reduction in phospho-AKT which confirmed the bioinformatic analysis of altered proteins (Figure 13B).

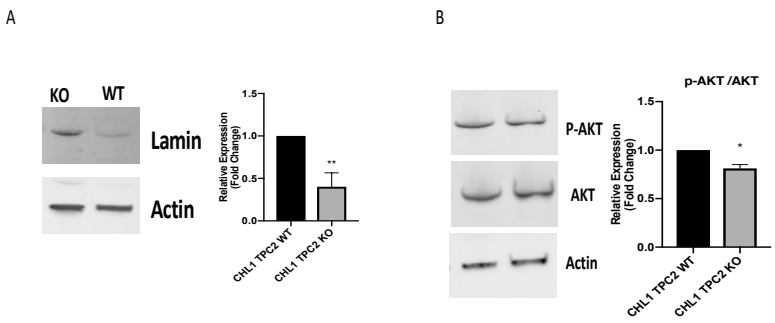

Figure 13. Lamin B and p-AKT/AKT proteins in WT and TPC2 KO CHL-1 melanoma cells.
A) Lamin B expression in WT and KO cells. Fold change representation of Lamin B is shown (n=4). **B)** The p-AKT/AKT ratio was analyzed in WT and KO cells. Fold change representation of p-AKT/AKT ratios is displayed (n=4).

Proteomics was also conducted to investigate the effect of TPC2 KO on the B16 cell line. Following filtering with the Perseus software, this resulted in a collection of 2,742 identified proteins (removing possible contaminants and considering only proteins identified at least with 1 unique peptide) (Figure 14A). To evaluate any differences in expression between WT and KO cells, a principal component analysis (PCA) was employed to estimate the degree of similarity, as depicted in Figure 14B. Histogram plots based on log2 transformations revealed distribution of all samples (Figure 18C). As a way to visualise the changes in expression levels between the samples, a scatter blot analysis was employed (Figure 14D). These data attest to the group's homogeneity. The fold change and p-value of each protein were plotted to detect enriched or depleted proteins in KO cells. 114 proteins showed significant expression change (59 upregulated and 54 downregulated). These proteins are visualised in a volcano plot and correlated using hierarchical clustering analysis and a heat map in Figure 14E and F.

A

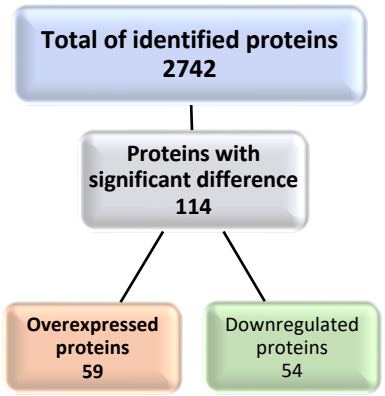
Total of identified proteins
2742
Proteins with significant difference
114
Overexpressed proteins
59
Downregulated proteins
54

B

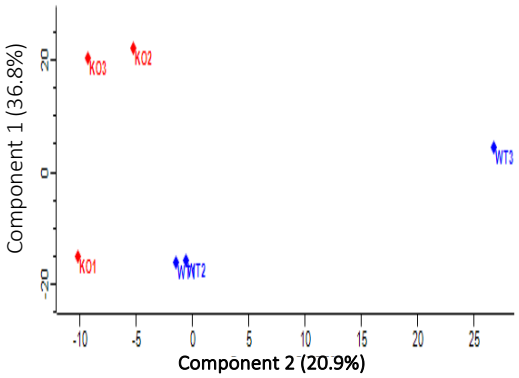
Component 1 (36.8%)
Component 2 (20.9%)
KO3
KO2
KO1
WT3
WT2
WT1

C

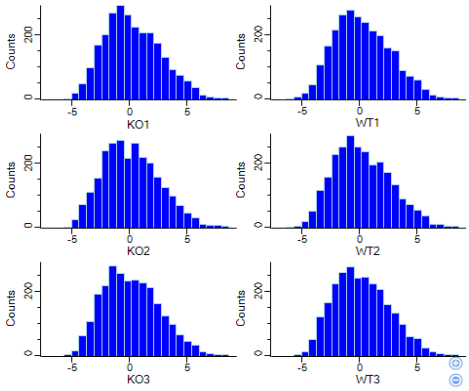
Counts
KO1
WT1
KO2
WT2
KO3
WT3

D

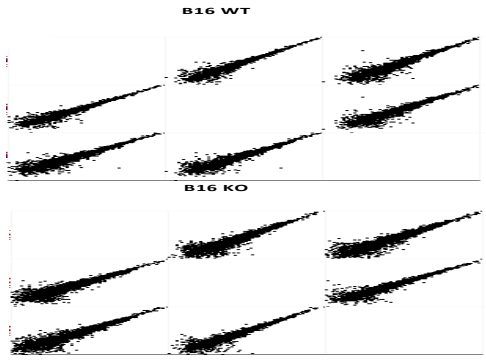
B16 WT
B16 KO

E

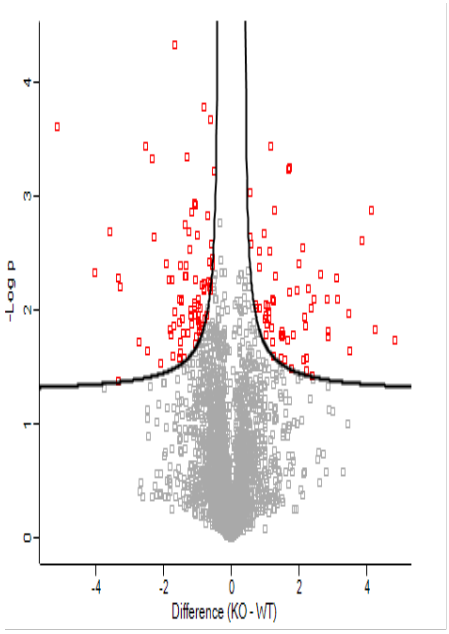
-Log P
Difference (KO - WT)

F

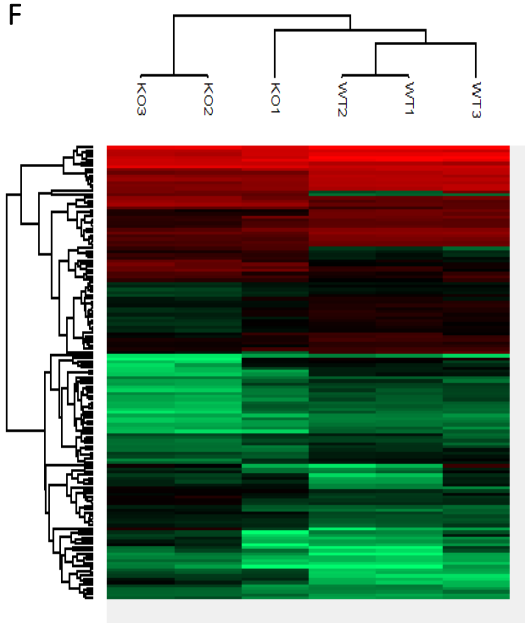
KO3
KO2
KO1
WT2
WT1
WT3

Figure 14. Identification of differentially expressed proteins between WT and TPC2 KO B16 melanoma cells. A) Number of identified proteins during analysis and filtering process. **B)** Principal component analysis of the measurements. KOs are shown in red, Ctrls in blue. **C)** Histogram plot of the fold-changes for all of the quantified proteins in log2-transformed ratios after normalization. **D).** Multiscatter analysis. To evaluate the similarity between samples, a multiscatter analysis was performed. A Pearson correlation index close to 1 indicates high similarity. **E)** Volcano plot analysis of KO vs WT cells. **F)**. Hierarchical clustering analysis with a heat map of the 114 proteins (rows) and the samples (columns).

To examine the alterations in gene ontology and signalling pathways associated with variably expressed proteins in B16 TPC2 KO cells, WebGestalt (WEB-based Gene SeT AnaLysis Toolkit) was used to perform gene set enrichment analysis (GSEA). Cellular component, vesicle membrane, trans-Golgi network, transport vesicle, endosomal component, and organelle inner membrane are the most enriched categories in gene ontology (Figure 15A). Among the categories that have been enriched for Biological Process study are reaction to virus, cell-cell signalling via Wnt, fatty acid metabolic process, protein localization to cytoskeleton, endosomal transport, and regulation of haemopoiesis (Figure 15B). Tubulin binding, kinase regulator activity, ATPase activity, and ubiquitin-like protein transferase activity were all elevated in KO samples when their molecular functions were evaluated (Figure 15C).

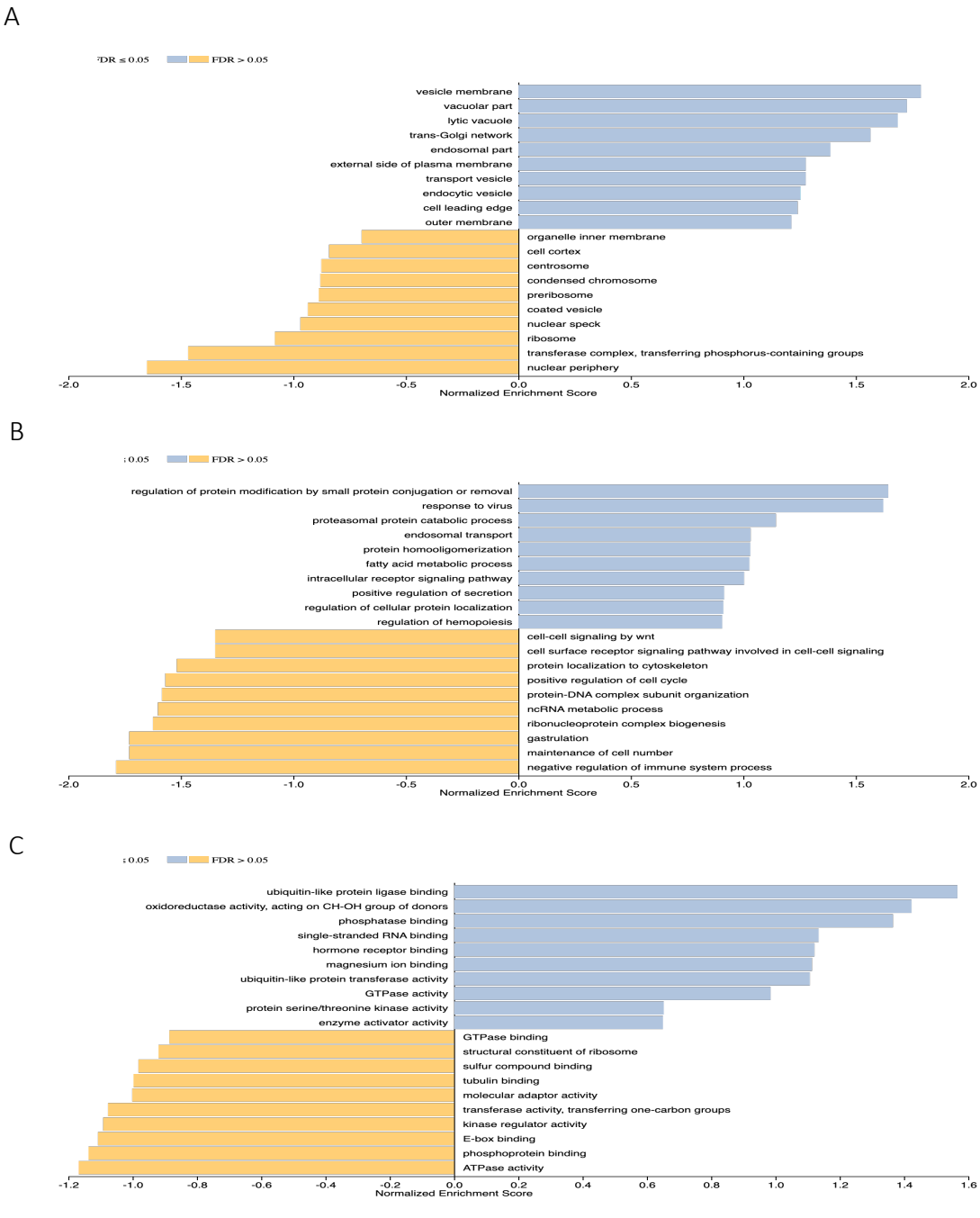

Figure 15. Gene set enrichment analysis (GSEA) using WebGestalt (WEB-based Gene SeT AnaLysis Toolkit) between differently expressed proteins in WT and TPC2 KO B16 melanoma cells. A) Cellular Component. B) Biological Process. C) Molecular Function of the differentially expressed proteins in B16 KO cells. Among the 103 unique entrezgene IDs, 72 IDs are annotated in Cellular Component. In Biological Process, 97 IDs are annotated to BP and 84 IDs are annotated to Molecular Function, which are used for the enrichment analysis. 10 positive related categories and 10 negative related categories are identified as enriched categories.

Furthermore, proteins were assigned to Reactome pathways in order to understand more about enriched pathways in KO samples (Figure 16A). The immune system, the antiviral mechanism of ISG15, interferon signalling, cytokine signalling in the immune system, and MAPK family signalling cascades were all elevated. The KEGG (Kyoto Encyclopedia of Genes and Genomes) pathway revealed an enrichment in the signalling pathway for RIG-I-like receptors, autophagy, and RNA transport (Figure 16 B).

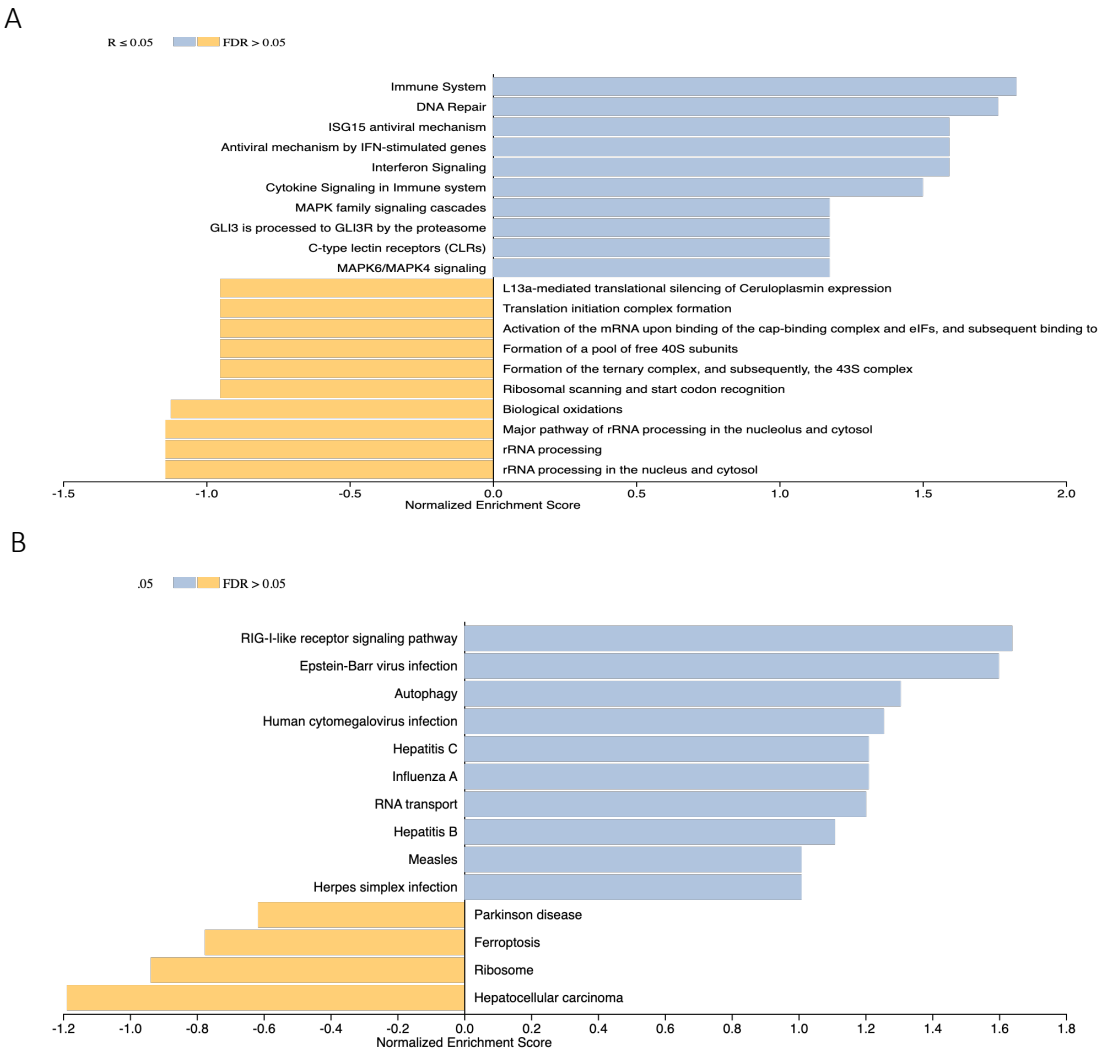

Figure 16. Gene set enrichment analysis (GSEA) using WebGestalt (WEB-based Gene SeT AnaLysis Toolkit) between differently expressed proteins in WT and TPC2 KO B16 melanoma cells. A) Pathway analysis by REACTOME. B) Pathway analysis by KEGG (Kyoto Encyclopedia of Genes and Genomes) C) Pathway enrichment by Wikipathway cancer of the differentially expressed proteins in CHL-1 KO cells. 10 positive related categories and 10 negative related categories are identified as enriched categories.

As a preliminary step in verifying the findings, the protein levels of some targets that were altered following TPC2 KO as assessed by proteomic quantification were further investigated by other approaches. In B16 KO cells, a proteomic analysis revealed more than a one-fold reduction in Fascin. The results of the Western blot and immunofluorescence experiments were consistent with the results of the MS quantification experiment. Fascin protein expression level was significantly reduced in B16 TPC2 KO cells (Figure 17A, C). The level of phospho-AKT was also measured. In B16 cells, p-AKT was reduced in the absence of TPC2, similar to the CHL-1 observation (Figure 17B).

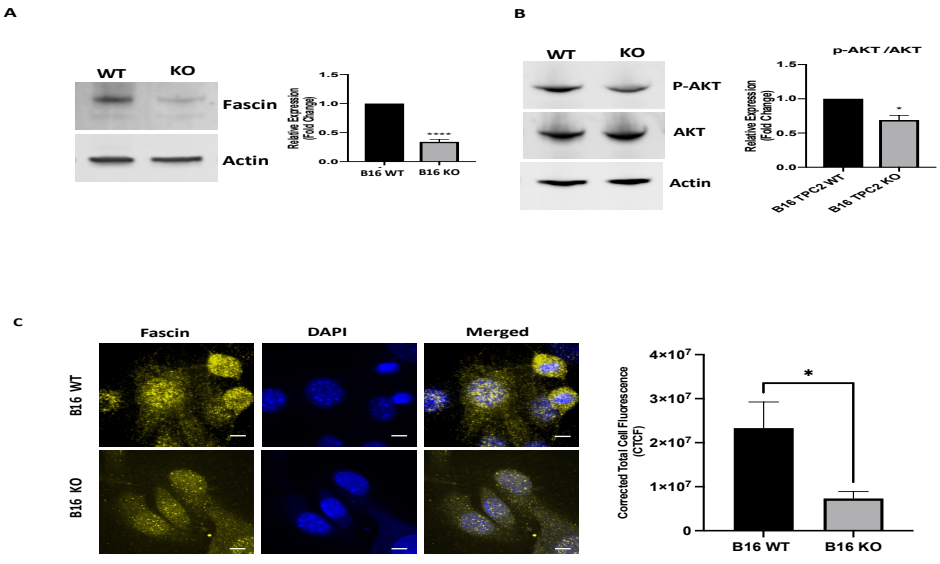

Figure 17. Fascin and p-AKT/AKT proteins in WT and TPC2 KO in B16 melanoma cells.
A) Fascin expression in WT and TPC2 KO cells. Fold change representation of fascin is shown (n=4). **B)** The p-AKT/AKT ratio was analyzed in WT and KO cells. Fold change representation of p-AKT/AKT ration is displayed (n=4). **C)** Immunofluorescence analysis of fascin expression. Quantification of fascin fluorescence staining intensity is shown (Mean CTCF values ± SEM). The scale bar represents 10 µm.

TPC2 and bioenergetic phenotypes

Oxidative phosphorylation (OXPHOS) and glycolysis are the two metabolic processes that produce energy in the form of ATP. OXPHOS is the most effective method of ATP production since it generates 19 times more ATP than glycolysis and occurs in the mitochondria. Tumour cells rewire their metabolism to favour growth, survival, proliferation, and long-term maintenance, as demonstrated by Otto Warburg and colleagues' pioneering investigations in the 1920s(84). Increased glucose absorption and glucose fermentation to lactate are prominent features of this altered metabolism. Our proteomic studies had previously revealed enrichment in cellular carbohydrate metabolic process, mitochondrial inner membrane, small molecule metabolic process regulation, mitochondrial protein complex after TPC2 KO in the CHL-1 cell line. Enrichment in previous categories was led by a significant increase in PCK1, phosphoenolpyruvate carboxykinase 1, COX7A2, cytochrome c oxidase subunit 7A2, NDUFB9, and NADH: ubiquinone oxidoreductase subunit B9. The PCK1 enzyme plays a key role in gluconeogenesis regulation. This gene's cytosolic enzyme catalyzes the synthesis of phosphoenolpyruvate from oxaloacetate, resulting in the release of carbon dioxide and GDP, and its expression can be controlled by insulin, glucocorticoids, glucagon, cAMP, and nutrition (85). COX7A2 catalyzes the electron transport from reduced cytochrome c to oxygen

as the terminal component of the mitochondrial respiratory chain (86). NDUFB9 is found in the inner membrane of mitochondria. It is also known as Complex I, and it is responsible for the transport of electrons from NADH to the respiratory chain (87). Consequently, we began by evaluating the ATP level in cell lines. ATP can be used either to store energy for future reactions or to pay for processes when the cell requires energy (88). In CHL-1 cells, TPC2 KO resulted in an increase in ATP synthesis and a decrease in lactate production relative to WT cells (Figure 18A, B). TPC2 KO thus appears to reduce anaerobic respiration in CHL-1 cells. In contrast, in the absence of glucose, ATP levels in CHL-1 TPC2 KO cells were unaffected, and lactate generation was enhanced (Figure 18C, D).

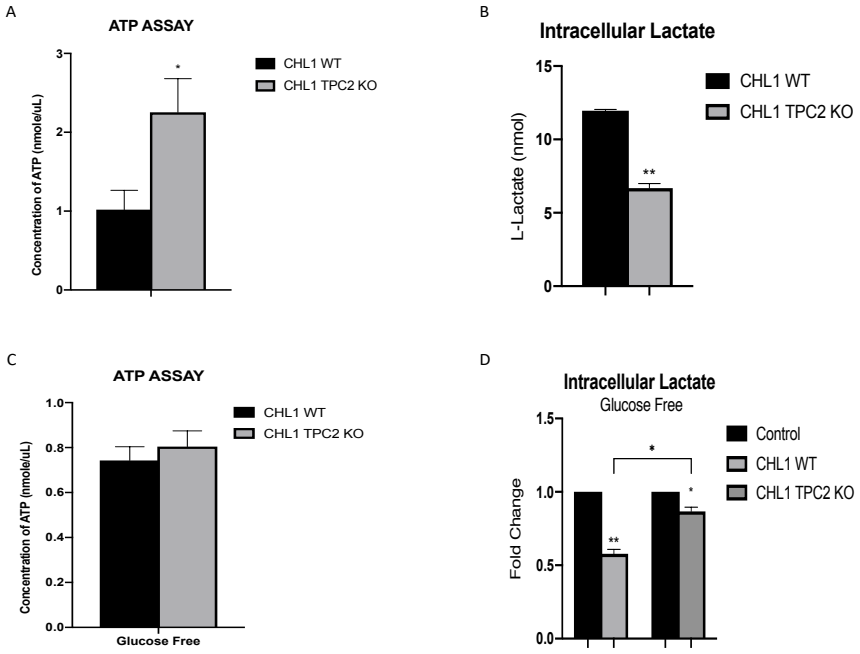

Figure 18. Intracellular ATP and Lactate concentration in CHL-1 (WT and TPC2 KO).
A) Intracellular ATP in CHL-1 WT and TPC2 KO cell lines. **B)** Intracellular lactate. **C**) Glucose deprivation effect on intracellular ATP. **D)** Glucose deprivation effect on intracellular lactate. Results obtained after incubating cells for 24 hours in normal media (supplemented with pyruvate, glucose, and glutamine) or normal media without glucose.

To acquire a deeper understanding of this energy shift, cellular metabolism was also evaluated using a Seahorse XF instrument that measures oxygen consumption rate [OCR] and extracellular acidification rate [ECAR] in the media surrounding cells in a microplate. Both glycolysis and oxidative phosphorylation (OXPHOS) processes are capable of contributing to the acidity of the assay medium. The conversion of glucose to lactate by glycolysis is followed by the release of one H^+ per lactate, whereas the TCA cycle that powers ETC/OXPHOS generates CO_2, which also acidifies the assay medium. Changes in extracellular

acidification are mostly caused by the sum of these reactions (ECAR) (89,90). The OCR/ECAR ratio was reduced in CHL-1 TPC2 KO cells under baseline conditions (Figure 19A). The level of OCR was significantly reduced in KO cells, whereas the level of ECAR was comparable to that of WT cells. Taking into account all previous findings regarding CHL-1 metabolism, KO cells exhibited a higher level of ATP and a lower level of intercellular lactate as well as an increased OCR/ECAR ratio. This may indicate that the higher level of ATP in CHL-1 KO cells is not entirely produced by OXPHOS or glycolysis, as oxygen consumption and lactate levels are both low. To examine these results, glucose-free media were used to cultivate cells and previous metabolic factors were measured. In KO cells, lactate levels increased significantly, and the OCR/ECAR ratio shifted to become higher (Figure 19B). CHL-1 KO cells exhibited a high oxygen consumption rate, indicating that OXPHOS was elevated under these circumstances. Under both conditions, KO cells demonstrated efficient energy production, which could be attributed to their mitochondria. In general, under normal conditions, CHL-1 KO cells may use the byproduct of glycolysis (pyruvate) to fuel mitochondria in order to produce a large amount of ATP as opposed to converting it to lactate. In this instance, mitochondrial ATP production occurred independently of oxygen consumption. In the absence of glucose, however, KO cells rely on OXPHOS to produce ATP.

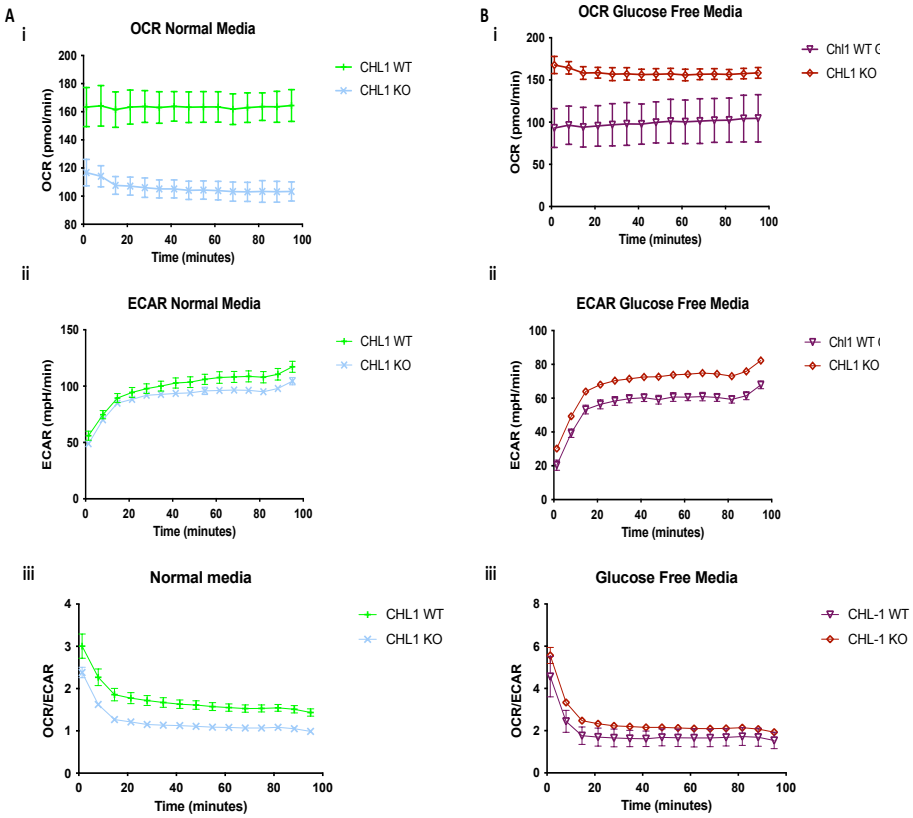

Figure 19. TPC2 KO alters the metabolic phenotype of cancer cells

(A-I, ii, iii) CHL-1 WT and TPC2 KO cells incubated in normal media. **(B-i, ii, iii)** CHL-1 WT and KO cells incubated in glucose free media. The OCR (oxygen consumption rate)/ECAR (extracellular acidification rate) ratio is displayed over time as the mean ± SEM, performed in triplicate (unpaired t test with Welch's correction). An increase of the OCR/ECAR ratio, indicating a decreased reliance on aerobic glycolysis of TPC2 KO cells, is visible.

In B16 proteomic analysis, the enrichments related to metabolism were cofactor metabolic process, sulfur, and ribose phosphate metabolic process. Acsl4, acyl-CoA synthetase long-chain family member, Aldoc, aldolase C, fructose-bisphosphate, and Sardh, sarcosine dehydrogenase, were the most commonly overexposed proteins in B16 KO cells, leading to an enrichment in the preceding categories. Aldoc is a glycolytic enzyme that converts fructose-1,6-bisphosphate to glyceraldehyde-3-phosphate and dihydroxyacetone phosphate from fructose-1,6-bisphosphate (91). ACSL4 belongs to an important family of lipid metabolic enzymes (92). SARDH is a mitochondrial enzyme that demethylates sarcosine via oxidation (93). The same phenomenon was investigated in B16 WT and TPC2 KO cells. TPC2 deletion increased ATP synthesis and lactate generation in B16 cells when compared to WT cells (Figure 20A-C). In the absence of glucose, ATP levels and lactate production were likewise increased in B16 KO cells (Figure 20B-D).

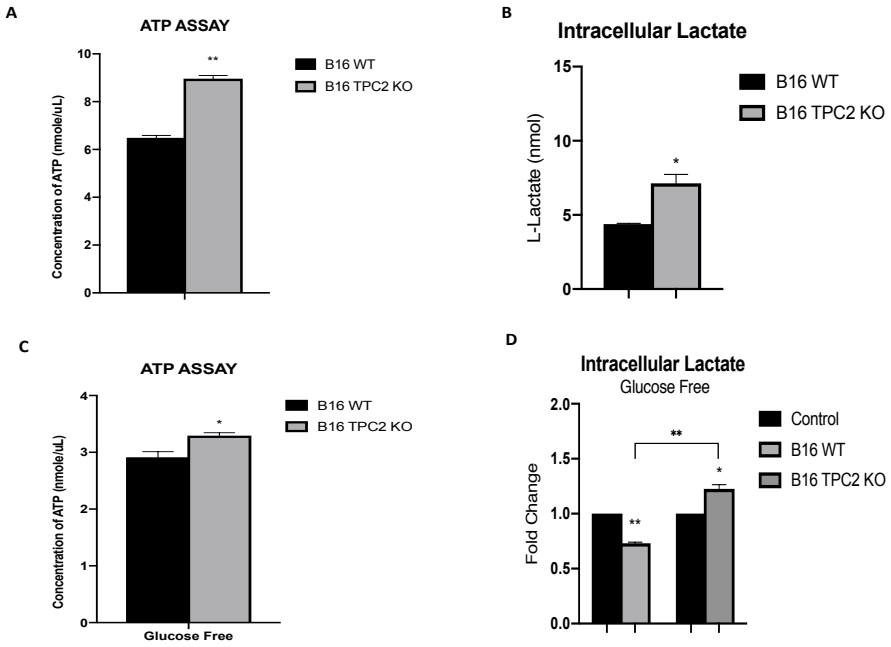

Figure 20. Intracellular ATP and lactate concentration in B16 (WT and TPC2 KO) cells.
A) Intracellular ATP in B16 WT and TPC2 KO cells. B) Intracellular lactate. C) Glucose deprivation effect on intracellular ATP. D) Glucose deprivation effect on intracellular lactate. Results obtained after incubating cells for 24 hours in normal media (supplemented with pyruvate, glucose, and glutamine) or normal media without glucose.

The Seahorse XF was used to detect oxygen flow, via OCR, and proton flux, via ECAR, in the media. Under baseline settings, B16 KO cells displayed an increase in OCR/ECAR ratio. This increase is a result of both a rise in oxygen consumption and extracellular acidification. Seahorse XF analysis was also conducted when cells were grown in a glucose-free culture. In the absence of glucose, the OCR of both cell lines increased, indicating a shift towards OXPHOS. ECAR followed the same pattern in this condition. The overall OCR/ECAR ratio between B16 WT and KO cells did not differ significantly (Figure 21). In the absence of the glycolysis source, glucose, both CHL-1 and B16 KO cells demonstrated an increase in their OCR. Additionally, the level of intercellular lactate was found to be elevated, which may indicate that these cells are utilizing pyruvate as a means of producing lactate. Pyruvate and lactate could then both be used to feed mitochondria in order to generate the necessary quantity of energy.

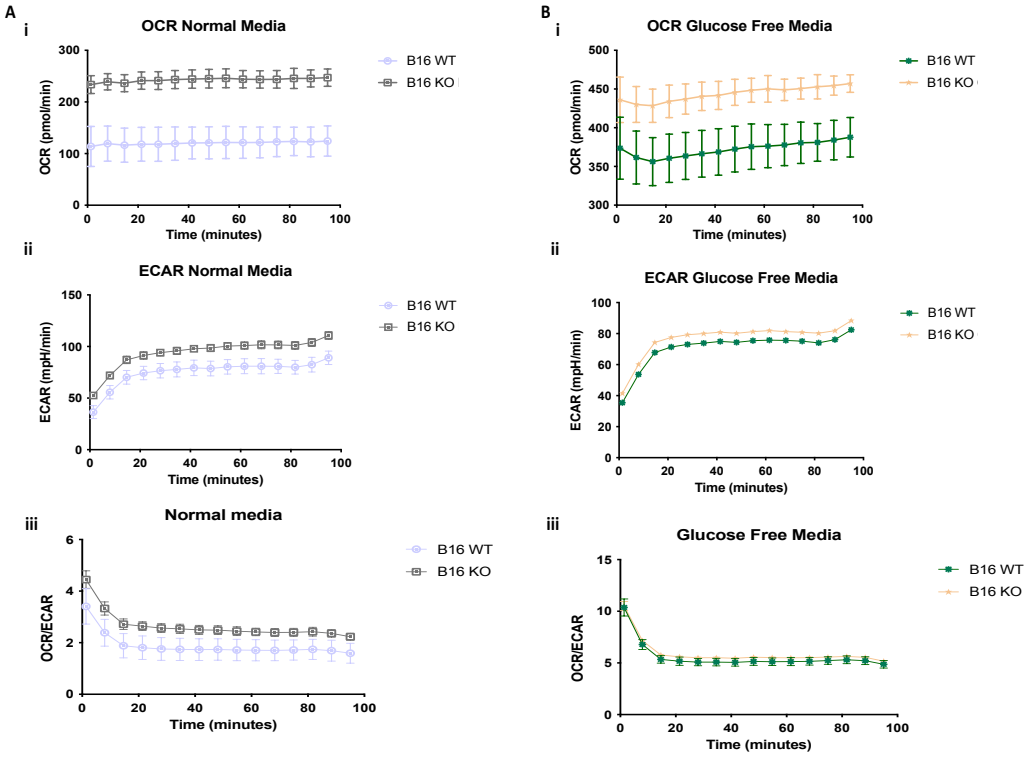

Figure 21. Intracellular ATP and lactate concentration in B16 (WT and TPC2 KO) cells.
A) Intracellular ATP in B16 WT and TPC2 KO cell lines. **B)** Intracellular lactate. **C**) Glucose deprivation effect on intracellular ATP. **D)** Glucose deprivation effect on intracellular lactate. Results obtained after incubating cells for 24 hours in normal media (supplemented with pyruvate, glucose, and glutamine) or normal media without glucose.

As a result, it is crucial to examine the mitochondria in the TPC2 KO cells. The mitochondria of cancer cells are structurally and functionally distinct from those of normal cells (94). Mitochondrial membrane potential (MMP) is an important indicator of mitochondrial activity because it reflects the process of electron transport and oxidative phosphorylation, which is the primary driver behind ATP production (95). Here, we stained cells with JC-1, a cationic dye that accumulates in mitochondria that are in an active state. At high concentrations (due to a high mitochondrial membrane potential), the dye aggregates to produce red fluorescence, whereas at low concentrations, JC-1 is predominantly a monomer that emits green light. Consequently, a decrease in the total fluorescent count indicates depolarization, whereas an increase indicates hyperpolarization. CHL-1 WT cell MMP did not demonstrate a significant increase in finished supplementary media (Figure 22A). CHL-1 KO cells, on the other hand, exhibited a significant increase in JC-1 dimers when grown in stressed conditions, that is media containing 1% FBS (Figure 22B).

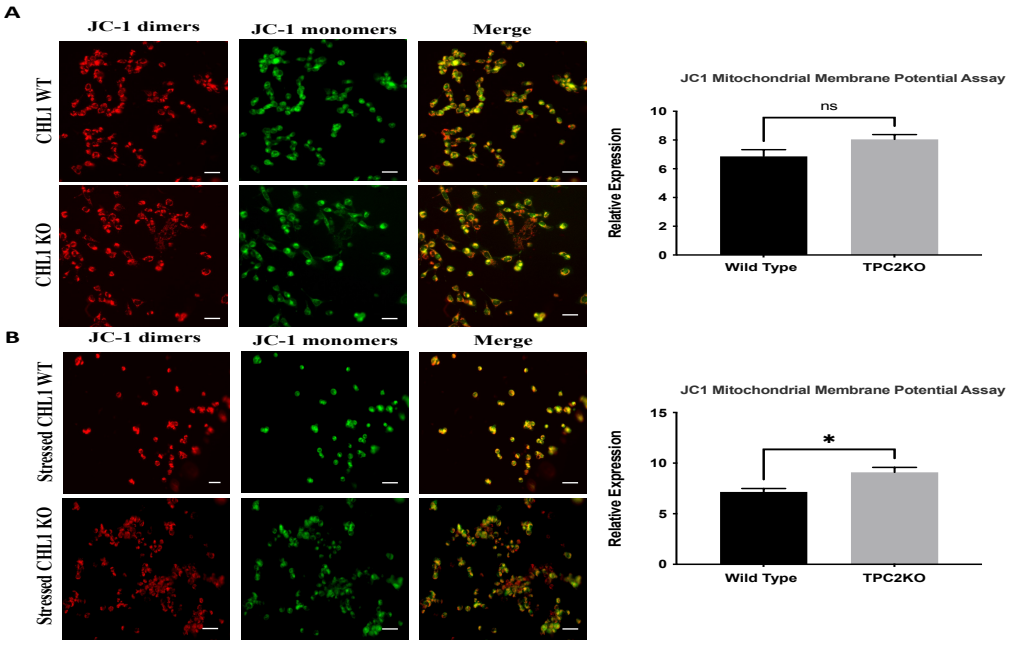

Figure 22. mitochondrial membrane potential as visualized by JC-1 staining in CHL-1 (WT and TPC2 KO).

A) Representative fluorescence images of CHL-1 cells grown in normal media captured after 24 h (h) stained with JC-1 and observed using fluorescent microscopy. Graph showing the ratio of the intensity of red to green fluorescence (JC-1 aggregate and JC-1 monomer). B) Stressed CHL-1 cells which were grown in 1% FBS media. Data represented are the mean ± SD of 5 separate experiments. * $p \leq 0.05$. The scale bar represents 20 µm.

MMP staining on B16 cells yielded comparable results to CHL-1 cell lines. Stressed B16 KO cells exhibited a greater mitochondrial membrane potential (Figure 23A, B).

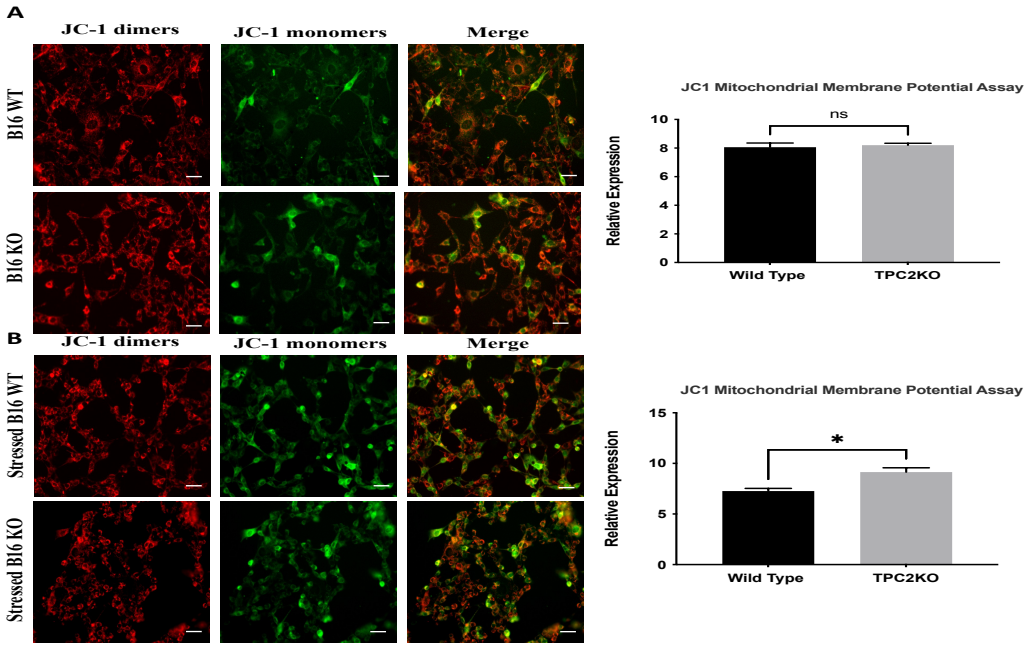

Figure 23. Mitochondrial membrane potential as visualized by JC-1 staining in B16 cells (WT and TPC2 KO). A) Representative fluorescence images of B16 cells grown in normal media captured after 24 h (h) stained with JC-1 and observed using fluorescent microscopy. Graph showing the ratio of the intensity of red to green fluorescence (JC-1 aggregate and JC-1 monomer). **B)** Stressed B16 cells which were grown in 1% FBS media. Data represented are the mean ± SD of 5 separate experiments. * $p \leq 0.05$. The scale bar represents 20 µm.

As shown in Figure 24A and B, the KO cells for both cell lines exhibited a significant upregulation of their MMP when maintained under a stressful condition, whereas WT cells exhibited no significant change in JC-1 dimers. To determine how TPC2 KO cells regulate their mitochondria differently, the expression of AKT/mTORC1 was analyzed. mTOR is a crucial regulator of mitochondrial biogenesis, as it regulates the expression of key factors in the regulation of mitochondrial biogenesis at both the transcriptional and translational levels (96). As a result, both KO cell lines exhibited a dramatic increase in mTOR expression, which may explain why KO cells respond differently to stress (Figure 24C, D). Mitochondria perform numerous roles in addition to energy production, including the creation of redox molecules and the regulation of cell signalling, cell death, biosynthetic metabolism, and the production of reactive oxygen species (ROS) (97). ROS, which are widely recognised for their signalling capabilities, play a dual role in cancer. Protumorigenic signalling is facilitated by ROS, allowing cancer cells to thrive and adapt to hypoxia. ROS, on the other hand, can increase antitumorigenic signalling and initiate oxidative stress–induced cancer cell death (98). ROS levels were elevated in response to serum stress in both CHL-1 and B16 cells (Figure 24E, F). Under serum deprivation, CHL-1TPC2-deficient cells produced significantly more reactive oxygen species than WT cells. Under the same conditions, both WT and TPC2 KO B16 cells generated comparable amounts of

ROS (Figure 24E, F). All of these cellular adaptations suggest that TPC2 may play a crucial role in cellular homeostasis.

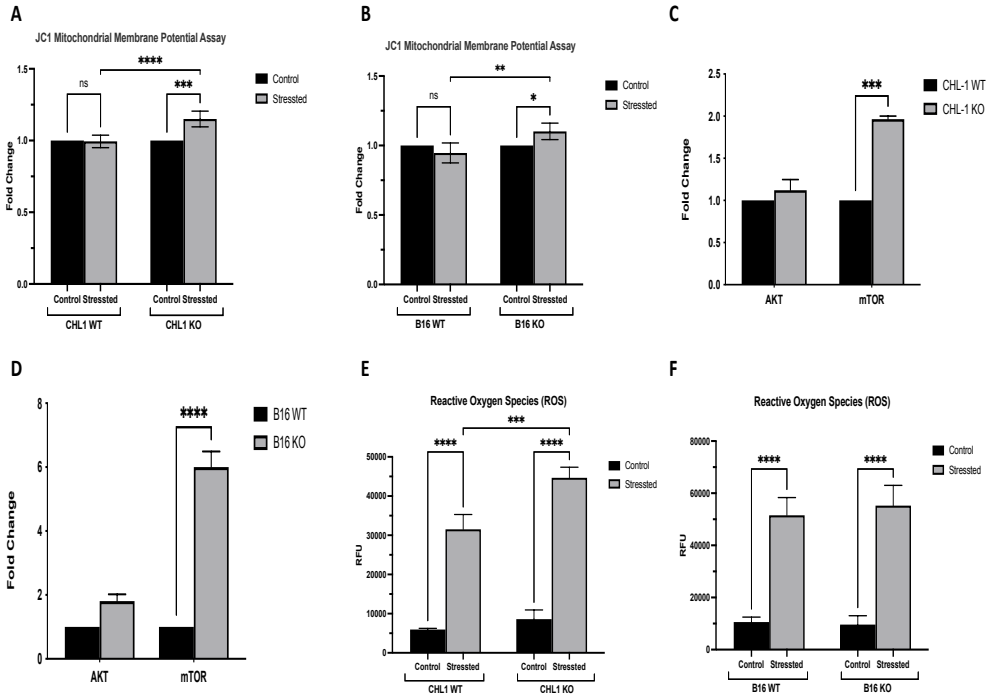

Figure 24. Mitochondrial membrane potential intensity fold change, related gene expression and ROS level in CHl-1 and B16 cell lines.

A) Fold change of quantities staining analysis of JC-1 in CHL-1 cells in normal and stressed conditions. **B)** JC-1 fold change in B16 cells. **C)** q-PCR analysis of AKT and mTOR in CHL-1 WT and TPC2 KO cell lines. **D)** q-PCR analysis of AKT and mTORC1 in B16 WT and TPC2 KO cell lines. **E)** The level of ROS in CHL-1 WT and KO cells under normal and 1% FBS supplemented media. **F)** ROS level in B16 cell line. Data represented is the mean ± SD of 5 separate experiments. * $p \leq 0.05$, ** $p \leq 0.001$, ****$p \leq 0.0001$.

Cellular cytoskeleton

The bioinformatic examination of differentially expressed proteins in TPC2 KO cells revealed that the cytoskeleton of the cells had been altered, which provides another phenotype to analyze further. Actin binding and cell adhesion molecule binding categories were altered as shown by CHL-1 KO cell proteomic analysis. In order to acquire a deeper understanding, microtubules and β-actin were stained and their co-localization in CHL-1 WT and TPC2 KO cells was examined (Figure 25A). In relation to WT cells, the value of Pearson's correlation coefficient in the KO cells was lower (Figure 25B, C).

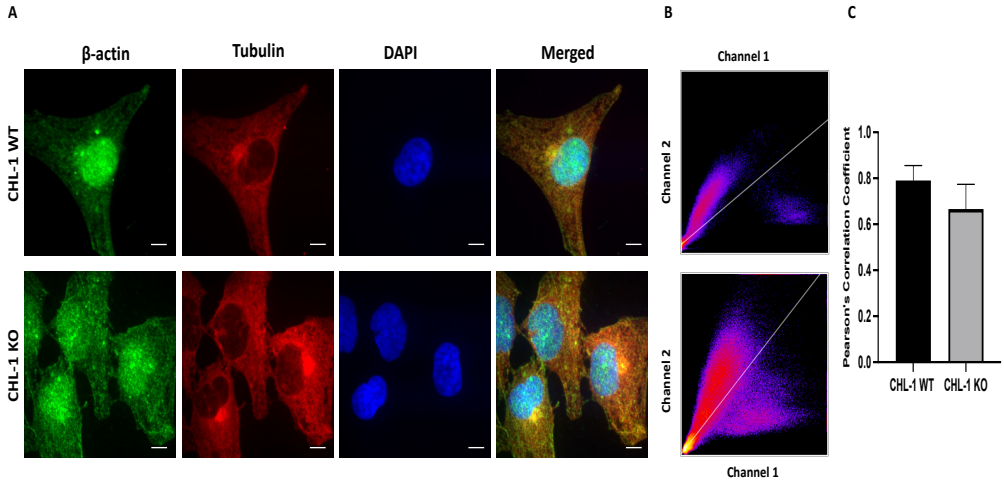

Figure 25. Immunofluorescence localization of microtubules and β-actin in CHL-1 (WT and TPC2 KO) cells

A) CHL-1 WT and KO cells showing microtubules (red), β-actin (green) and nuclei (blue). **B)** 2D Histogram of Intensity Relationship of cells in A. Channel 1 is correlated to β-actin while channel 2 represents tubulin. **C**) Pearson's correlation coefficient values for colocalization. The average Pearson's correlation coefficients ± SEM were calculated from five randomly selected cells. ****, $P < 0.0001$. The scale bar represents 10 µm.

In B16 KO cells, actin cytoskeleton and nuclear envelope groups were altered. These changes were revealed as lamin B, tropomyosin 3, Pdlim5; PDZ and LIM domain 5 and CTTNBP2 N-terminal like, which were significantly upregulated. As illustrated in Figure 17A and 17C, fascin was significantly downregulated. Tropomyosin 3, Pdlim5, and CTTNBP2 are involved in the organization of the actin cytoskeleton, whereas lamin B is essential for nuclear structure and, together with other lamin family members, contributes to the formation of the nuclear matrix (99–102). With relation to the above, the co-localization of microtubules and actin in B16 WT and TPC2 KO cells was investigated (Figure 26A). The value of Pearson's correlation coefficient in KO cells was significantly reduced compared to that in WT cells (Figure 26B, C).

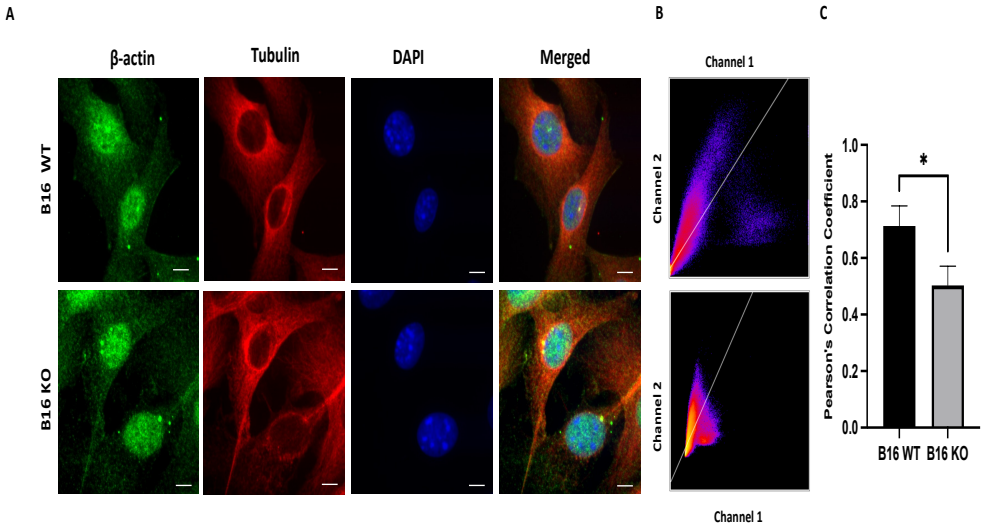

Figure 26. Immunofluorescence localization of microtubules and β-actin in B16 (WT and TPC2 KO) cells.

A) B16 WT and TPC2 KO cells showing microtubules (red), β-actin (green) and nuclei (blue). **B)** 2D Histograms of Intensity Relationship of cells in A. Channel 1 is correlated to β-actin while channel 2 represents tubulin. **C**) Pearson's correlation coefficient values for colocalization. The average Pearson's correlation coefficients ± SEM were calculated from five randomly selected cells. *, $P < 0.05$. The scale bar represents 10 µm.

TPC2 and Melanin

Over recent years, researchers have been examining the role of melanin in melanoma, specifically the effect of melanin pigmentation on the metastatic behaviour of melanoma cells. To date, however, the results have been ambiguous(103). TPC2-GFP overexpression has been demonstrated to change the melanin content of the MNT1 melanoma cell line in a transitory manner (58). TPC2-deficient melanosomes exhibited an alkalinization of the lumen pH, which increased the activity of tyrosinase, the enzyme responsible for melanin formation. In addition, MNT1 TPC2 KO cells exhibited larger melanosomes than MNT1 WT cells (58). Melanin content or production per cell have been commonly utilised to compare melanin content in different cell lines or at various phases of growth (e.g., growing stage and senescent stage)(104). When cells reach full confluence *in vitro*, the colour shift in the medium can be detected vividly. As demonstrated in Chapter 1, B16 TPC2 KO cells grow faster than WT cells. The melanin was evaluated at two distinct time intervals. The first time point was after three days, when cells were still growing and had not reached full confluence; the second time point was after five days, when both WT and KO cells had reached full confluence. After three days, the content and release of melanin dramatically increased in B16 KO cells. However, after five days when both cell lines were fully confluent, there was no difference between WT and KO cells (Figure 27A, B). Tyrosinase and melanoregulin were evaluated

in order to assess the molecular changes in the KO cells. Tyrosinase catalyses the first two stages of tyrosine to melanin synthesis (105). Figure 27D illustrates a higher level of tyrosinase expression in TPC2 KO cells, which is consistent with earlier studies investigating the relationship between TPC2 and melanin(58). MREG, or melanoregulin, is a cargo-recognition protein that connects cytoplasmic vesicles to the transport machinery (106). MREG is involved in the movement of melanosomes from the cell's periphery to its centre. MREG overexpression in melanocytes results in the hyperaccumulation of melanosomes at microtubule minus ends, which coalesce at the microtubule organising centre (MTOC) close to the nucleus (107,108). MREG was considerably elevated in TPC2 KO cells, and three-dimensional imaging revealed an increase in melanosomes around the cell periphery (Figure 27C, D). These observations provide further evidence that TPC2 has a function in the production of melanin and is also involved in the trafficking of melanosomes.

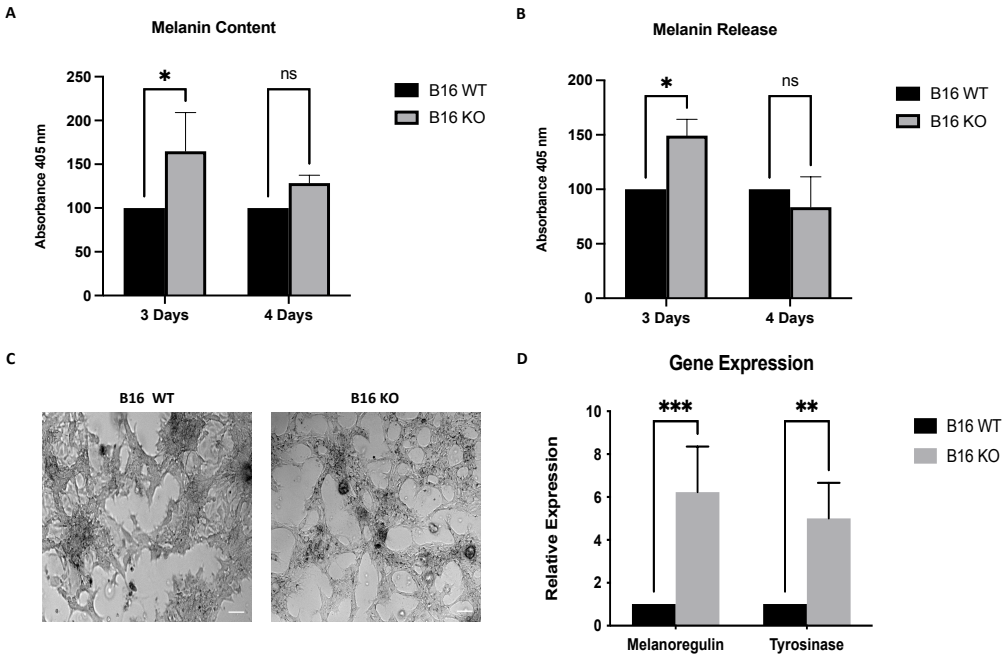

Figure 27. Effects of TPC2 knockout on melanin release in B16 murine melanoma cells.
A) Intracellular melanin content of WT and TPC2 KO cells in basal conditions at 72h and 120h. B) Melanin release assay on WT and TPC2 KO cells in basal conditions at 72h and 120h. C) 3D culture of B16 WT and KO cells. Cells were maintained in 3D culture condition for 10 days. D) q-PCR analysis of melanoregulin and tyrosinase in B16 WT and TPC2 KO cell lines. The scale bar represents 20 µm.

Discussion

Proteomics is gaining popularity in cancer research. By analyzing protein expression patterns, proteomics-based technologies can identify potential biomarkers and classify malignancies. Proteomics has also been utilized to decipher how signalling pathways in tumour cells are altered, expanding our understanding of how to target various pathways for cancer therapy(83).

In this chapter, the proteomic signatures of CHL-1 and B16 TPC2 KO cell lines were analyzed in comparison to their WT counterparts. The differential expression of proteins between WT and KO cells enabled us to characterize TPC2's involvement in a variety of critical pathways and processes.

Out of 2772 identified proteins, 303 proteins were highly expressed in the CHL-1 cell line. Gene set enrichment analysis (GSEA) was used to determine the alterations in gene ontology and signalling pathways associated with differentially expressed proteins in CHL-1 KO cells using WebGestalt (WEB-based Gene SeT AnaLysis Toolkit). The three categories of enrichment were cellular components, biological processes, and molecular activities. The enrichment analysis of gene ontology annotations associated with these categories revealed enrichment in the intercellular junction, actin cytoskeleton, endoplasmic reticulum, extracellular matrix, mitochondrial inner membrane, regulation of metabolic processes, organelle localization, cytoskeleton organization, regulation of intracellular transport, and sensitivity to oxygen

levels. Additionally, proteins were assigned to Reactome, KEGG, and Wikipathway pathways in order to obtain insight into pathways that were enriched in TPC2 KO samples. The TGF-beta receptor complex, WNT signalling, small molecule transport, Rho GTPase signalling, cell-cell communication, TGF-beta signalling, cell cycle, focal adhesion-PI3K-Akt-mTOR signalling, and DNA Damage Response were all significantly enhanced.

The B16 cell line showed 114 differently expressed proteins out of 2742 identified proteins. The GSEA analysis identified the following categories as enriched: vesicle membrane, trans-Golgi network, transport vesicle, endosomal component, viral response, cell-cell signalling via Wnt, fatty acid metabolic pathway, and protein localization to the cytoskeleton. Further, proteins were assigned to Reactome and KEGG pathways in order to gain a better understanding of pathways that were enriched in B16 KO samples. We found that proteins related to the immune system, ISG15's antiviral mechanism, interferon signalling, cytokine signalling in the immune system, MAPK family signalling cascades, RIG-I-like receptors, and autophagy, are all upregulated. In general, the proteomic signatures of KO cell lines revealed intriguing categories that warrant further investigation. Metabolic regulation, organelle location, and cytoskeleton arrangement were all significantly altered in both cell lines.

As a result, the bioenergetic phenotype of TPC2-deficient cells was investigated. Normal cells derive the majority of their energy from mitochondrial oxidative

phosphorylation (OXPHOS), which is more efficient and produces more adenosine triphosphate (ATP) than glycolysis. Nonetheless, one of the metabolic characteristics of cancer cells is their voracious glucose uptake for aerobic glycolysis. The German scientist Otto Warburg first identified this inefficient method for energy production in cancer cells in the 1920s, since then it has been known as the Warburg effect (109). Cancers are tremendously heterogeneous diseases, and each malignancy has its own metabolic characteristics. Even within a single malignancy, cells are diverse, and their metabolic characteristics differ. However, despite the presence of aerobic glycolysis in malignant tumours, OXPHOS still plays a significant role in cancer energy production (110). TPC2 depletion increased ATP synthesis in both CHL-1 and B16 TPC2 KO cells relative to WT controls; however, whereas knockout decreased lactate production in CHL-1 cells, knockout increased lactate production in B16 cells. This implies that TPC2 deficiency enhances anaerobic respiration in B16 cells but decreases it in CHL-1 cells. The OCR/ECAR ratio confirmed the TPC2 KO cells' metabolic shift. CHL-1 TPC2 KO cells have a lower OCR/ECAR ratio than WT cells, indicating they are more aerobic. In glucose-free media, TPC2 KO cells showed increase in oxygen consumption and intercellular lactate. OCR/ECAR increased in B16 KO cells in complete media. In the absence of glucose, B16 KO cells increased their oxygen use and lactate generation.

This raises questions regarding the molecular mechanisms driving these distinctions, as well as the possible functional significance of how changes in TPC2 expression alter tumour cell properties depending on whether the changes occur in a primary tumour or one that has metastasized. Interestingly, a recent study reported that knocking out TPC2 in another type of cancer cell, hepatocellular carcinoma cells, resulted in a shift toward OXPHOS in glucose-free medium(111). Shifting toward OXPHOS raises questions about the status of the mitochondrion in KO cells. Cancer cell mitochondria are physically and functionally unique from normal cell mitochondria [89]. Mitochondrial membrane potential (MMP) is a significant indication of mitochondrial activity because it reflects the process of electron transport and oxidative phosphorylation, the fundamental generator of ATP synthesis [90]. Under stress conditions, KO cells exhibited a significant capacity to hyperpolarize mitochondria by elevating MMP in both cell lines. In addition to making energy, mitochondria also make redox molecules, control cell signalling, cell death, biosynthetic metabolism, and make reactive oxygen species (ROS) [92]. ROS, whose signalling abilities are well-known, have a dual role in cancer. ROS facilitate pro-tumourigenic signalling, allowing cancer cells to survive and adapt to hypoxia. ROS can boost antitumourigenic signalling and initiate oxidative stress-induced cancer cell death [93]. CHL-1 and B16 cell lines did not exhibit a significant change in ROS levels under baseline conditions. However, serum

starvation drastically increased ROS levels, and CHL-1 KO cells were able to produce more than their WT counterparts. Alterations in the generation of energy and adaptations to various stress conditions suggest that TPC2 may play an important part in the process of cellular homeostasis.

Homeostasis is the mechanism through which an organism maintains balance while adapting to survival-optimal environmental conditions. Consequently, precise coordination between cellular compartments is becoming a vital part of cellular homeostasis. The molecular elements that facilitate this intracellular communication, on the other hand, are still being identified. In the process of fine-tuning cell metabolism and function, autophagosomes, lysosomes, and mitochondria take the lead. Endosomes and lysosomes are essential organelles that link nutrition and metabolic status with responses such as autophagy and organelle biosynthesis(112). Due to elevated biosynthetic needs, hyperproliferation, mutational load, immunological attack, and oxidative stress, cancer cells are continuously exposed to stress. Cancer cells demonstrate increased activity of homeostatic mechanisms to maintain the proteome's functional condition in response to these stresses (113). The mechanistic target of rapamycin (mTOR) synchronizes many environmental cues to regulate a variety of cellular activities, including protein translation, cell growth, proliferation, metabolism, migration, and survival. In mammalian cells, mTOR works as two signalling complexes: mTOR complex 1 (mTORC1) and

mTOR complex 2 (mTORC2)(114). TPC2 is necessary for efficient growth development transition in Dictyostelium and modulates mTORC1 activity to achieve this (115). In numerous models, the crosstalk between TPC2 and mTOR has been demonstrated. TPC2 regulates a Na^+ conductance that is blocked by mTOR(116). In pulmonary arterial myocytes, TPC2 also appears to contribute to autophagy termination by enabling mTOR reactivation (117). Therefore, shifts in cellular metabolism under glucose deprivation and the induction of mitochondrial membrane potential under serum deprivation in TPC2 KO cells may be attributable to mTOR's differential adaptation to these conditions.

The cytoskeleton is a complex network of highly structured intracellular filaments that controls cell shape, division, functions, and interactions in human organs and tissues. It is well established that the cytoskeleton has a role in cancer. The cytoskeleton has the potential to stimulate cell proliferation and activate oncogenes, leading to cancer progression (118,119). The co-localization of microtubules and actin was examined in WT and TPC2 KO cells. Pearson's correlation coefficient was generally lower in KO cells than in WT controls. Mechanotransduction of actin is critical for metastasis and differentiation of epithelial cells into mesenchymal ones (120). Intracellular Ca^{2+} is a critical signalling agent that regulates a variety of cellular processes, including migration. When Ca^{2+} levels are elevated intracellularly, it binds to actin and promotes a conformational shift in its structure. This enhances the

cytoskeleton's fluidity and alters its mechanical characteristics, hence boosting cell motility in cancer (121,122). Our findings suggest that TPC2 may play a role in the regulation of the cytoskeleton.

Melanoma is a malignant tumour that arises from altered melanocytes, which typically produce melanin (123). In contrast to melanocytes, where melanin synthesis is controlled by several stimuli and serves a specific biological function, melanin pigmentation in melanoma is significantly dysregulated (124,125). The significance of melanin in melanoma, specifically the effect of melanin pigmentation on the metastatic activity of melanoma cells, has been intensively studied for years, with ambiguous results (126,127). It is generally accepted that during the process of melanin synthesis, melanoma cells become less aggressive; thus, the formation of melanin requires the involvement of particular genes that decrease invasion. However, what occurs after the pigment has been created is something that is still up for debate(128).

A melanosome-mediated contact between melanoma cells and the microenvironment has been demonstrated recently (129) and shown to contribute to the formation of the primary tumour niche through fibroblast accumulation in the dermis prior to melanoma invasion. Melanosome content is critical for tumour niche establishment and reprogramming distant fibroblasts to facilitate metastasis (130). TPC2 has been shown to be expressed on the melanosome membrane and has been linked to the regulation of human

pigmentation in recent investigations. TPC2 KO affects the pH and size of the melanosome luminal membrane in MNT1 cell line. These TPC2 KO cells had a higher melanosome luminal pH than WT cells, resulting in increased tyrosinase activity, a critical enzyme in melanin production (58). It can be difficult to determine the melanin content of pigment-containing tissues or cultured cells. Melanin production can be determined using the melanin content and cell count at the beginning and completion of a culture to compare the melanin concentration at various stages of the culture (104). Here, we found that B16 KO cells displayed an increase in melanin content and release after 72 hours of culturing, whereas after 5 days, this significant difference disappeared. Tyrosinase is an important enzyme in melanogenesis. Tyrosinase is responsible for the first two steps of the melanin-to-tyrosine conversion (105). This enzyme was induced in TPC2 KO MNT melanoma cells, followed by the formation of alkaline melanosomes (58). Therefore, TPC2 is essential to regulate melanosome pH in B16 KO cells. We also evaluated the melanoregulin gene, which plays significant role in melanogenesis. Melanoregulin, also known as MREG, is a cargo-recognition protein that connects cytoplasmic vesicles to the transport machinery. MREG is involved in the transport of melanosomes from the cell's periphery to its centre (106,108). MREG overexpression in melanocytes results in the hyperaccumulation of melanosomes at microtubule minus ends, which coalesce at the microtubule organising centre (MTOC)

adjacent to the nucleus(107). In TPC2 KO cells, MREG expression was significantly enhanced, and 3-D imaging revealed accumulation of melanosomes near the nucleus. After five days, there was no difference in melanin content and release between WT and KO cells. This may result from how these cells react to stress. At the conclusion of the experiment, the cells were over-confluent, which triggered stress responses in the cells. As previously demonstrated, KO cells appear to respond differently to stress conditions such as serum and glucose deprivation, which may explain why the melanin level increase was slowed. MTOR can have a negative regulatory effect on melanogenesis (131). As a result of the increased mTOR expression in KO cells, melanogenesis may regulate differently in this case. The effect of melanin presence on the elasticity of melanoma cells has been neglected for a long time, despite the fact that pigment granules were discovered to be extremely rigid and difficult to bend (132). *In vitro*, the pigment granules reduced the invasive capabilities of melanoma cells in a manner depending on the amount of granules (133). Melanoma cells that had melanin were less able to spread within mice than those that lacked the pigment (134).

Overall, in this chapter, the proteomic signature of TPC2 KO cells suggests involvement of TPC2 in various cellular processes, including cellular metabolism and cytoskeleton regulation. Moreover, TPC2 involvement in melanin regulation has been confirmed in the B16 cell line (Figure 28).

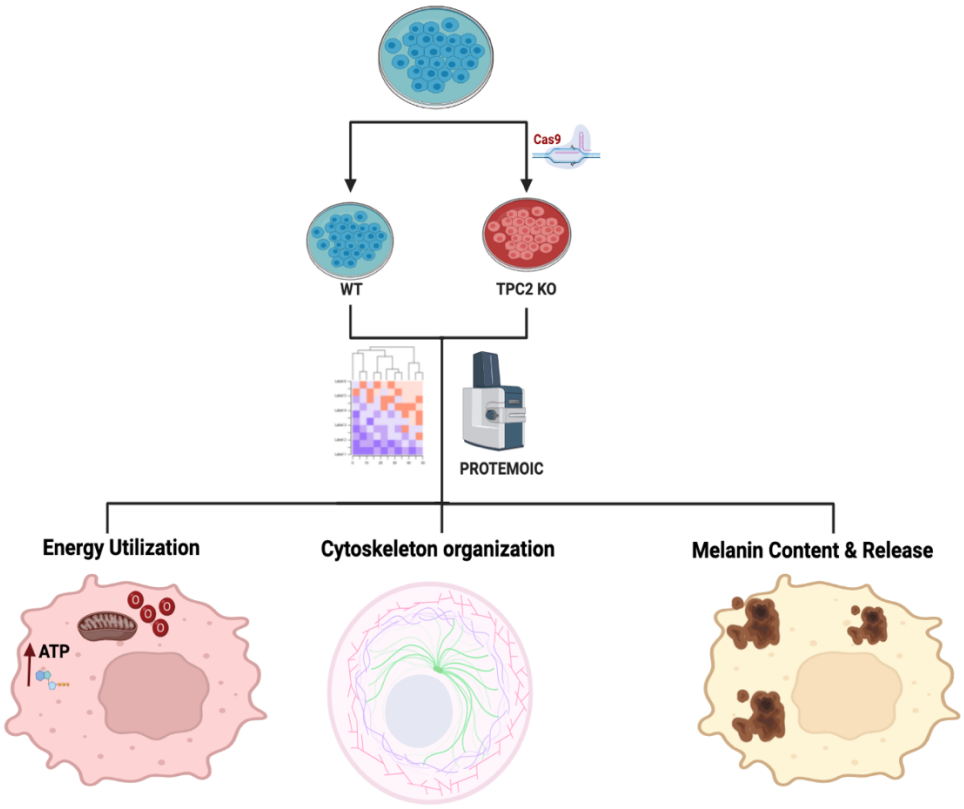

Figure 28. An overview of the chapter's methods and findings.

Chapter 5

In vivo characterization of TPC2 KO melanoma cell lines

TPC2 deletion in melanoma cell lines impaired tumour growth

In spite of the numerous benefits of *in vitro* cancer models, *in vivo* systems are necessary for evaluating the contribution of the tumour microenvironment, host immune system, and angiogenesis in tumourigenesis and metastasis. Subcutaneous injection of cancer cells into a mouse often results in tumour growth at the injection site. Here, we injected B16 WT and KO cells and monitored tumour growth, and the effect on the histopathology of various organs. Early post-transplantation days revealed no significant difference in tumour volume between the two groups of mice. However, mice injected with WT B16 melanoma cells demonstrated significantly greater tumour growth than mice injected with B16 TPC2 KO cells. This pattern persisted throughout the experiment (Figure 29A). The KO group had a modest reduction in body weight at the start of the experiment, but this was not statistically significant. Toward the end, both groups demonstrated a slight decrease in body weight, which is consistent with an increased tumour burden. Throughout the experiment, there was no statistically significant difference between the groups (Figure 29B).

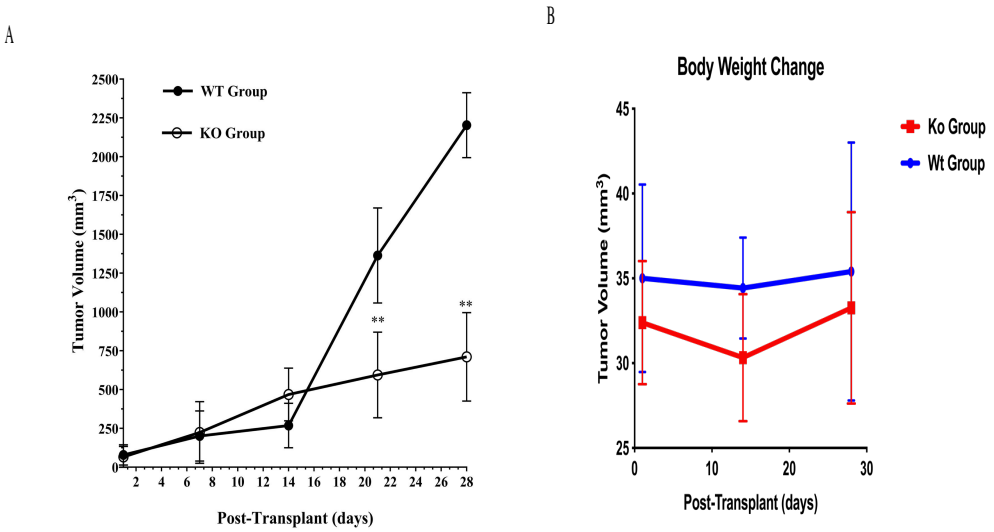

Figure 29. Tumour growth and body weight change in mice subcutaneously injected with either WT or TPC2 KO melanoma cells and monitored *in vivo*.

A) Change in tumour growth. **B)** Body weight monitoring during experiment. Data was presented as mean ± SD.

Pathological alterations in liver and spleen

To examine the effect of TPC2 KO cells on liver and spleen, histopathological analysis was performed at the end of the *in vivo* experiment. This analysis was performed on organs from animals that were not injected as a control, organs from animals injected with B16 WT cells, and organs from animals injected with B16 KO cells. Mice control liver showed normal appearance of hepatic tissue consisting of veins surrounded by strands of hepatocytes separated from each other by blood sinusoids with abundant rod-shaped Kuppfer cells (Figure 30A.a). In the second group, the livers of the B16 WT injected group displayed relative healthy hepatic structure with small foci of inflammatory cells besides activation of Kuppfer cells in the sinusoids (Figure 30A.b). Meanwhile, the hepatic structure in the third group, the B16 TPC2 KO injected group, revealed severe alterations manifested by incidence of fibrosis surrounded by massive infiltrations which are deposited in wide necrotic areas (Figure 30A.c), Moreover, congested veins with erythrocytes and oedema with their walls looking thickened appeared in the section in addition to cytoplasmic degeneration of hepatocytes (Figure 30A-d).

In spleen tissues, mice control spleen displayed normal architecture with well-defined white pulp consisting mainly of lymphocytes, and red pulp which consisted of splenic parenchyma called cords of Billroth (Figure 30B.a). The B16 WT injected group showed a well-defined splenic structure (Figure 30B.b), with less area and volume of lymph nodes compared to the control group. In contrast, the third group, B16-TPC2 KO injected mice, showed marked pathological alterations in the spleen represented by hyaline degeneration in the lymph nodes which in turn looked minimized and showed significant decrease of lymph node areas and volumes compared to the control group, an ill-defined appearance with white pulp diffused in the red pulp which was mostly congested, and also observed was the presence of numerous large macrophages (Figure 30B.c-d). Overall, the liver and spleen tissues of animals injected with B16 KO cells exhibited far more pathological characteristics than those of mice injected with WT B16 melanoma cells.

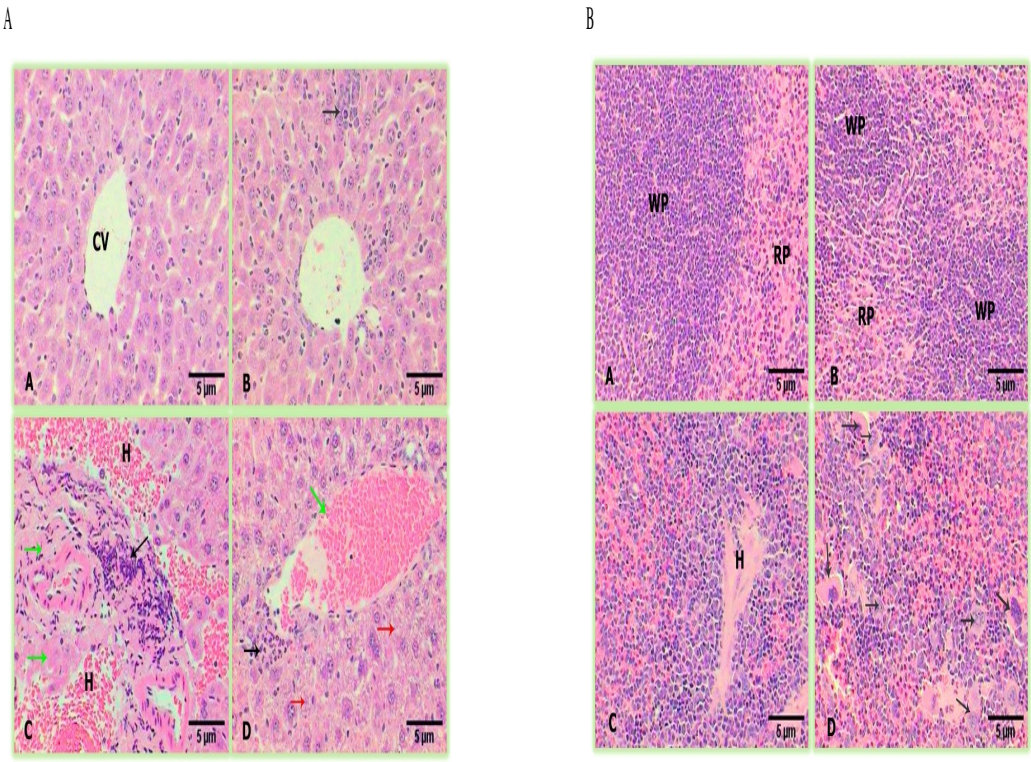

Figure 30.Photomicrographs of liver and splenic tissues.

(A) Liver tissue, a. control group showing normal structure, b. liver from mice injected with B16 WT cells revealing small foci of infiltrative cells (black arrow), c. liver from mice injected with B16 TPC2 KO cells displaying fibrosis (green arrows) aggregations of infiltrative cells (black arrow), haemorrhage (H), d. liver from mice injected with B16 TPC2 KO cells displaying congested vein with haemorrhage and oedema (green arrow), infiltrative cells (black arrow), cytoplasmic degeneration (red arrows). (HE-400X). (**B) Spleen tissue,** (a) control spleen showing well-defined splenic structure, white pulp (WP), red pulp (RP), (b) spleen of B16 WT group revealing healthy splenic tissue white pulp (WP), red pulp (RP), (c) spleen of B16 TPC2 KO group displaying pathological changes with minimized lymph node centred with hyaline degeneration (h, (d) spleen of B16 TPC2 KO group displaying ill-defined structure, numerous large macrophages (black arrows).

Clinical association

The Cancer Genome Atlas (TCGA) has helped to establish the importance of cancer genomics, revolutionised our understanding of cancer, and even begun to change how cancer is treated in clinics (135). It is thus critical to assess the correlations between our molecular findings and cancer patient survival. GEPIA is a new advanced interactive web service that uses a standard processing pipeline to analyse the RNA sequencing expression data of 9,736 cancers and 8,587 normal samples from the TCGA and GTEx studies(136). Prognosis was determined using skin cutaneous melanoma (SKCM) in patients with high and low TPC2 expression. The overall survival time of patients in the high-expression group was substantially shorter than the overall survival time of patients in the low-expression group, according to a logrank test with a P-value of 0.013. By contrast, if we consider disease-free survival, the log-rank test reveals a non-significant P-value. It suggests that TPC2 expression could be a predictor of prognosis rather than relapse (Figure 31A, B). OncoDB's "Pathological Stage Plot" module was also utilised to examine the relation between TPC2 expression and various tumour stages. The median amount of TPC2 exposure rose in proportion to the stage of the malignancy. The medians for stages I ii, iii, and iv were 8.8, 9.4, 8.4, and 17.2 respectively (Figure 31C).

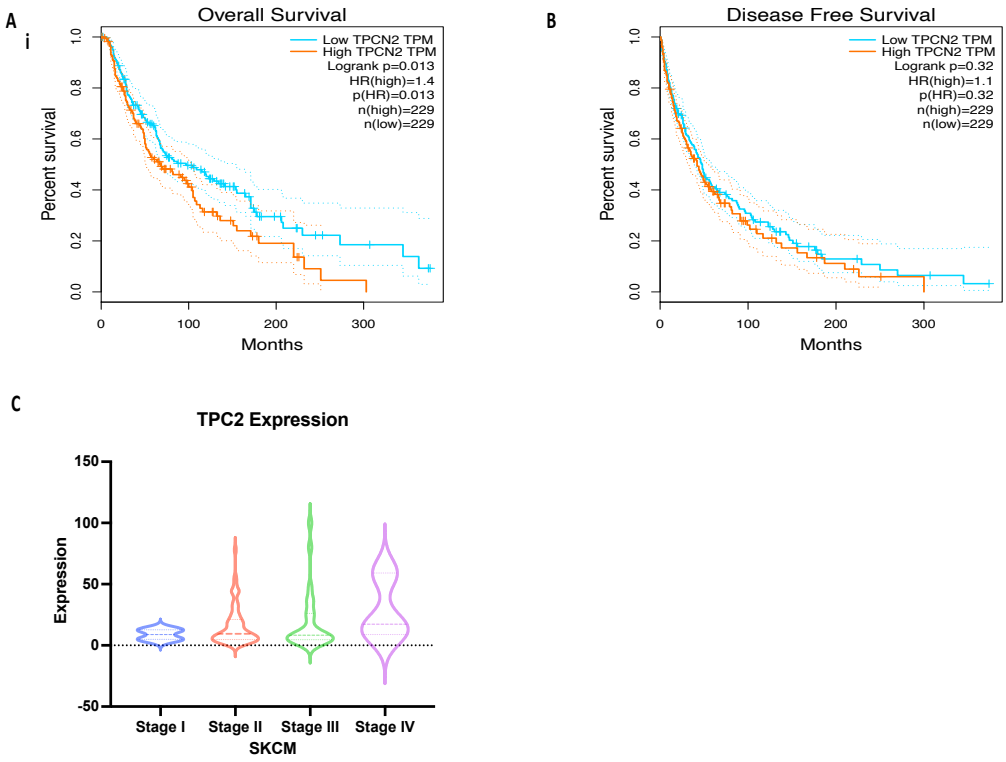

Figure 31.Kaplan–Meier survival curves for patients with high versus low TPC2 expression and the correlations between TPC2 expression and tumour stages.

(A) OS between patients with high and low TPC2 expression. There was a significant difference in OS (p = 0.0005) between the two arms. **(B)** DFS between patients with high and low TPC2 expression; there was no significant difference. DFS, disease-free survival; OS, overall survival. **C)** Violin plots showing TPC2 expression at different stages of melanoma determined via OncoDB**.** Samples number in stage I, II,III, and IV are 2, 61, 25, and 3,respectively.

TPC2 expression in melanoma subtypes was investigated further to determine its impact on overall survival. Melanoma is classified as BRAF mutant, NF1 mutant, RAS mutant, or triple WT. Only in the BRAF mutant group did high TPC2 expression result in a reduction in overall survival (Figure 32A). As previously stated, CHL-1 is a triple WT melanoma cell line and in this genetic background TPC2 expression was not found to have a substantial effect on survival (Figure 32D).

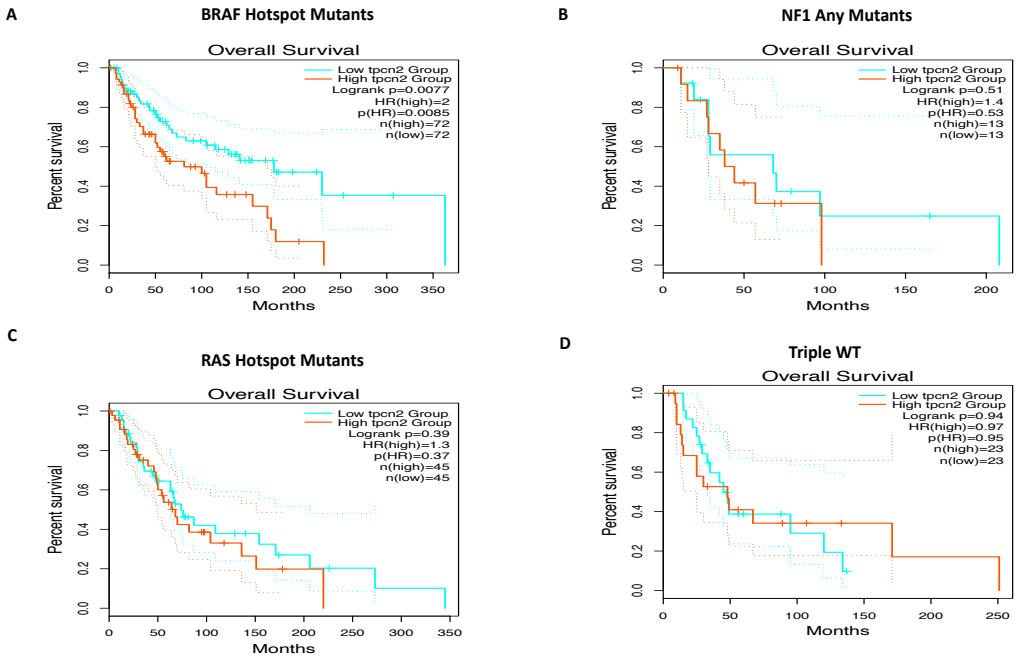

Figure 32. Kaplan–Meier survival curves for patients with high versus low TPC2 in different subtype of melanoma.

A) OS between patients with high and low TPC2 in BRAF Hotspot Mutants; there was a significant difference in OS (p = 0.0077) between the two arms. **(B)** NF1 Any Mutants (**C)** RAS Hotspot Mutants **D)** Triple WT.

Discussion

Cancer cell lines are simple to cultivate *in vitro*, allow direct comparison of experimental data, and are frequently employed to investigate the molecular principles underlying tumour cell biology. However, *in vivo* models better represent the complexity of the tumourigenic and metastatic processes in a real organism, which cannot be replicated *in vitro* (137). To examine the effect of TPC2 deficiency *in vivo*, we injected WT and TPC2 KO B16 cells subcutaneously into mice. We observed that WT B16 cells developed into a significantly larger tumour than KO cells. These *in vivo* findings are consistent with *in vitro* findings in which KO cells exhibited a severe reduction in cell growth rate after 4 days and a considerable loss in invasion potential. Angiogenesis is another trait that could contribute to this outcome. Angiogenesis is the process through which new blood vessels develop from pre-existing vessels, allowing for the progression of tumours. As the tumour grows subcutaneously, it is crucial for it to form new blood vessels. TPC2 has been identified as a major regulator of processes associated with the pathophysiology of neovascular age-related macular degeneration (138). In addition, there is evidence that TPC2 has a function in signalling pathways that promote angiogenesis triggered by VEGF (139). Consequently, when KO tumours lack TPC2, this may lead to alterations

in the vasculogenesis around the tumour, which is essential for providing growth-promoting nutrients to the tumour.

Histopathological examination showed that B16 TPC2 KO cells significantly altered the hepatic and splenic structures as compared to B16 WT cells. These data raise the question of how a smaller growing tumour might produce greater tissue damage. Immunity of the host has a crucial role in regulating tumour growth. Immunosuppression is a hallmark of the vast majority of cancer types and is crucial to the development and progression of cancer (140,141). In recent years, studies have identified myeloid-derived suppressor cells (MDSC) as a major contributor to an immunosuppressive tumour microenvironment (TME) (142). Interestingly, these MDSC were discovered to accumulate in tumour-bearing animals. Animals with cancer accumulate MDSC in the liver (143) and spleen (144). MDSC-induced liver damage was tumour-specific, as not all studied tumour models resulted in liver damage, despite the fact that MDSC proliferation was found in all models (145). Subcutaneous growth of B16 (melanoma) tumour cell lines on a C57BL/6 background results in moderate liver damage due to the accumulation of MDSC in the liver (145). All of this evidence provides a rational explanation for the histopathological abnormalities observed following injection of WT and KO B16 cells in comparison to the control group. In spite of the fact that B16 KO cells showed lesser tumourigenic traits *in vitro* and tumour growth in vivo, histopathology

analysis revealed that B16 KO cells had a worse toxic effect on the organs of the host mice than their WT counterparts. These findings suggest that TPC2 KO cells may result in an increase in MDSC accumulation in the liver and spleen. Accumulation of MDSC is the consequence of two processes: activation and expansion. MDSCs can be induced *in vitro* by a variety of tumour-derived substances, including prostaglandin E2, interleukin-6, interleukin-10, interleukin-1, transforming growth factor (TGF), stem cell factor (SCF), and proangiogenic factors including vascular endothelial growth factor (VEGF) (VEGF) (146). Interestingly, TPC2 was identified to be associated with a number of these markers (50,147,148). Therefore, the loss of a functional TPC2 may result in the over-expression of certain markers, resulting in an abnormal response of the host animal and the accumulation of excessive MDSC in organs. The latter finding further emphasises how crucial it is to combine *in vitro* and *in vivo* investigations.

The Cancer Genome Atlas (TCGA) has contributed to the recognition of the relevance of cancer genomics, redefined our understanding of cancer, and has even begun to influence how cancer is treated in clinics (149).Thus, it is crucial to determine the links between our molecular discoveries and cancer patient survival. Overall survival time was significantly shorter for patients in the TPC2 high-expression group than for those in the low-expression group. As a result, we will gain a better understanding of why TPC2 downregulation causes

tumourigenesis in certain cases, while it slows cancer progression in others, by analyzing survival in melanoma subgroups (150–152). There are four subtypes of melanoma: those with BRAF, NF1, and RAS mutations, or those that are triple WT. TPC2 overexpression resulted in a reduction in overall survival only in the BRAF mutant group (Figure 14). As highlighted, CHL-1 is a triple-WT melanoma cell line, and this is a genetic background in which TPC2 expression had no discernible influence on survival. This association demonstrates the critical role of TPC2 based on melanoma subtype. Figure 33 summarizes the approaches applied and the main findings in this chapter.

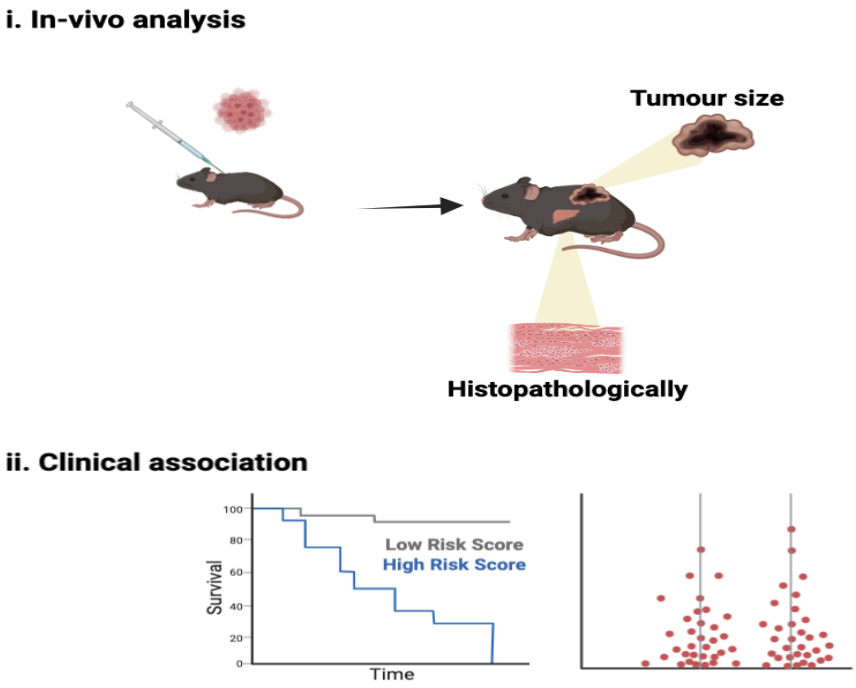

Figure 33. An overview of the chapter's methods and findings.

Chapter 6

Conclusions and future directions

Conclusions and future directions

Melanoma is a cancer of the melanocytes that has spread widely across the Western world and is on the rise (11). Furthermore, it is the most dangerous and lethal type of skin cancer, with an intrinsic resistance to both radiotherapy and chemotherapy. As a result, finding new therapeutic approaches is essential.

Tumourigenesis and metastasis

In Chapter 3, TPC2 knockout cells were generated in CHL-1 and B16 cell lines to investigate the role of TPC2 in melanoma tumorigenesis and metastasis. The CHL-1 cells are a model of human amelanotic melanoma. Neither BRAF, NRAS, nor NF1 were mutated in CHL-1 cells. CHL-1 is therefore categorized as a triple WT metastatic melanoma cell line based on the aforementioned premises. B16 cells are a highly pigmented mouse melanoma cell line widely used in melanoma research. CRISPR/Cas9 gene editing was used to create TPC2 depleted CHL-1 and B16 cell lines. Previously in this study, cancer's traits were studied by looking at its invasion potential. When CHL-1 KO cells were compared to CHL-1 WT cells, CHL-1 KO cells demonstrated a statistically significant increase in their ability to infiltrate membranes, whereas B16 KO cells exhibited decreased invasion ability. To further elucidate and validate our findings, the expression of YAP/TAZ target genes was examined in CHL-1 WT

and TPC2 KO cells. YAP/TAZ are tumour initiators and growth factors. Their activity has the potential to inhibit proliferation, invasion, and metastasis, and is frequently associated with a poor prognosis (153). It has been demonstrated that elevated YAP levels are associated with a decrease in melanoma patient survival (154). In this study several of their target genes, including ANKRD, CYR61, and CTGF, were found to be significantly up regulated. The data were also confirmed following transient inhibition of TPC2 in the human CHL-1 cell line. The expression of ORAI1, a component of SOCE, and PKC-II, were also studied in order to better understand the crosstalk between TPC-2 and YAP/TAZ. Until our recent studies, the only known connection between YAP/TAZ activity and Ca^{2+} signalling was through store-operated Ca^{2+} entry (SOCE) (82). Interestingly, TPC2 KO cells exhibited a significant decrease in ORAI1 and PKC-II expression, while STIM1 and INF2 expression remained unchanged [3]. Additionally, a decrease in ORAI1 expression was observed following TPC2 transient silencing. To establish a link between ORAI1, TPC2, and YAP/TAZ, a rescue of ORAI1 protein was performed in our TPC2 KO model and a reduction in YAP/TAZ target gene expression was observed when ORAI1 was overexpressed compared to mock-transfected cells (151). Through our collaborators, additionally, the levels of vimentin and ZEB1 was determined and they were found to be decreased when ORAI1 was overexpressed. To determine whether mechanotransduction plays a role in YAP/TAZ activation

following TPC2 knockdown, the activation of YAP/TAZ target genes and N-Cadherin was examined in conditions of extremely low cell attachment and no activation (151). This suggests that the absence of TPC2 may result in the activation of YAP/TAZ target genes and thus increased metastasis, as a result of changes in SOCE and the cytoskeleton's ability to inhibit the Hippo pathway.

Future directions

- How might a change in TPC2 expression or function affect primary and advanced melanoma cell lines?

As a side note, we have been using mouse B16-F0 cells as an example of cancer cells that originate from the primary tumour and human CHL-1 cells as an example of cancer cells that originate from the metastatic stage. Our analysis revealed striking differences in the effects of TPC2 KO on these two cell types, which may reflect the stage of the tumour from which they originate. We cannot, however, rule out the possibility that these differences are due to the cell lines' species of origin. Thereby, obtaining mouse melanoma lines derived from more advanced tumours and human melanoma lines derived from primary tumours, creating TPC2 KOs in these lines, and studying their characteristics will allow us to determine whether the differences in TPC2 KO between B16 and CHl-1 cells reflect the stage of the tumour from which they originated and the role of the genetic background of these cell lines.

- What effect does the absence of TPC2 have on the Hippo pathway?

As we have recently discovered, activation of the tumour-promoting YAP/TAZ pathway occurs when TPC2 expression is knocked out or reduced via RNA interference (RNAi). Our findings suggest that this activation is caused by a decrease in the expression of ORAI1, a key component of store-operated calcium entry (SOCE), which inhibits the Hippo pathway, a negative regulator of YAP/TAZ. It is critical to understand how the loss of TPC2, an endolysosomal cation channel, results in such decreased ORAI1 expression. This can be accomplished by examining the upstream regulation of ORAI1 gene expression and how TPC2 deficiency affects it. Additionally, it will be interesting to determine whether this link between TPC2 and SOCE is mediated by changes in Ca^{2+} signals. It will be essential to examine the activity, post-translational state, and intracellular location of individual Hippo pathway components in WT vs TPC2 KO cells and to correlate any changes to TPC2's role in Ca^{2+} signalling in order to gain insight into the relationship between TPC2 and Hippo signalling.

Proteomic signature and cellular hemostasis

Our next chapter looked at how different the proteomic signatures of CHL-1 and B16 knockout cell lines are from those of their wild-type counterparts. We were able to characterize TPC2's involvement in a variety of critical pathways and processes in CHL-1 and B16 cell lines. Following the proteomic findings, we investigated the energy utilization of WT and TPC2 KO cells. TPC2 depletion increased ATP synthesis in CHL-1 and B16 cells compared to WT cells, but increased lactate production in B16 cells. So TPC2 deficiency increases anaerobic respiration in B16 cells but reduces it in CHL-1 cells. The OCR/ECAR ratio confirmed the TPC2 knockout cells' metabolic shift. TPC2 KO cells are more aerobic than WT cells, with a lower OCR/ECAR ratio. TPC2 KO cells showed reduced aerobic respiration on glucose-free media. OCR/ECAR increased in B16 KO cells compared to WT. The previously significant difference in aerobic glycolysis was eliminated in glucose-free media.

The effect of TPC2 KO on the cytoskeleton is also noteworthy. This network of highly structured intracellular filaments controls cell shape, division, functions, and interactions in human organs and tissues. The cytoskeleton is known to play a role in cancer. The cytoskeleton can promote cell growth and activation of oncogenes, leading to cancer progression (Gaspar et al., 2015; X. Zhang et al., 2017). Microtubule and actin colocalization were studied in WT and KO cells.

Pearson's correlation coefficient was generally lower in TPC2-deficient cells than in WT cells.

The final phenotype examined in this chapter was the content and release of melanin in WT and KO cell lines. There was no difference between WT and KO B16 cell lines in the content of melanin. On the other hand, KO cells produced significantly less melanin. These results suggest that TPC2 may also regulate melanin production and secretion.

Future directions

- What relationship exists between differences in the metabolic state of various types of melanoma cells and their other biological properties?

Our research has shown that both B16 and CHL-1 TPC2 KO melanoma cells seem to have undergone a transition to a more aerobic state. Interestingly, while CHL-1 WT cells are more aerobic in normal medium than CHL-1 TPC2 KO cells, the TPC2 KO CHL-1 cells are more aerobic in glucose-free media. CHL-1 and B16 TPC2 KO cells behave in a different manner in glucose-free media, which suggests that there is a difference between the two types of cells. Our previous studies have shown that TPC2 KO decreases the invasiveness of B16 cells but increases the invasiveness of CHL-1 cells, with the latter displaying both cellular and molecular signs that TPC2 KO increases the likelihood of metastatic spread. Notably, TPC2 KO CHL-1 cells exhibit activation of two key tumorigenesis and metastasis drivers, YAP and TAZ, in contrast to B16 TPC2 KO

cells, which do not exhibit such activation. Naturally, there may be additional distinctions between B16 and CHL-1 TPC2 KO cells in melanin trafficking.

- Why do TPC2-deficient melanoma cells have a higher rate of aerobic respiration? What does this have to do with glycolysis and oxidative phosphorylation, as well as their regulation?

Understanding the molecular mechanisms that underlie this shift is critical because this will be an important discovery about the regulation of metabolism in melanoma cells. To investigate this further, the utilization rate of various metabolites in WT and KO cell lines could provide insight into the relationship between TPC2's normal role in this process and these observations. Similar investigations can be conducted in normal and glucose-free media, based on the differences observed between B16 and CHL-1 cells in these media.

- What is the relationship between TPC2 KO B16 and CHL-1 cells exhibiting enhanced metastatic potential and mechanotransduction?

Following TPC2 KO, mechanotransduction may play a role in the activation of YAP/TAZ. To further investigate this issue, it may be necessary to determine whether changes in the cell surface and cytoskeleton contribute to the activation of YAP/TAZ in the absence of TPC2 function. Indeed, our recent studies have revealed differences in the cytoskeleton of B16 and CHL-1 TPC2 KO cells when compared to WT cells. We will investigate the molecular basis for these changes and whether they contribute to our understanding of how

YAP/TAZ activity is enhanced in the absence of TPC2 function via a mechanism involving reduced SOCE. Recent research has identified Ca^{2+} permeable Piezo channels as significant transducers of mechanical stress into Ca^{2+}-dependent signals, as well as key players in the development of various cancer types (155). We will investigate whether the expression, intracellular location, and activity of Piezo channels changes in TPC2 KO cells compared to WT controls, and whether these changes are associated with the changes in ORAI1 expression and presumably SOCE activity observed in TPC2 CHL-1 cells.

In vivo studies and clinical association

In the next chapter of results, we examined the *in vivo* characteristics of B16 WT and TPC2 KO cells and their effects on other organs. Further, we correlated our molecular findings with cancer patient survival. In order to better understand the molecular processes behind tumour cell biology, cancer cell lines are routinely used to develop them. However, *in vivo* models are better at capturing the complexities of metastatic disease in a living creature, which cannot be recreated *in vitro*. We injected WT and TPC2 KO B16 cells into mice to determine the effect of TPC2 deficiency on melanoma cells *in vivo*. We noticed that WT B16 cells grew into a tumour that was much larger than the tumour formed by KO cells. Histopathological analysis revealed that KO cells dramatically affected the hepatic and splenic architecture when compared to WT cells. Next, a correlation study revealed that patients with a high level of TPC2 expression had a significantly shorter overall survival than those with a low level of TPC2. When we used a similar technique in melanoma subtypes, we discovered that overexpression of TPC2 decreased overall survival exclusively in BRAF mutants. There was no significant difference in the triple WT subgroup, which may explain why TPC2 KO in CHL-1 resulted in induction of tumourigenesis in the first place.

Future directions

- What role does TPC expression have in the tumorigenic/metastatic capacity of primary versus advanced melanoma cells *in vivo*?

We recently demonstrated that injecting WT B16 cells into mice results in significantly larger tumours than injecting TPC2 KO variants of the same cells. It will be interesting to observe the growth of metastatic melanoma cell lines *in vivo* and compare the results to our *in vivo* studies. Furthermore, hepatic and splenic architecture were drastically altered by B16 KO cells when compared to WT cells, according to histopathological analyses. In addition, it will be critical to perform the same analysis after CHL-1 injection into nude mice in order to link this to either TPC2 expression or tumour features. *In vitro*, metastatic characteristics of B16 and CHL-1 TPC2 KO cells appear to be highly distinct. Therefore, it will be critical to determine whether CHL-1 TPC2 KO cells have an increased metastatic potential *in vivo* in order to correlate *in vitro* findings with *in vivo* findings.

- Can TPC2 be a potential therapeutic target in specific melanoma subtype?

When TPC2 was overexpressed, only the BRAF mutant subtype demonstrated a substantial decrease in overall patient survival. Following on from these findings, targeting TPC2 in several cell lines derived from various melanoma subtypes and evaluating their tumourigenicity may enable us to define the specific type of melanoma that is affected by targeting TPC2.

In general, this thesis thoroughly examined the role of TPC2 in melanoma (Figure 34). We created TPC2 knockout cell lines using the cutting-edge gene editing technique CRISPR/Cas9, allowing us to compare the impact of TPC2 KO on these cell lines. The first chapter of results described the discovery of tumourigenesis and a novel connection to the YAP/TAZ pathway. The proteomic signatures of these cell lines enabled us to establish a critical connection between TPC2 and several cellular activities, including energy utilization and cytoskeleton organization. Finally, *in vivo* observations were made to confirm the *in vitro* results at the whole animal level. Additionally, a connection with overall patient survival was made, which revealed a link between TPC2 overexpression and decreased patient survival in the BRAF mutant group exclusively. These ground-breaking findings emphasize the critical role of TPC2 in melanoma and the significance of additional research in this area.

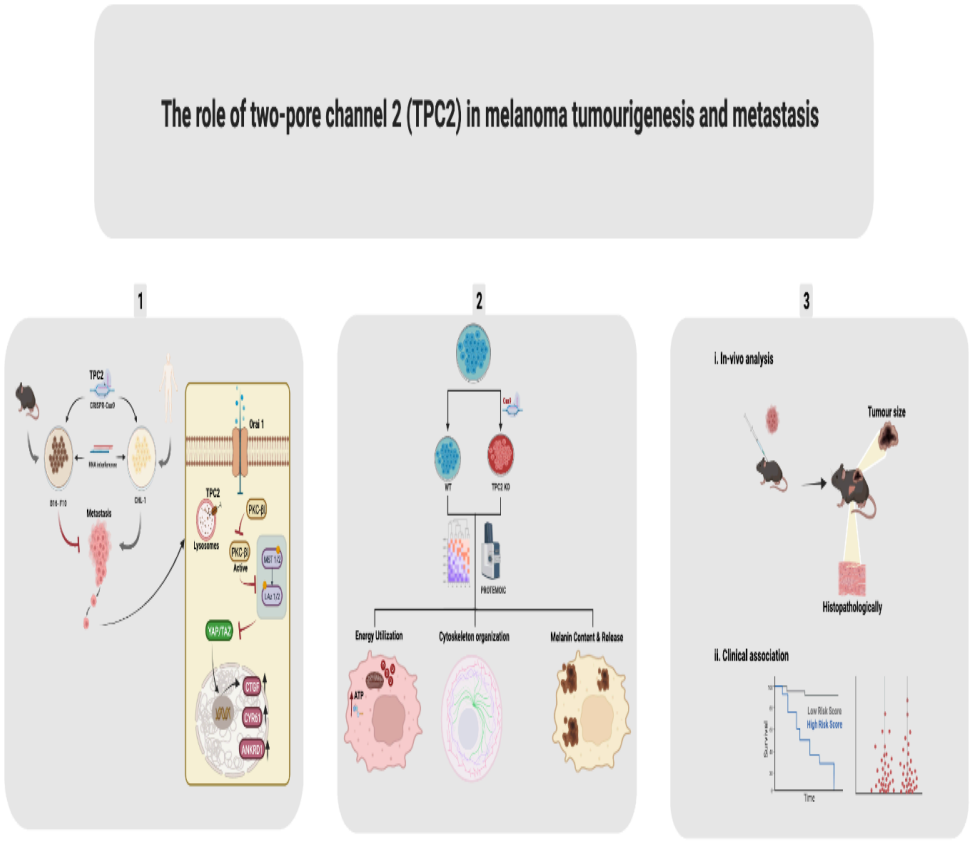

Figure 34. An overview of the thesis's methods and findings.

Chapter 7

References

1. Tsatmali M, Ancans J, Thody AJ. Melanocyte function and its control by melanocortin peptides. Journal of Histochemistry and Cytochemistry [Internet]. 2002 Jun 26 [cited 2022 Apr 26];50(2):125–33. Available from: https://journals.sagepub.com/doi/full/10.1177/002215540205000201
2. Lerner AB, McGuire JS. MELANOCYTE-STIMULATING HORMONE AND ADRENOCORTICOTROPHIC HORMONE. THEIR RELATION TO PIGMENTATION. N Engl J Med [Internet]. 1964 Mar 12 [cited 2022 Apr 26];270(11):539–46. Available from: https://pubmed.ncbi.nlm.nih.gov/14091524/
3. Abdel-Malek Z, Suzuki I, Tada A, Im S, Akcali C. The melanocortin-1 receptor and human pigmentation. Ann N Y Acad Sci [Internet]. 1999 [cited 2022 Apr 26];885:117–33. Available from: https://pubmed.ncbi.nlm.nih.gov/10816645/
4. Erdei E, Torres SM. A new understanding in the epidemiology of melanoma. Expert Rev Anticancer Ther [Internet]. 2010 Nov [cited 2022 Apr 26];10(11):1811–23. Available from: https://pubmed.ncbi.nlm.nih.gov/21080806/
5. Kosary CL, Altekruse SF, Ruhl J, Lee R, Dickie L. Clinical and prognostic factors for melanoma of the skin using SEER registries: Collaborative

stage data collection system, version 1 and version 2. Cancer. 2014 Dec 1;120(S23):3807–14.

6. Linos E, Swetter S, Cockburn M, … GCJ of I, 2009 undefined. Increasing burden of melanoma in the United States. Elsevier [Internet]. [cited 2022 Apr 26]; Available from: https://www.sciencedirect.com/science/article/pii/S0022202X15344262

7. Rigel DS, Carucci JA. Malignant melanoma: prevention, early detection, and treatment in the 21st century. CA Cancer J Clin. 2000 Jul 1;50(4):215–36.

8. Erdei E, Torres SM. A new understanding in the epidemiology of melanoma. Expert Rev Anticancer Ther. 2010 Nov;10(11):1811–23.

9. Ray L. Future prospective of nanotechnology in skin cancer therapeutics. Skin Aging & Cancer: Ambient UV-R Exposure. 2020 Jan 1;87–100.

10. Goodson A, of DGJ of the AA, 2009 undefined. Strategies for early melanoma detection: Approaches to the patient with nevi. Elsevier [Internet]. [cited 2022 Apr 26]; Available from: https://www.sciencedirect.com/science/article/pii/S0190962208024730

11. Wolchok JD, Chiarion-Sileni V, Gonzalez R, Rutkowski P, Grob JJ, Cowey CL, et al. Overall Survival with Combined Nivolumab and Ipilimumab in Advanced Melanoma. New England Journal of Medicine. 2017 Oct 5;377(14):1345–56.

12. Radiation: Ultraviolet (UV) radiation and skin cancer [Internet]. [cited 2022 Apr 26]. Available from: https://www.who.int/news-room/questions-and-answers/item/radiation-ultraviolet-(uv)-radiation-and-skin-cancer

13. PDQ Adult Treatment Editorial Board. Melanoma Treatment (PDQ®): Health Professional Version. PDQ Cancer Information Summaries [Internet]. 2002 [cited 2022 Apr 26]; Available from: http://www.ncbi.nlm.nih.gov/pubmed/26389469

14. Melanoma skin cancer statistics | Cancer Research UK [Internet]. [cited 2022 Apr 26]. Available from: https://www.cancerresearchuk.org/health-professional/cancer-statistics/statistics-by-cancer-type/melanoma-skin-cancer

15. Parsons HM, Harlan LC, Schmidt S, Keegan THM, Lynch CF, Kent EE, et al. Who Treats Adolescents and Young Adults with Cancer? A Report from the AYA HOPE Study. J Adolesc Young Adult Oncol [Internet]. 2015 Sep 1 [cited 2022 Apr 26];4(3):141. Available from: /pmc/articles/PMC4575540/

16. Rastrelli M, Tropea S, Rossi C, vivo MAI, 2014 undefined. Melanoma: epidemiology, risk factors, pathogenesis, diagnosis and classification. iv.iiarjournals.org [Internet]. [cited 2022 Apr 26]; Available from: https://iv.iiarjournals.org/content/28/6/1005.short

17. surgery DRS in cutaneous medicine and, 2010 undefined. Epidemiology of melanoma. cdn.mdedge.com [Internet]. 2010 [cited 2022 Apr 26];29:204–9. Available from: https://cdn.mdedge.com/files/s3fs-public/issues/articles/vol29_i4_Epidemiology.pdf

18. Heasley D, Toda S, America MMJSC of N, 1996 undefined. Pathology of malignant melanoma. Elsevier [Internet]. [cited 2022 Apr 26]; Available from: https://www.sciencedirect.com/science/article/pii/S0039610905705120

19. Rastrelli M, Tropea S, Rossi C, vivo MAI, 2014 undefined. Melanoma: epidemiology, risk factors, pathogenesis, diagnosis and classification. iv.iiarjournals.org [Internet]. [cited 2022 Apr 26]; Available from: https://iv.iiarjournals.org/content/28/6/1005.short

20. Viros A, Fridlyand J, Bauer J, Lasithiotakis K, Garbe C, Pinkel D, et al. Improving melanoma classification by integrating genetic and morphologic features. PLoS Med. 2008 Jun;5(6):0941–52.

21. Long G v., Menzies AM, Nagrial AM, Haydu LE, Hamilton AL, Mann GJ, et al. Prognostic and clinicopathologic associations of oncogenic BRAF in metastatic melanoma. Journal of Clinical Oncology. 2011;29(10):1239–46.

22. Akbani R, Akdemir K, Aksoy B, Albert M, Cell AA, 2015 undefined. Genomic classification of cutaneous melanoma. Elsevier [Internet]. [cited 2022 Apr 26]; Available from: https://www.sciencedirect.com/science/article/pii/S0092867415006340

23. Mattia G, Puglisi R, Ascione B, Malorni W, … ACCD&, 2018 undefined. Cell death-based treatments of melanoma: conventional treatments and new therapeutic strategies. nature.com [Internet]. [cited 2022 Apr 27]; Available from: https://www.nature.com/articles/s41419-017-0059-7

24. Clinics RES, 2003 undefined. Surgical treatment of malignant melanoma. surgical.theclinics.com [Internet]. [cited 2022 Apr 27]; Available from: https://www.surgical.theclinics.com/article/S0039-6109(02)00205-0/abstract

25. Sanada M, Takagi Y, Ito R, repair MSD, 2004 undefined. Killing and mutagenic actions of dacarbazine, a chemotherapeutic alkylating agent, on human and mouse cells: effects of Mgmt and Mlh1 mutations.

Elsevier [Internet]. [cited 2022 Apr 27]; Available from: https://www.sciencedirect.com/science/article/pii/S1568786404000059

26. Middleton E, Kandaswami C, Theoharides TC. The Effects of Plant Flavonoids on Mammalian Cells: Implications for Inflammation, Heart Disease, and Cancer. 2000 [cited 2022 Jul 25]; Available from: http://www.pharmrev.org

27. Bhatia S, Tykodi S, Park JTO (Williston, NY) undefined, 2009 undefined. Treatment of metastatic melanoma: an overview. ncbi.nlm.nih.gov [Internet]. [cited 2022 Apr 27]; Available from: https://www.ncbi.nlm.nih.gov/pmc/articles/PMC2737459/

28. Wilson MA, Schuchter LM. Chemotherapy for melanoma. Cancer Treat Res. 2016;167:209–29.

29. Hayward N, Wilmott J, Waddell N, Nature PJ, 2017 undefined. Whole-genome landscapes of major melanoma subtypes. nature.com [Internet]. [cited 2022 Apr 27]; Available from: https://www.nature.com/articles/nature22071

30. Kudchadkar R. Novel Targeted Therapies for the Treatment of Metastatic Melanoma.

31. van Rooij N, van Buuren MM, Philips D, Velds A, Toebes M, Heemskerk B, et al. Tumor Exome Analysis Reveals Neoantigen-Specific T-Cell

Reactivity in an Ipilimumab-Responsive Melanoma. J Clin Oncol [Internet]. 2013 Nov 10 [cited 2022 Apr 27];31(32). Available from: /pmc/articles/PMC3836220/

32. Zhu MX, Ma J, Parrington J, Calcraft PJ, Galione A, Evans AM. Calcium signaling via two-pore channels: Local or global, that is the question. Am J Physiol Cell Physiol. 2010 Mar;298(3).

33. Marchant J, Transactions SPBS, 2015 undefined. Two-pore channels at the intersection of endolysosomal membrane traffic. portlandpress.com [Internet]. [cited 2022 Apr 27]; Available from: https://portlandpress.com/biochemsoctrans/article-abstract/43/3/434/65036

34. Ogunbayo O, Zhu Y, Shen B, Agbani E, … JLJ of B, 2015 undefined. Organelle-specific subunit interactions of the vertebrate two-pore channel family. ASBMB [Internet]. [cited 2022 Apr 27]; Available from: https://www.jbc.org/article/S0021-9258(20)57884-8/abstract

35. Morgan A, Platt F, … ELEB, 2011 undefined. Molecular mechanisms of endolysosomal Ca2+ signalling in health and disease. portlandpress.com [Internet]. [cited 2022 Apr 27]; Available from: https://portlandpress.com/biochemj/article-abstract/439/3/349/45679

36. Pitt SJ, Reilly-O'Donnell B, Sitsapesan R. Exploring the biophysical evidence that mammalian two-pore channels are NAADP-activated

calcium-permeable channels. Journal of Physiology. 2016 Aug 1;594(15):4171–9.

37. Cang C, Zhou Y, Navarro B, Seo Y, Aranda K, Cell LS, et al. mTOR regulates lysosomal ATP-sensitive two-pore Na+ channels to adapt to metabolic state. Elsevier [Internet]. [cited 2022 Apr 27]; Available from: https://www.sciencedirect.com/science/article/pii/S0092867413000755

38. Wang X, Zhang X, Dong X, Samie M, Li X, Cell XC, et al. TPC proteins are phosphoinositide-activated sodium-selective ion channels in endosomes and lysosomes. Elsevier [Internet]. [cited 2022 Apr 27]; Available from: https://www.sciencedirect.com/science/article/pii/S0092867412011051

39. biology AGCSH perspectives in, 2011 undefined. NAADP receptors. cshperspectives.cshlp.org [Internet]. [cited 2022 Apr 27]; Available from: https://cshperspectives.cshlp.org/content/3/1/a004036.short

40. Calcraft P, Ruas M, Pan Z, Cheng X, Nature AA, 2009 undefined. NAADP mobilizes calcium from acidic organelles through two-pore channels. nature.com [Internet]. [cited 2022 Apr 27]; Available from: https://www.nature.com/articles/nature08030

41. Ruas M, Davis LC, Chen C, Morgan AJ, Chuang K, Walseth TF, et al. Expression of Ca 2+ -permeable two-pore channels rescues NAADP signalling in TPC -deficient cells . EMBO J. 2015 Jul 2;34(13):1743–58.

42. Jha A, Ahuja M, Patel S, Brailoiu E, Muallem S. Convergent regulation of the lysosomal two-pore channel-2 by Mg 2+, NAADP, PI(3,5)P2 and multiple protein kinases. EMBO Journal. 2014 Mar 3;33(5):501–11.

43. Walseth T, Lin-Moshier Y, Jain P, … MRJ of B, 2012 undefined. Photoaffinity Labeling of High Affinity Nicotinic Acid Adenine Dinucleotide Phosphate (NAADP)-Binding Proteins in Sea Urchin Egg*♦. ASBMB [Internet]. [cited 2022 Apr 27]; Available from: https://www.jbc.org/article/S0021-9258(20)53193-1/abstract

44. Lin-Moshier Y, Walseth T, … DCJ of B, 2012 undefined. Photoaffinity Labeling of Nicotinic Acid Adenine Dinucleotide Phosphate (NAADP) Targets in Mammalian Cells*♦. ASBMB [Internet]. [cited 2022 Apr 27]; Available from: https://www.jbc.org/article/S0021-9258(20)53192-X/abstract

45. Zhang C, He Y, Okutsu M, Ong LC, Jin Y, Zheng L, et al. Autophagy is involved in adipogenic differentiation by repressesing proteasome-dependent PPARγ2 degradation. Am J Physiol Endocrinol Metab. 2013 May 8;305(4).

46. Aley P, Singh N, Brailoiu G, … EBJ of B, 2013 undefined. Nicotinic acid adenine dinucleotide phosphate (NAADP) is a second messenger in muscarinic receptor-induced contraction of guinea pig trachea. ASBMB [Internet]. [cited 2022 Apr 27]; Available from: https://www.jbc.org/article/S0021-9258(20)67179-4/abstract

47. Sugahara K, … YMI, 2011 undefined. Combination effects of distinct cores in 11q13 amplification region on cervical lymph node metastasis of oral squamous cell carcinoma. spandidos-publications.com [Internet]. [cited 2022 Apr 27]; Available from: https://www.spandidos-publications.com/ijo/39/4/761

48. Huang X, Godfrey TE, Gooding WE, McCarty KS, Gollin SM. Comprehensive genome and transcriptome analysis of the 11q13 amplicon in human oral cancer and synteny to the 7F5 amplicon in murine oral carcinoma. Genes Chromosomes Cancer. 2006 Nov;45(11):1058–69.

49. Nam O, Nguyen P, Grimm C, Schneider LS, Chao YK, Atzberger C, et al. Two-pore channel function is crucial for the migration of invasive cancer cells. AACR [Internet]. 2017 [cited 2022 Apr 27];77(6). Available from: https://cancerres.aacrjournals.org/content/77/6/1427.short

50. Favia A, Desideri M, Gambara G, D'alessio A, Ruas M, Esposito B, et al. VEGF-induced neoangiogenesis is mediated by NAADP and two-pore

channel-2–dependent Ca2+ signaling. National Acad Sciences [Internet]. [cited 2022 Apr 27]; Available from: https://www.pnas.org/content/111/44/E4706.short

51. Patel S, Cell BKBEBA (BBA) M, 2018 undefined. Two-pore channels and disease. Elsevier [Internet]. [cited 2022 Apr 27]; Available from: https://www.sciencedirect.com/science/article/pii/S0167488918300880

52. Pho L, ufficiale SL, e S italiana di dermatologia, 2010 undefined. Genetics of pigmentation and melanoma predisposition. europepmc.org [Internet]. [cited 2022 Apr 27]; Available from: https://europepmc.org/article/med/20197744

53. genetics RSH molecular, 2009 undefined. Molecular genetics of human pigmentation diversity. academic.oup.com [Internet]. [cited 2022 Apr 27]; Available from: https://academic.oup.com/hmg/article-abstract/18/R1/R9/2901093

54. Alharbi AF, Parrington J. The role of genetic polymorphisms in endolysosomal ion channels TPC2 and P2RX4 in cancer pathogenesis, prognosis, and diagnosis: a genetic association in the UK Biobank. npj Genomic Medicine 2021 6:1 [Internet]. 2021 Jul 12 [cited 2022 May 15];6(1):1–12. Available from: https://www.nature.com/articles/s41525-021-00221-9

55. Chao YK, Schludi V, Chen CC, Butz E, Nguyen ONP, Müller M, et al. TPC2 polymorphisms associated with a hair pigmentation phenotype in humans result in gain of channel function by independent mechanisms. National Acad Sciences [Internet]. 2017 [cited 2022 Apr 27]; Available from: https://www.pnas.org/content/114/41/E8595.short

56. Bellono N, Escobar I, reports EOS, 2016 undefined. A melanosomal two-pore sodium channel regulates pigmentation. nature.com [Internet]. [cited 2022 Apr 27]; Available from: https://www.nature.com/articles/srep26570

57. research MMP cell & melanoma, 2008 undefined. FIG4, Charcot-Marie Tooth disease, and hypopigmentation: a role for phosphoinositides in melanosome biogenesis? ncbi.nlm.nih.gov [Internet]. [cited 2022 Apr 27]; Available from: https://www.ncbi.nlm.nih.gov/pmc/articles/PMC2773460/

58. Ambrosio A, Boyle J, … AAP of the, 2016 undefined. TPC2 controls pigmentation by regulating melanosome pH and size. National Acad Sciences [Internet]. [cited 2022 Apr 27]; Available from: https://www.pnas.org/content/113/20/5622.short

59. Bellono N, Escobar I, reports EOS, 2016 undefined. A melanosomal two-pore sodium channel regulates pigmentation. nature.com [Internet].

[cited 2022 Apr 27]; Available from: https://www.nature.com/articles/srep26570

60. Davis S, Charles PD, He L, Mowlds P, Kessler BM, Fischer R. Expanding proteome coverage with CHarge Ordered Parallel Ion aNalysis (CHOPIN) combined with broad specificity proteolysis. ACS Publications [Internet]. 2017 Mar 3 [cited 2022 Jul 25];16(3):1288–99. Available from: https://pubs.acs.org/doi/abs/10.1021/acs.jproteome.6b00915

61. Tyanova S, Temu T, Sinitcyn P, Carlson A, Hein MY, Geiger T, et al. The Perseus computational platform for comprehensive analysis of (prote)omics data. Nature Methods 2016 13:9 [Internet]. 2016 Jun 27 [cited 2022 Jul 25];13(9):731–40. Available from: https://www.nature.com/articles/nmeth.3901

62. Wang J, Duncan D, Shi Z, research BZN acids, 2013 undefined. WEB-based gene set analysis toolkit (WebGestalt): update 2013. academic.oup.com [Internet]. [cited 2022 May 1]; Available from: https://academic.oup.com/nar/article-abstract/41/W1/W77/1105552

63. Li C, Tang Z, Zhang W, Ye Z, Liu F. GEPIA2021: integrating multiple deconvolution-based analysis into GEPIA. Nucleic Acids Res [Internet]. 2021 Jul 2 [cited 2022 Apr 27];49(W1):W242–6. Available from: https://academic.oup.com/nar/article/49/W1/W242/6288438

64. Lin JY, Fisher DE. Melanocyte biology and skin pigmentation. Nature 2007 445:7130 [Internet]. 2007 Feb 21 [cited 2022 Jan 23];445(7130):843–50. Available from: https://www.nature.com/articles/nature05660

65. Animal models of skin disease - ClinicalKey [Internet]. [cited 2022 Jan 23]. Available from: https://www.clinicalkey.com/#!/content/book/3-s2.0-B9780702069833000360

66. IJ F, GL N. Organ selectivity for implantation survival and growth of B16 melanoma variant tumor lines. J Natl Cancer Inst [Internet]. 1976 [cited 2022 Jan 23];57(5):1199–202. Available from: https://pubmed.ncbi.nlm.nih.gov/1003551/

67. Maniotis AJ, Folberg R, Hess A, Seftor EA, Gardner LMG, Pe'er J, et al. Vascular Channel Formation by Human Melanoma Cells in Vivo and in Vitro: Vasculogenic Mimicry. Am J Pathol [Internet]. 1999 Sep 1 [cited 2022 Jan 24];155(3):739–52. Available from: http://ajp.amjpathol.org/article/S0002944010651735/fulltext

68. Dobrokhotov O, Samsonov M, Sokabe M, Hirata H. Mechanoregulation and pathology of YAP/TAZ via Hippo and non-Hippo mechanisms. Clin Transl Med [Internet]. 2018 Dec [cited 2022 Jan 18];7(1):23. Available from: /pmc/articles/PMC6087706/

69. Menzel M, Meckbach D, Weide B, Toussaint NC, Schilbach K, Noor S, et al. In melanoma, Hippo signaling is affected by copy number alterations and YAP1 overexpression impairs patient survival. Pigment Cell Melanoma Res [Internet]. 2014 [cited 2022 Jan 18];27(4):671–3. Available from: https://pubmed.ncbi.nlm.nih.gov/24703331/

70. Hoj JP, Mayro B, Pendergast AM. A TAZ-AXL-ABL2 feed-forward signaling axis promotes lung adenocarcinoma brain metastasis. Cell Rep [Internet]. 2019 Dec 10 [cited 2022 Jan 18];29(11):3421. Available from: /pmc/articles/PMC7254883/

71. Dupont S, Morsut L, Aragona M, Enzo E, Giulitti S, Cordenonsi M, et al. Role of YAP/TAZ in mechanotransduction. Nature [Internet]. 2011 Jun 8 [cited 2022 Jan 18];474(7350):179–84. Available from: https://pubmed.ncbi.nlm.nih.gov/21654799/

72. Faviaa A, Desiderib M, Gambaraa G, D'Alessioa A, Ruas M, Esposito B, et al. VEGF-induced neoangiogenesis is mediated by NAADP and two-pore channel-2 -dependent ca2+signaling. Proc Natl Acad Sci U S A. 2014 Nov 4;111(44):4706–15.

73. Calcraft PJ, Ruas M, Pan Z, Cheng X, Arredouani A, Hao X, et al. NAADP mobilizes calcium from acidic organelles through two-pore channels. Nature. 2009 May 28;459(7246):596–600.

74. Mercer JC, DeHaven WI, Smyth JT, Wedel B, Boyles RR, Bird GS, et al. Large store-operated calcium selective currents due to co-expression of Orai1 or Orai2 with the intracellular calcium sensor, Stim1. Journal of Biological Chemistry. 2006 Aug 25;281(34):24979–90.

75. Liu Z, Wei Y, Zhang L, Yee PP, Johnson M, Zhang X, et al. Induction of store-operated calcium entry (SOCE) suppresses glioblastoma growth by inhibiting the Hippo pathway transcriptional coactivators YAP/TAZ. Oncogene. 2019 Jan 3;38(1):120–39.

76. Nguyen ONP, Grimm C, Schneider LS, Chao YK, Atzberger C, Bartel K, et al. Two-Pore Channel Function Is Crucial for the Migration of Invasive Cancer Cells. Cancer Res [Internet]. 2017 Mar 15 [cited 2022 Apr 25];77(6):1427–38. Available from: https://pubmed.ncbi.nlm.nih.gov/28108508/

77. Thompson BJ. YAP/TAZ: Drivers of Tumor Growth, Metastasis, and Resistance to Therapy. Bioessays [Internet]. 2020 May 1 [cited 2022 Apr 23];42(5). Available from: https://pubmed.ncbi.nlm.nih.gov/32128850/

78. Hwang SM, Jin MH, Shin YH, Choi SK, Namkoong E, Kim MK, et al. Role of LPA and the Hippo pathway on apoptosis in salivary gland epithelial cells. Experimental & Molecular Medicine 2014 46:12 [Internet]. 2014 Dec 12 [cited 2022 Apr 23];46(12):e125–e125. Available from: https://www.nature.com/articles/emm201477

79. Hoj JP, Mayro B, Marie A, Correspondence P. A TAZ-AXL-ABL2 Feed-Forward Signaling Axis Promotes Lung Adenocarcinoma Brain Metastasis. CellReports [Internet]. 2019 [cited 2022 Apr 23];29:3421-3434.e8. Available from: https://doi.org/10.1016/j.celrep.2019.11.018

80. D'amore A, Hanbashi AA, di Agostino S, Palombi F, Sacconi A, Voruganti A, et al. Loss of Two-Pore Channel 2 (TPC2) Expression Increases the Metastatic Traits of Melanoma Cells by a Mechanism Involving the Hippo Signalling Pathway and Store-Operated Calcium Entry. Cancers 2020, Vol 12, Page 2391 [Internet]. 2020 Aug 24 [cited 2022 Jul 12];12(9):2391. Available from: https://www.mdpi.com/2072-6694/12/9/2391/htm

81. Jin X, Zhang Y, Alharbi A, Hanbashi A, Alhoshani A, Parrington J. Targeting Two-Pore Channels: Current Progress and Future Challenges. Trends Pharmacol Sci. 2020 Aug 1;41(8):582–94.

82. Smyth JT, DeHaven WI, Jones BF, Mercer JC, Trebak M, Vazquez G, et al. Emerging perspectives in store-operated Ca2+ entry: Roles of Orai, Stim and TRP. Biochimica et Biophysica Acta (BBA) - Molecular Cell Research. 2006 Nov 1;1763(11):1147–60.

83. Kwon YW, Jo HS, Bae S, Seo Y, Song P, Song M, et al. Application of Proteomics in Cancer: Recent Trends and Approaches for Biomarkers Discovery. Front Med (Lausanne). 2021 Sep 22;8:1644.

84. Läsche M, Emons G, Gründker C. Shedding New Light on Cancer Metabolism: A Metabolic Tightrope Between Life and Death. Front Oncol. 2020 Mar 31;10:409.

85. PCK1 phosphoenolpyruvate carboxykinase 1 [Homo sapiens (human)] - Gene - NCBI [Internet]. [cited 2022 May 18]. Available from: https://www.ncbi.nlm.nih.gov/gene?Db=gene&Cmd=ShowDetailView&TermToSearch=5105

86. COX7A2 cytochrome c oxidase subunit 7A2 [Homo sapiens (human)] - Gene - NCBI [Internet]. [cited 2022 May 18]. Available from: https://www.ncbi.nlm.nih.gov/gene/1347

87. NDUFB9 NADH:ubiquinone oxidoreductase subunit B9 [Homo sapiens (human)] - Gene - NCBI [Internet]. [cited 2022 May 18]. Available from: https://www.ncbi.nlm.nih.gov/gene?Db=gene&Cmd=ShowDetailView&TermToSearch=4715

88. Dunn J, Grider MH. Physiology, Adenosine Triphosphate. StatPearls [Internet]. 2022 Feb 17 [cited 2022 May 18]; Available from: https://www.ncbi.nlm.nih.gov/books/NBK553175/

89. Technologies A. Agilent Technologies Agilent Seahorse XF Cell Mito Stress Test Kit User Guide Kit 103015-100.

90. Guide U. Agilent Technologies Agilent Seahorse XF Glycolytic Rate Assay Kit.

91. Aldoc aldolase C, fructose-bisphosphate [Mus musculus (house mouse)] - Gene - NCBI [Internet]. [cited 2022 May 18]. Available from: https://www.ncbi.nlm.nih.gov/gene/?term=11676

92. Küch EM, Vellaramkalayil R, Zhang I, Lehnen D, Brügger B, Stremmel W, et al. Differentially localized acyl-CoA synthetase 4 isoenzymes mediate the metabolic channeling of fatty acids towards phosphatidylinositol. Biochim Biophys Acta [Internet]. 2014 Feb [cited 2022 May 18];1841(2):227–39. Available from: https://pubmed.ncbi.nlm.nih.gov/24201376/

93. SARDH protein expression summary - The Human Protein Atlas [Internet]. [cited 2022 May 18]. Available from: https://www.proteinatlas.org/ENSG00000123453-SARDH

94. Gogvadze V, Orrenius S, Zhivotovsky B. Mitochondria in cancer cells: what is so special about them? Trends Cell Biol [Internet]. 2008 Apr 1 [cited 2022 May 25];18(4):165–73. Available from: http://www.cell.com/article/S0962892408000482/fulltext

95. Lee YX, Lin PH, Rahmawati E, Ma YY, Chan C, Tzeng CR. Mitochondria Research in Human Reproduction. The Ovary. 2019 Jan 1;327–35.

96. de la Cruz López KG, Toledo Guzmán ME, Sánchez EO, García Carrancá A. mTORC1 as a Regulator of Mitochondrial Functions and a Therapeutic Target in Cancer. Front Oncol. 2019 Dec 13;9:1373.

97. Vyas S, Zaganjor E, Cell MH, 2016 undefined. Mitochondria and cancer. Elsevier [Internet]. [cited 2022 May 26]; Available from: https://www.sciencedirect.com/science/article/pii/S0092867416309084

98. Reczek CR, Chandel NS. The Two Faces of Reactive Oxygen Species in Cancer. http://dx.doi.org/101146/annurev-cancerbio-041916-065808 [Internet]. 2017 Mar 6 [cited 2022 May 26];1:79–98. Available from: /pb-assets/assets/images/social-media/facebook-cover/CA_Journal_Cover_Facebook-1539113409273.png

99. Tpm3 tropomyosin 3, gamma [Mus musculus (house mouse)] - Gene - NCBI [Internet]. [cited 2022 May 18]. Available from: https://www.ncbi.nlm.nih.gov/gene/?term=59069

100. Pdlim5 PDZ and LIM domain 5 [Mus musculus (house mouse)] - Gene - NCBI [Internet]. [cited 2022 May 18]. Available from: https://www.ncbi.nlm.nih.gov/gene/?term=56376

101. Cttnbp2nl CTTNBP2 N-terminal like [Mus musculus (house mouse)] - Gene - NCBI [Internet]. [cited 2022 May 18]. Available from: https://www.ncbi.nlm.nih.gov/gene/?term=80281

102. LMNB1 lamin B1 [Homo sapiens (human)] - Gene - NCBI [Internet]. [cited 2022 May 18]. Available from:

https://www.ncbi.nlm.nih.gov/gene?Db=gene&Cmd=ShowDetailView&TermToSearch=4001

103. Slominski RM, Zmijewski MA, Slominski AT. The role of melanin pigment in melanoma. Exp Dermatol [Internet]. 2015 Apr 1 [cited 2022 Jan 27];24(4):258–9. Available from: https://onlinelibrary.wiley.com/doi/full/10.1111/exd.12618

104. Hu DN. Methodology for evaluation of melanin content and production of pigment cells in vitro. Photochem Photobiol [Internet]. 2008 May [cited 2022 May 30];84(3):645–9. Available from: https://pubmed.ncbi.nlm.nih.gov/18435617/

105. TYR tyrosinase [Homo sapiens (human)] - Gene - NCBI [Internet]. [cited 2022 May 30]. Available from: https://www.ncbi.nlm.nih.gov/gene/7299

106. MREG melanoregulin [Homo sapiens (human)] - Gene - NCBI [Internet]. [cited 2022 May 30]. Available from: https://www.ncbi.nlm.nih.gov/gene/55686

107. Ohbayashi N, Maruta Y, … MIJ of cell, 2012 undefined. Melanoregulin regulates retrograde melanosome transport through interaction with the RILP–p150Glued complex in melanocytes. journals.biologists.com [Internet]. [cited 2022 May 30]; Available from: https://journals.biologists.com/jcs/article-abstract/125/6/1508/33297

108. Damek-Poprawa M, Diemer T, Lopes V, … CLJ of B, 2009 undefined. Melanoregulin (MREG) modulates lysosome function in pigment epithelial cells. ASBMB [Internet]. [cited 2022 May 30]; Available from: https://www.jbc.org/article/S0021-9258(20)39929-4/abstract

109. Koppenol WH, Bounds PL, Dang C v. Otto Warburg's contributions to current concepts of cancer metabolism. Nat Rev Cancer [Internet]. 2011 May [cited 2022 May 26];11(5):325–37. Available from: https://pubmed.ncbi.nlm.nih.gov/21508971/

110. Zheng J. Energy metabolism of cancer: Glycolysis versus oxidative phosphorylation (review). Oncol Lett [Internet]. 2012 Dec 1 [cited 2022 May 26];4(6):1151–7. Available from: http://www.spandidos-publications.com/10.3892/ol.2012.928/abstract

111. Müller M, Gerndt S, Chao YK, Zisis T, Nguyen ONP, Gerwien A, et al. Gene editing and synthetically accessible inhibitors reveal role for TPC2 in HCC cell proliferation and tumor growth. Cell Chem Biol. 2021 Aug 19;28(8):1119-1131.e27.

112. Tooze S, Zoncu R. Control of cellular homeostasis: organelles take the pilot's seat. Mol Biol Cell [Internet]. 2015 Mar 3 [cited 2022 May 26];26(6):1009. Available from: /pmc/articles/PMC4357499/

113. Eales KL, Hollinshead KER, Tennant DA. Hypoxia and metabolic adaptation of cancer cells. Oncogenesis 2016 5:1 [Internet]. 2016 Jan

25 [cited 2022 May 26];5(1):e190–e190. Available from: https://www.nature.com/articles/oncsis201550

114. Keating R, McGargill MA. mTOR regulation of lymphoid cells in immunity to pathogens. Front Immunol. 2016;7(MAY):180.

115. Chang FS, Wang Y, Dmitriev P, Gross J, Galione A, Pears C. A two-pore channel protein required for regulating mTORC1 activity on starvation. BMC Biol [Internet]. 2020 Jan 22 [cited 2022 May 27];18(1):1–16. Available from: https://bmcbiol.biomedcentral.com/articles/10.1186/s12915-019-0735-4

116. Cang C, Zhou Y, Navarro B, Seo YJ, Aranda K, Shi L, et al. mTOR Regulates Lysosomal ATP-Sensitive Two-Pore Na+ Channels to Adapt to Metabolic State. Cell. 2013 Feb 14;152(4):778–90.

117. Ogunbayo OA, Duan J, Xiong J, Wang Q, Feng X, Ma J, et al. mTORC1 controls lysosomal Ca2+ release through the two-pore channel TPC2. Sci Signal [Internet]. 2018 Apr 4 [cited 2022 May 27];11(525). Available from: /pmc/articles/PMC6055479/

118. Gaspar P, Holder M v., Aerne BL, Janody F, Tapon N. Zyxin antagonizes the FERM protein expanded to couple F-actin and Yorkie-dependent organ growth. Curr Biol [Internet]. 2015 Mar 16 [cited 2022 Apr

25];25(6):679–89. Available from: https://pubmed.ncbi.nlm.nih.gov/25728696/

119. Zhang X, Pei Z, Ji C, Zhang X, Xu J, Wang J. Novel Insights into the Role of the Cytoskeleton in Cancer. Cytoskeleton - Structure, Dynamics, Function and Disease [Internet]. 2017 May 17 [cited 2022 Apr 25]; Available from: https://www.intechopen.com/chapters/53708

120. Thiery JP, Acloque H, Huang RYJ, Nieto MA. Epithelial-mesenchymal transitions in development and disease. Cell [Internet]. 2009 Nov 25 [cited 2022 Apr 25];139(5):871–90. Available from: https://pubmed.ncbi.nlm.nih.gov/19945376/

121. Aseervatham J. Cytoskeletal Remodeling in Cancer. Biology (Basel) [Internet]. 2020 Nov 1 [cited 2022 Apr 25];9(11):1–40. Available from: /pmc/articles/PMC7695181/

122. Chen YF, Chen YT, Chiu WT, Shen MR. Remodeling of calcium signaling in tumor progression. J Biomed Sci [Internet]. 2013 [cited 2022 Apr 25];20(1):23. Available from: /pmc/articles/PMC3639169/

123. Lin J, Nature DF, 2007 undefined. Melanocyte biology and skin pigmentation. nature.com [Internet]. [cited 2022 May 30]; Available from: https://www.nature.com/articles/nature05660

124. Slominski A, Zmijewski MA, Pawelek J. L-tyrosine and L-dihydroxyphenylalanine as hormone-like regulators of melanocyte

functions. Pigment Cell Melanoma Res [Internet]. 2012 Jan 1 [cited 2022 May 30];25(1):14–27. Available from: https://onlinelibrary.wiley.com/doi/full/10.1111/j.1755-148X.2011.00898.x

125. Mishra R, Kneitz S, … MS and PPCT&, 2014 undefined. Comparative analysis of melanoma deregulated miRNAs in the medaka and Xiphophorus pigment cell cancer models. Elsevier [Internet]. [cited 2022 May 30]; Available from: https://www.sciencedirect.com/science/article/pii/S1532045614000040

126. Slominski R, … MZE, 2015 undefined. The role of melanin pigment in melanoma. ncbi.nlm.nih.gov [Internet]. [cited 2022 May 30]; Available from: https://www.ncbi.nlm.nih.gov/pmc/articles/PMC4450257/

127. Hoek KS, Schlegel NC, Brafford P, Sucker A, Ugurel S, Kumar R, et al. Metastatic potential of melanomas defined by specific gene expression profiles with no BRAF signature. Pigment Cell Res [Internet]. 2006 Aug 1 [cited 2022 May 30];19(4):290–302. Available from: https://onlinelibrary.wiley.com/doi/full/10.1111/j.1600-0749.2006.00322.x

128. Carreira S, Goodall J, Denat L, Rodriguez M, Nuciforo P, Hoek KS, et al. Mitf regulation of Dia1 controls melanoma proliferation and

invasiveness. Genes Dev [Internet]. 2006 Dec 15 [cited 2022 May 30];20(24):3426–39. Available from: http://genesdev.cshlp.org/content/20/24/3426.full

129. Dror S, Sander L, Schwartz H, Sheinboim D, Barzilai A, Dishon Y, et al. Melanoma miRNA trafficking controls tumour primary niche formation. Nature Cell Biology 2016 18:9 [Internet]. 2016 Aug 22 [cited 2022 May 27];18(9):1006–17. Available from: https://www.nature.com/articles/ncb3399

130. Dror S, Sander L, Schwartz H, Sheinboim D, Barzilai A, Dishon Y, et al. Melanoma miRNA trafficking controls tumour primary niche formation. Nat Cell Biol [Internet]. 2016 Sep 1 [cited 2022 Apr 25];18(9):1006–17. Available from: https://pubmed.ncbi.nlm.nih.gov/27548915/

131. Ohcuchi K, Banno Y, Nakagawa Y, Akao Y, Nozawa Y. Negative regulation of melanogenesis by phospholipase D1 through mTOR/p70 S6 kinase 1 signaling in mouse B16 melanoma cells. J Cell Physiol [Internet]. 2005 Dec 1 [cited 2022 May 30];205(3):444–51. Available from: https://onlinelibrary.wiley.com/doi/full/10.1002/jcp.20421

132. Guo S, Hong L, Akhremitchev BB, Simon JD. Surface elastic properties of human retinal pigment epithelium melanosomes. Photochem Photobiol. 2008 May;84(3):671–8.

133. Sarna M, Zadlo A, Czuba-Pelech B, Urbanska K. Nanomechanical Phenotype of Melanoma Cells Depends Solely on the Amount of Endogenous Pigment in the Cells. International Journal of Molecular Sciences 2018, Vol 19, Page 607 [Internet]. 2018 Feb 18 [cited 2022 May 30];19(2):607. Available from: https://www.mdpi.com/1422-0067/19/2/607/htm

134. Sarna M, Krzykawska-Serda M, Jakubowska M, Zadlo A, Urbanska K. Melanin presence inhibits melanoma cell spread in mice in a unique mechanical fashion. Scientific Reports 2019 9:1 [Internet]. 2019 Jun 26 [cited 2022 May 30];9(1):1–9. Available from: https://www.nature.com/articles/s41598-019-45643-9

135. Tomczak K, Czerwińska P, Wiznerowicz M. The Cancer Genome Atlas (TCGA): an immeasurable source of knowledge. Contemp Oncol [Internet]. 2015 [cited 2022 Jan 26];19(1A):A68. Available from: /pmc/articles/PMC4322527/

136. Tang Z, Li C, Kang B, Gao G, Li C, Zhang Z. GEPIA: a web server for cancer and normal gene expression profiling and interactive analyses. Nucleic Acids Res [Internet]. 2017 Jul 3 [cited 2022 Jan 26];45(W1):W98–102. Available from: https://academic.oup.com/nar/article/45/W1/W98/3605636

137. Katt ME, Placone AL, Wong AD, Xu ZS, Searson PC. In vitro tumor models: Advantages, disadvantages, variables, and selecting the right platform. Front Bioeng Biotechnol. 2016 Feb 12;4(FEB):12.

138. Li Y, Schön C, Chen CC, Yang Z, Liegl R, Murenu E, et al. TPC2 promotes choroidal angiogenesis and inflammation in a mouse model of neovascular age-related macular degeneration. Life Sci Alliance [Internet]. 2021 Aug 1 [cited 2022 May 31];4(8). Available from: https://www.life-science-alliance.org/content/4/8/e202101047

139. Favia A, Desideri M, Gambara G, D'alessio A, Ruas M, Esposito B, et al. VEGF-induced neoangiogenesis is mediated by NAADP and two-pore channel-2–dependent Ca2+ signaling. National Acad Sciences [Internet]. [cited 2022 May 31]; Available from: https://www.pnas.org/content/111/44/E4706.short

140. Ostrand-Rosenberg S. Immune surveillance: a balance between protumor and antitumor immunity. Curr Opin Genet Dev. 2008 Feb;18(1):11–8.

141. Cavallo F, de Giovanni C, Nanni P, Forni G, Lollini PL. 2011: The immune hallmarks of cancer. Cancer Immunology, Immunotherapy. 2011 Mar;60(3):319–26.

142. Umansky V, Sevko A. Tumor microenvironment and myeloid-derived suppressor cells. Cancer Microenvironment. 2013 Aug;6(2):169–77.

143. Ilkovitch D, Lopez DM. The Liver is a Site for Tumor Induced Myeloid-Derived Suppressor Cell Accumulation and Immunosuppression. Cancer Res [Internet]. 2009 Jul 7 [cited 2022 Jun 1];69(13):5514. Available from: /pmc/articles/PMC2706931/

144. Fu Y, Watson G, Jimenez J, Wang Y, research DLC, 1990 undefined. Expansion of immunoregulatory macrophages by granulocyte-macrophage colony-stimulating factor derived from a murine mammary tumor. AACR [Internet]. [cited 2022 Jun 1]; Available from: https://cancerres.aacrjournals.org/content/50/2/227.short

145. Eggert T, Medina-Echeverz J, Kapanadze T, Kruhlak MJ, Korangy F, Greten TF. Tumor Induced Hepatic Myeloid Derived Suppressor Cells Can Cause Moderate Liver Damage. PLoS One [Internet]. 2014 Nov 17 [cited 2022 Jun 1];9(11):112717. Available from: /pmc/articles/PMC4234460/

146. Lechner M, Immunology DLTJ of, 2010 undefined. Characterization of cytokine-induced myeloid-derived suppressor cells from normal human peripheral blood mononuclear cells. Am Assoc Immnol [Internet]. 2022 [cited 2022 Jun 1];185:2273–84. Available from: https://www.jimmunol.org/content/185/4/2273.short

147. Davis LC, Morgan AJ, Galione A. NAADP-regulated two-pore channels drive phagocytosis through endo-lysosomal Ca2+ nanodomains,

calcineurin and dynamin. EMBO J [Internet]. 2020 Jul 7 [cited 2022 Jun 1];39(14). Available from: /pmc/articles/PMC7360967/

148. Li Y, Schön C, Chen CC, Yang Z, Liegl R, Murenu E, et al. TPC2 promotes choroidal angiogenesis and inflammation in a mouse model of neovascular age-related macular degeneration. Life Sci Alliance [Internet]. 2021 Aug 1 [cited 2022 Jun 1];4(8). Available from: https://www.life-science-alliance.org/content/4/8/e202101047

149. Tomczak K, Czerwińska P, Wiznerowicz M. Review
The Cancer Genome Atlas (TCGA): an immeasurable source of knowledge. Contemporary Oncology/Współczesna Onkologia [Internet]. 2015 [cited 2022 Jul 25];2015(1):68–77. Available from: https://tcga-data.nci.nih.gov/datareports/codeTablesReport.

150. Müller M, Gerndt S, Chao YK, Zisis T, Nguyen ONP, Gerwien A, et al. Gene editing and synthetically accessible inhibitors reveal role for TPC2 in HCC cell proliferation and tumor growth. Cell Chem Biol. 2021 Aug 19;28(8):1119-1131.e27.

151. D'amore A, Hanbashi AA, di Agostino S, Palombi F, Sacconi A, Voruganti A, et al. Loss of Two-Pore Channel 2 (TPC2) Expression Increases the Metastatic Traits of Melanoma Cells by a Mechanism Involving the Hippo Signalling Pathway and Store-Operated Calcium Entry. Cancers 2020, Vol 12, Page 2391 [Internet]. 2020 Aug 24 [cited 2022 Apr

25];12(9):2391. Available from: https://www.mdpi.com/2072-6694/12/9/2391/htm

152. Nguyen ONP, Grimm C, Schneider LS, Chao YK, Atzberger C, Bartel K, et al. Two-Pore Channel Function Is Crucial for the Migration of Invasive Cancer Cells. Cancer Res [Internet]. 2017 Mar 15 [cited 2022 Apr 25];77(6):1427–38. Available from: https://pubmed.ncbi.nlm.nih.gov/28108508/

153. Dobrokhotov O, Samsonov M, Sokabe M, Hirata H. Mechanoregulation and pathology of YAP/TAZ via Hippo and non-Hippo mechanisms. Clin Transl Med. 2018 Dec;7(1).

154. Menzel M, Meckbach D, … BWP cell &, 2014 undefined. In melanoma, Hippo signaling is affected by copy number alterations and YAP1 overexpression impairs patient survival. pubmed.ncbi.nlm.nih.gov [Internet]. [cited 2022 May 3]; Available from: https://pubmed.ncbi.nlm.nih.gov/24703331/

155. Felice D de, Cancers AA, 2020 undefined. Mechanosensitive piezo channels in cancer: focus on altered calcium signaling in cancer cells and in tumor progression. mdpi.com [Internet]. [cited 2022 May 4]; Available from: https://www.mdpi.com/760174